NUMERICAL MODELING OF DAM BREACH IN CONCRETE GRAVITY DAMS

A THESIS SUBMITTED TO
THE GRADUATE SCHOOL OF NATURAL AND APPLIED SCIENCES
OF
MIDDLE EAST TECHNICAL UNIVERSITY

BY

FARSHID MOSADDEGHI

IN PARTIAL FULFILLMENT OF THE REQUIREMENTS
FOR
THE DEGREE OF DOCTOR OF PHILOSOPHY
IN
CIVIL ENGINEERING

SEPTEMBER 2021

Approval of the thesis:

NUMERICAL MODELING OF DAM BREACH IN CONCRETE GRAVITY DAMS

submitted by **FARSHID MOSADDEGHI** in partial fulfillment of the requirements for the degree of **Doctor of Philosophy** i**n Civil Engineering, Middle East Technical University** by,

Prof. Dr. Halil Kalıpçılar

Dean, Graduate School of **Natural and Applied Sciences**

Prof. Dr. Ahmet Türer

Head of the Department, **Civil Engineering**

Prof. Dr. Mete Köken

Supervisor, **Civil Engineering, METU**

Prof. Dr. İsmail Aydın

Co-Supervisor, **Civil Engineering, METU**

Examining Committee Members:

Prof. Dr. Zafer Bozkuş

Civil Engineering, METU

Prof. Dr. Mete Köken

Civil Engineering, METU

Assoc.Prof.Dr. Alper Aldemir

Civil Engineering, Hacettepe Uni.

Assoc.Prof.Dr. Müsteyde Baduna Koçyiğit

Civil Engineering, Gazi Uni.

Assoc.Prof.Dr. A. Ersin Dinçer

Civil Engineering, Abdullah Gül Uni.

Date: 08.09.2021

I hereby declare that all information in this document has been obtained and presented in accordance with academic rules and ethical conduct. I also declare that, as required by these rules and conduct, I have fully cited and referenced all material and results that are not original to this work.

Name Last name : Farshid Mosaddeghi

Signature : 

ABSTRACT

NUMERICAL MODELING OF DAM BREACH IN CONCRETE GRAVITY DAMS

Farshid Mosaddeghi
Doctor of Philosophy, Civil Engineering
Supervisor: Prof. Dr. Mete Köken
Co-Supervisor: Prof. Dr. Ismail Aydin

September 2021, 168 pages

When a dam fails, a large amount of water is suddenly released that may create large flood waves capable of causing devastating impacts to downstream areas. This is even more important when the damage is caused by an earthquake, because it is unpredictable. The main objective of the research is a detailed simulating of the water surface profile from the first crack to the entire breaking of dams' body during earthquake using Finite Volume Method (FVM). The next objective is detecting of vulnerable zones on the dams' body during earthquake using Finite Element Method (FEM). Due to the complexity of the issue, it is necessary to first ensure the capability of the Flow 3D software in the field of dam failure simulation. For this purpose, the third part of the thesis, which includes simulation of pressure inside cracks during an earthquake, is used to verify the Volume of Fluid method (VOF), and the fourth chapter of the thesis, which includes the study of different motion types of solid objects due to the earthquake, is used to verify the General Moving Object method (GMO) in the scope of dam failure study. Finally, in the fifth chapter of the thesis, using the results and information obtained from the third and fourth chapters, models for the dam failure mechanism will be presented in sudden and gradual forms. The most important findings can be summarize in this way: Firstly, an important result

obtained from the simulation of the pressure inside the cracks is that by changing the length of the crack or its opening, the pressure distribution inside it changes. Therefore, considering that the failure of the concrete dam begins with the cracking of the body, modeling dam failure is almost impossible with small scale. Secondly, the failure of the dam in a sudden mode that is the results of terrible earthquake, is more dangerous than the gradual failure of the dam, which is very likely in concrete hydraulic structures. According to the discharge hydrographs of the two failure modes, for the gradual mode, the step-by-step increase to the maximum output flow rate occurs, while in the sudden failure of the dam, the discharge quickly tends to its maximum. finally, by a closer look at the sudden failure of the dam resulted in the conclusion that, with decreasing oscillation frequencies in constant magnitude of earthquake, the probability of failure in the sudden state increases. However, after cracking of the body, higher oscillation frequencies will be able to break it in less time. from this perspective the earthquakes that start with small oscillation frequencies and end with higher frequencies are the most destructive ones.

Keywords: Dam breach, Numerical simulation, Free-surface flow, Seismic stability, Flood inundation

ÖZ

BETON AĞIRLIK BARAJLARDA BARAJ YIKILMASININ SAYISAL MODELLEMESİ

Farshid, Mosaddeghi
Doktora, İnşaat Mühendisliği
Tez Yöneticisi: Prof. Dr. Mete Köken
Ortak Tez Yöneticisi: Prof. Dr. Ismail Aydin

Eylül 2021, 168 sayfa

Bir baraj çöktüğünde, aniden büyük miktarda su salınır ve bu da mansap bölgelerinde yıkıcı etkilere neden olabilir. Baraj yıkılması, bir depremden kaynaklandığı durumlarda daha da önemlidir, çünkü önceden tahmin edilemez. Araştırmanın temel amacı, ilk çatlaktan baraj gövdesinin tüm kırılmasına kadar su yüzeyi profilinin, FVM yöntemini kullanılarak detaylı bir simülasyonudur. Bir sonraki hedef, deprem sırasında baraj gövdesi üzerindeki hassas bölgelerin, FEM yöntemini kullanılarak tespit edilmesidir. Konunun karmaşıklığı nedeniyle öncelikle Flow 3D yazılımının baraj çökme simülasyonu alanında yeterliliğinin sağlanması gerekmektedir. Bu amaçla, VOF yöntemini doğrulamak için deprem sırasında çatlak içi basıncın simülasyonunu içeren tezin üçüncü bölümü ve katı cisimlerin farklı hareket türlerinin çalışılmasını içeren dördüncü bölüm kullanılmıştır. Son olarak, tezin beşinci bölümünde, üçüncü ve dördüncü bölümlerden elde edilen sonuçlar ve bilgiler kullanılarak baraj yıkılma mekanizmasına ilişkin modeller anlık ve kademeli formlarda sunulacaktır. En önemli sonuçlar şu şekilde özetlenebilir: İlk olarak, çatlakların içindeki basıncın simülasyonundan elde ettiğimiz önemli bir sonuç, çatlağın uzunluğunu veya açıklığını değiştirerek içindeki basınç dağılımının değişmesidir. Bu nedenle beton barajın yıkılmasının gövdenin çatlaması ile başladığı

düşünülürse, baraj yıkılmasının küçük ölçekli modellenmesi neredeyse imkansızdır. İkinci olarak, ani baraj yıkılması, kademeli baraj yıkılmasından daha tehlikelidir. İki yıkılma modelin deşarj hidrograflarına göre, kademeli mod için, maksimum çıkış debisinde adım adım artış meydana gelirken, barajın ani yıkılmasında deşarj hızla maksimuma yönelir. Son olarak, barajın ani göçmesine daha yakından bakıldığında, sabit büyüklükteki depremde salınım frekanslarının azalmasıyla ani durumda yıkılması olasılığının arttığı sonucuna varılmıştır. Ancak gövde çatladıktan sonra daha yüksek salınım frekansları onu daha kısa sürede kırabilecektir. bu açıdan küçük salınım frekanslarıyla başlayan ve yüksek frekanslarla biten depremler en yıkıcı olanlardır.

Anahtar Kelimeler: Baraj yıkılması, Sayısal modelleme, Serbest yüzey akışı, Sismik risk, Sel kontrolü

To My Mother and Father...

ACKNOWLEDGMENTS

I would like to express my deepest gratitude to my supervisor Prof. Dr. Mete Köken and my co-supervisor Prof. Dr. Ismail Aydin for their guidance, advice, criticism, encouragement, and insight throughout the research.

I would also like to thank Prof. Dr. Yalın Arıcı for his suggestions and comments. Without his vision and ambition, this study would not have been possible.

Many thanks to my dissertation progress committee members Prof. Dr. Zafer Bozkuş, Assoc. Prof. Dr. Müsteyde Baduna Koçyiğit, Assoc. Prof. Dr. Alper Aldemir and Assoc. Prof. Dr. Ali Ersin Dinçer for their valuable suggestions, comments and support.

This work is partially funded by the Scientific and Technological Research Council of Turkey under grant number TUBİTAK 116M524.

TABLE OF CONTENTS

LIST OF TABLES

TABLES

LIST OF FIGURES

FIGURES

CHAPTER 1

INTRODUCTION

Various definitions can be given for the dam. In a general definition, a structure that is built on the river to stop and store water is called a dam. These structures are very strong walls that can control the flow of water. On the other hand, they are often used to change the direction of the water. Behind the dams, a lake-shaped reservoir is usually created and this water is used when necessary. It can be said that all dams have a section called overflow, which is very necessary to maintain the water level. The most important and biggest benefit of constructing a dam is water storage. The water stored behind these structures is used in various ways and each dam is built depending on the purpose. For example, the water collected in the reservoir of dams can be used for agriculture or industrial purposes. Water power by turbines and electric generators can also be used to generate electricity. Dams are being built in many areas to control and prevent floods, However, these dams can cause floods on a much larger scale if broken.

1.1 Dams Failure

When a dam fails, a large amount of water is suddenly released that may create large flood waves capable of causing devastating impacts to downstream areas. Consequently, there is a need for the prediction of flood inundation due to dam failure to be prepared for the flood risks. Dams are extremely expensive structures that directly affect the economy of the watershed by water supply, irrigation, navigation, power generation, etc. therefore, lots of people will be gathered around dams to benefit from its advantages to improve their life condition. As the population

of an area grows, the structural failure of large dams can cause great danger for the residence of the watershed due to sudden flooding.

The risk of dam break has long been one of the most important issues in dam construction. Due to the advances made in various branches of science, it has always been tried to minimize the risk of their destruction by building resistant dams. Therefore, numerous researches have been done in this field. According to the International Commission on Large Dams (Moigne & Barghouti, 1990), during a review of 14,700 dams built before 1983, 7.5 percent of these had serious defects. From the study, before 1950 the percentage of broken dams worldwide was 1.2%, and after 1950 this figure dropped to 0.3%. Today, dams' failure have increased due to the age of dams, earthquakes, and climate change. Failure of a dam can cause irreparable damage at various levels, such as the loss of human and animal life, as well as the loss of a significant portion of a country's national capital. Examples include the failure of the Vajont Dam (1963) in Italy and the Teton Dam (1976) in the United States, which left 2,600 and 1,000 deaths, respectively. Other incidents include the failure of the Austin Concrete Dam in September 1911 in the United States, which killed 87 people and caused 88 million $ in financial losses, and the collapse of the Malpasset Arc Concrete Dam in December 1959 in France, which killed 441 people and caused significant economic damage (Jansen, 1980).

1.2 Problem Statement and Research Objectives

Important factors in the process of dam failure can be divided into two main categories: natural and human. Natural factors can be divided into two categories: external and internal. Human factors are just as important as natural factors. The most important human causes of dam failure are terrorist attacks and war. Internal natural factors are the second category of natural factors affecting failure. Among these factors, defects in the dam body or defects in the dam foundation can be mentioned. External natural factors, including heavy rains, storms, earthquakes, etc., are the second category of natural factors affecting failure. Heavy rains and storms

cause rivers to overflow, increasing the volume of water behind the dam. If the water inlet is more than the outlet, a lot of pressure is applied to the dam body, which if the proper arrangements are not provided, the dam will be damaged. Another important natural and external factor that can destroy a dam is an earthquake. At the time of the earthquake, due to the basic excitation, there is a possibility of cracking of the dam body, which can collapse the whole body if it spreads.

After identifying the failure factors, its process should be examined. For the emergency system, it should be noted that the failure process can take from a few minutes to several hours. For example, the Glashütte Dam in Germany in 2002 failed in few minutes, but the South Fork Dam in the United States in 1889 broke in several hours. The dam failure process should be evaluated by two important methods of experimental and mathematical modeling. Mathematical models are the main methods for modeling flood propagation; For example, Aureli et al. (2006) introduced the two-dimensional MUSCL-Hancock model, which is a finite element model to simulate the velocity of flood currents that propagate horizontally despite obstacles. Cao et al. (2006) also presented one-dimensional and two-dimensional hydrodynamic models of shallow considered to study flood propagation due to dam failure on a sedimentary bed with erodible properties. There are three important things in dam safety management including 1. Dam failure factors 2. Dam breaking process 3. Flood release. Dam failure factors are directly related to the type of dam and its structural features. The process of dam failure is also very important from a time perspective. After the failure of the dam, the most important disaster is the flood. Studies on flood propagation and mathematical modeling are of great help in combating and controlling flood risks.

The main goal of the research is to provide a realistic insight into the hypothetical flood caused by dam break. As mentioned in summary simulating free-surface flow is one of the most challenging parts of computational and numerical analysis of hydraulic structures, therefore it attracts lots of attention among researchers. Admittedly, by effectively tracking free surfaces, gaining the value of time

dependent dischrage would be possible, which will lead the study to have a realistic prediction about the hypothetical flood and its adverse consequences.

Given the above, it is important to be aware of the dam failure process and the risks of flooding after its failure. In other words, preparedness for dam failure can minimize the risks of flooding, while in some cases it is not possible to predict dam failure, which can be catastrophic. The most important type of dam failure that is not predictable, is failure due to an earthquake. In general, this type of dam failure has a very complex failure mechanism due to the simultaneous effect of seismic, hydrodynamic, and hydrostatic forces on the dam body.

In general, research objectives can be summarized in two main categories, which include:

First and foremost, the main objective of the research is a detailed simulating of the water surface profile from the first crack to the whole break of the body. Admittedly, by gaining an accurate fluid flow profile, time-dependent discharge (Q_t) would be predicted precisely, therefore the governments and authorities will be able to control the flood (caused by dam break) in an efficient way and with fewer costs.

Last but not least, formulating a dam break mechanism, to assist construction engineers in decreasing their constructing errors would be the other objective of the study. In other words, if designers and construction engineers are aware of the vulnerable areas of the dam body under the combination of hydraulic and seismic forces, they can design and build dams with confidence.

CHAPTER 2

LITERATURE REVIEW

2.1 Free Surface Flow

Amid the most recent decades expanding consideration is focused on the figuring strategies in the case of flow with free-surface, which exist in many hydraulic engineering issues like the Dam-Break case. Free surface flow can be defined as two immiscible fluids separated by sharp interfaces, mostly water, and air in hydraulic engineering problems, which continuously alter with time. Numerous strategies for surface tracking are introduced in the literature. Admittedly free-surface flow hydrodynamic is not fully known yet because of the flow discontinuities, air entrapments, turbulence effects, etc., that cause a greater degree of nonlinearity to this kind of problem besides the free-surface geometry complexities. Generally, there are three defined theories for the numerical solution of free-surface: 1. Lagrangian 2. Eulerian 3. Arbitrary Lagrangian-Eulerian description.

2.1.1 Shallow Water Equations

In a brief review of the past works in the case of hydraulic engineering problems that are open to the atmosphere, Barré de Saint-Venant (1871) presented the first known classical model for open channel flow problems. It was the wave formations in one dimension that the equations are still valid in many cases of fluid mechanics. (see Fig. 2.1)

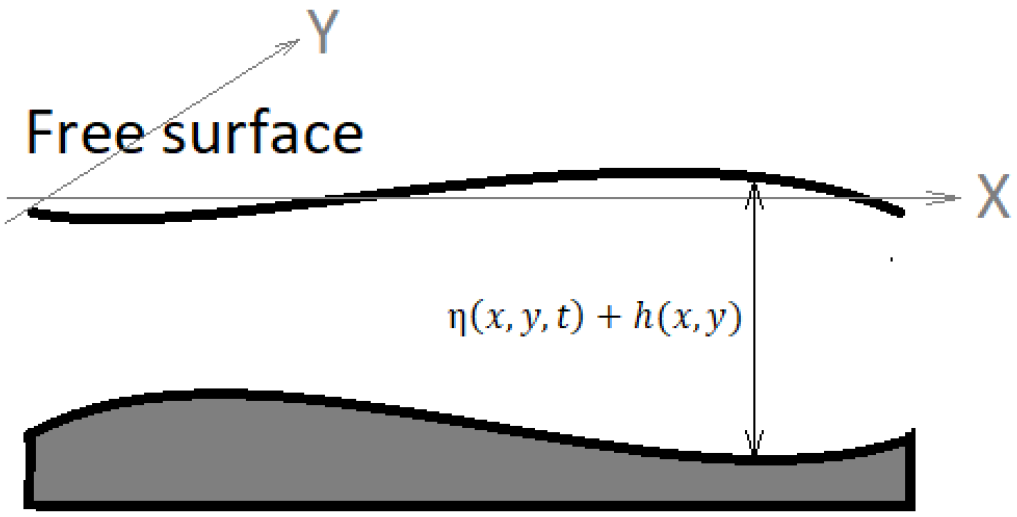

Figure 2.1. Shallow water equations

$$\partial u / \partial t + u\, \partial u / \partial x + v\, \partial u / \partial y + g\, \partial \eta / \partial x = 0 \quad (2.1)$$

$$\partial v / \partial t + u\, \partial v / \partial x + v\, \partial v / \partial y + g\, \partial \eta / \partial y = 0 \quad (2.2)$$

$$\partial \eta / \partial t + \partial / \partial x\, [(\eta + h)u] + \partial / \partial y\, [(\eta + h)v] = 0 \quad (2.3)$$

Here, p, η, u = (u,v,w), ρ, g, and h(x,y) are respectively representative of pressure, vertical displacement of the free surface, velocity, density, gravity acceleration, and the bottom topography. By evaluating existing methods to forecast the dam failure impacts, acquired outcomes demonstrated that the shallow water scheme is sensibly reasonable in solving the dam breach case and it has acceptable concurrence with experimental results according to Wang et al. (2000). Solving the SWEs concludes the method of characteristics, limited content, and finite-difference modeling techniques from past and most recently the finite volume technique. The drawback to this model is that SWEs neglect the surge acceleration, therefore it can't precisely represent profiles of the water exactly. As a matter of fact, in the brief time step soon after the dam crumple, the stream is mostly affected by pelt in vertical direction because of its weight, which is disregarded in shallow water scheme. The mentioned phenomenon is known as the wrong assumption of SWEs, which brings some doubt about the exactness of results. In the same field of study, Biscarini et al. (2010)

compared open-surface flow simulations persuaded from a dam failure by the three-dimensional simulations to SWEs. To present a conclusion experimental data are used together with numerical results. Outcomes demonstrated regardless of the possibility of shallow water to acceptably present principle measurements of the fluid streams, disregard several 3D features, because of inaccurate shallow water idealization. Generally, the doubt about the reliability of SW equations in the dam failure case existed from the past, and in this research similar to some other studies, it has proved.

2.1.2 VOF Technique

Numerical methods for solving free and moving boundary problems may be classified into three categories: Lagrangian, Eulerian and Arbitrary Lagrangian-Eulerian methods. In the first group of methods, any point on the free or moving boundary moves with the fluid. The so-called Line Segments method and the Marker Particles method lie in this category. These methods are very accurate but frequent remeshings are required. In the Eulerian description based methods, actual positions of the points of the free boundary are localized in a fixed mesh. The equations of the fluid are solved in a large domain than that really occupied by the fluid, the interface between the dry and wet regions has to be distinguished by using the notion of characteristic function (e.g. Volume of Fluid Method). In principle, these methods can be employed for general free and moving boundary problems, however, the identification of the interface needs a refined mesh in order to obtain a sufficient accuracy. Arbitrary Lagrangian-Eulerian Methods (ALE) are intended to combine the respective advantages of the previous methods. Predetermined numerical modeling of dam-breach has included the N-S equations resolving alongside surface tracking calculations, such as level set. Volume of Fluid (VOF) strategy was presented during the past decades to find the most robust method (Yue & Wang, 2006). These days VOF method is the most prevalent approach in the simulation of water flow around structures, nevertheless, some gaps need to be filled. Going into

the depth of the issue, VOF uses averaging process to get the values of fluid in each cell, however, in reality, the fluid properties can change inside of the grid. Therefore, to capture reliable results from VOF methods, grid generation quality is very important and must be done with strong insight into fluid characteristics. (Fig. 2.2)

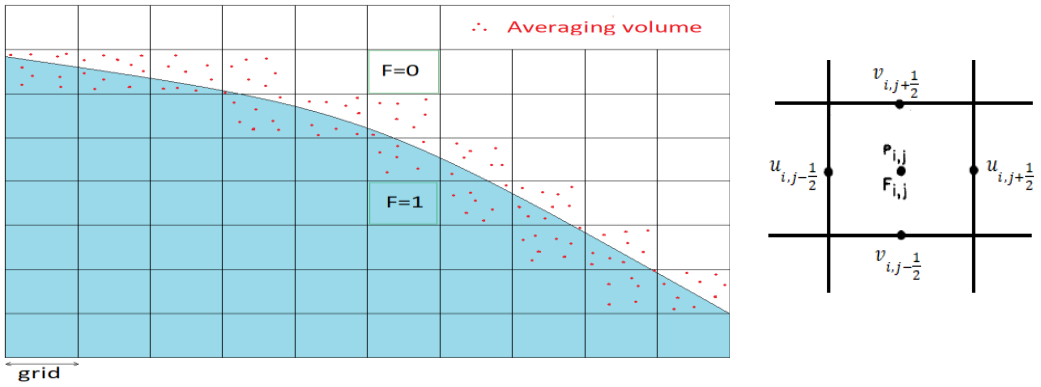

a) Free surface tracking b) A VOF grid

Figure 2.2. VOF technique

The VOF method is computationally friendly, as it introduces only one additional equation and thus requires minimal storage. The method is also characterized by its capability of dealing with highly non-linear problems in which the free-surface experiences sharp topological changes. By using the VOF method, one also evades the use of complicated mesh deformation algorithms used by surface-tracking methods. The major difficulty associated with the method is the smearing of the free-surface. This problem originates from excessive diffusion of the transport equation. The volume of fluid (VOF) technique is on of the most prevalent free surface modeling strategy. However, the first VOF method, which depends on the finite difference method, is constrained to issues with complicated calculation areas. Therefore, there is an expanding enthusiasm among analysts toward compensating for this confinement. Jeong and Yang (1998) developed the method for solving the VOF function and introduced a numerical model that combined the VOF method with finite element analysis, which can be applied to adaptive meshes. This study was the starting of decades' affords in the development of VOF. As one of the main

researches in the scope of the study, Löhner et al. (2006) offer another VOF model, which can be utilized on adaptive grids to present actions and reactions between structures and surges. In other words, a volume of fluid (VOF) technique has been developed and coupled with an incompressible Euler/Navier– Stokes solver operating on adaptive, unstructured grids to simulate the interactions of extreme waves and three-dimensional structures. As mentioned, the accuracy of VOF results is highly dependent on the mesh exactness, therefore using adaptive mesh was a huge step in the scope of the study. This study was improved by Kocaman et al. (2015), who presented a simulation of a dam-breach stream in an initially arid chute. In this study, the triangular-shaped water break was situated in the down part of the dam to give the impacts of unexpected change in topography on engendering of dam-break surge waves. Examination among the figured outcomes and the empirical information demonstrated N-S equations (RANS) and the SWEs give the stream behavior with worthy exactness.

2.1.3 SPH Method

Another common method that has shown acceptable answers in the field of dam failure study is the Smoothed Particle Hydrodynamics (SPH) method. SPH was invented to simulate nonaxisymmetric phenomena in astrophysics (Lucy 1 977, Gingold & Monaghan 1977). The SPH method is a particle method. Unlike the particle in cell method (PIC) (Harlow 1 957, 1 974, 1 988), SPH does not need a grid to calculate spatial derivatives. Instead, they are found by analytical differentiation of interpolation formulae. The equations of momentum and energy become sets of ordinary differential equations which are easy to understand in mechanical and thermodynamical terms.

Chang et al. (2011) expanded a numerical mesh-less method to deal with the shallow water wave equation based on Smoothed-particle hydrodynamics (SPH) in dam breach cases. As said over, the most critical goal in the reproduction of multiphase stream models is locating the moving fluid free-surface (Fig. 2.3). In the numerical

calculations of an Eulerian grid, points must be dynamically included or disposed of from the computational space. In this method, each particle has its own physical properties, therefore, there is no need for any special free-surface treatment. SPH can be considered as a completely Lagrangian approach for CFD simulations, firstly was presented by Gingold and Monaghan (1977). Afterward, lots of works have been done to develop the main SPH, for instance, Hui Pu et al. (2013) compared SWEs and SPH methods in the dam-breach stream. By reproducing a recorded exploratory dam-break stream, they showed that both model reproduction comes about gave great concurrence with the test information at various estimation areas. Besides, Chen et al. (2016) remedied SPH techniques for solving SWEs. Six SPH techniques with various types of numerical viscosity are tried against analytical solutions for dam breach stream. Correlation demonstrates that the revised SPH reproduction can catch shock waves more precisely. This revised SPH method can be utilized to tackle shallow-water equations well. Admittedly, the mentioned study was a huge step in the development of the existing SPH method.

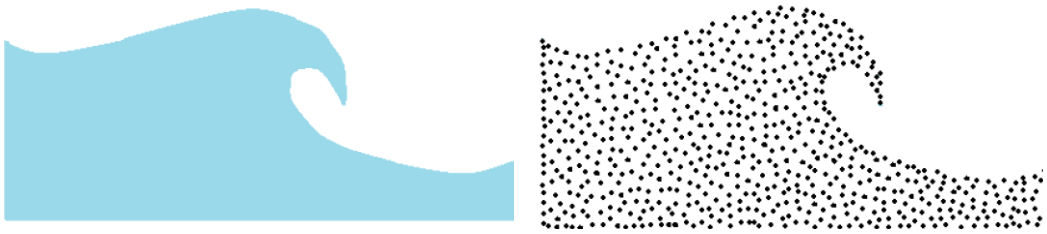

a) Continuum b) SPH

Figure 2.3. Comparison of SPH with reality

The grid-based classical Euler methods are now widely applied to solve the SWEs, such as the finite difference method and the finite volume method. However, due to restrictions of grid, grid-based methods suffer many limitations in simulating multi-phase effects, most importantly, the debris flows in flood modeling. On the other hand, the particle method requires no grid, therefore, the grid distortion and reconstruction problems can be avoided, with a natural advantage in dealing with

large deformation for free interface. This feature makes particle methods promising in solving the SWEs. (Chen, Liao, & Huang, 2016)

2.1.4 Comparison of Common Methods for Dam Breach Capturing

In summary, the best answers in free surface flow simulation in the field of dam failure analysis are obtained from two methods comprising VOF and SPH. Songdong Shao et al. (2003) Conducted a general study of three conventional free surface simulation methods, including VOF, MAC, and SPH, which included both Newtonian and non-Newtonian fluids. (see Fig. 2.4)

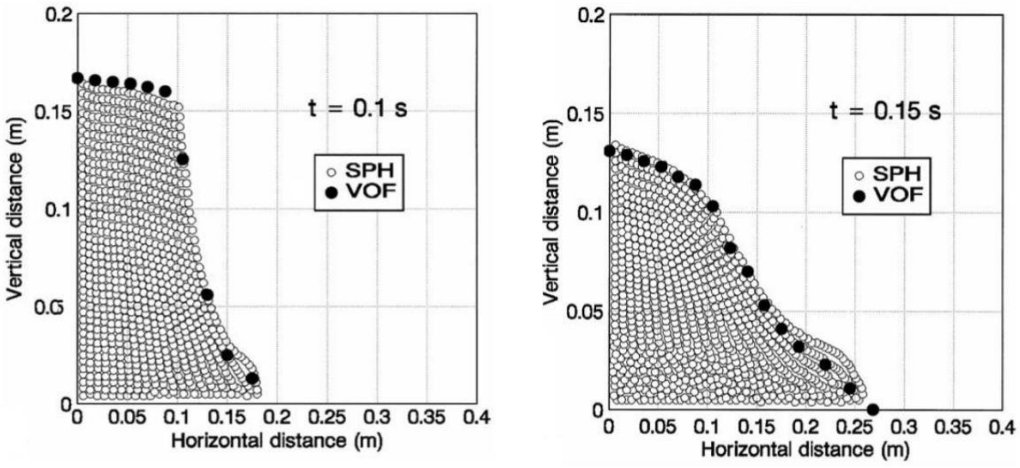

a) 0.1 second after failure b) 0.15 second after failure

Figure 2.4. Comparison of SPH and VOF results in sudden dam break case reprinted from Shao & Lo, (2003). P. 794

In this study, the immediate failure of the dam was investigated and the results obtained from both methods showed good agreement with the experimental results. More precisely, the results obtained from the VOF method by selecting the appropriate size cells showed better agreement with the experimental results. Non-Newtonian and unsteady mudflow (two-dimensional) from a reservoir of limited size on a sloping canal was also investigated in this study and the results showed that water flow after breaking the dam is faster than mudflow. Figure 2.5 compares the

results obtained by SPH, VOF, and MAC methods with laboratory experimental results.

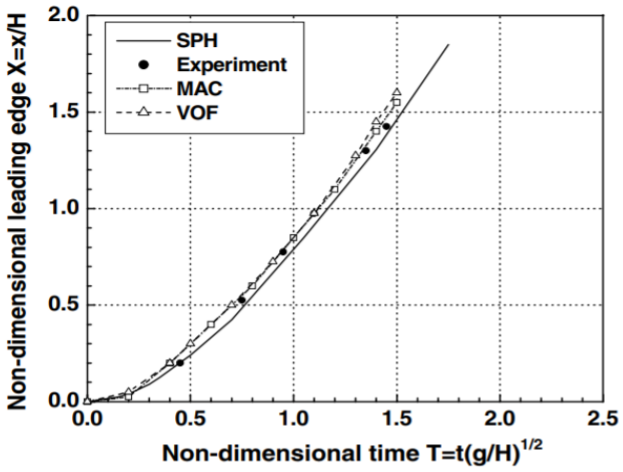

Figure 2.5. Verification of VOF, MAC, and SPH results with reprinted from Shao & Lo, (2003). P. 794

Wave propagation due to dam break using SPH and VOF methods in open-source software of Open-FOAM (two-phases, unsteady flow) was compared by Farzin et al. (2014). The obtained results are compared with reliable empirical and numerical solutions in the literature. It was shown again that the two presented approaches can handle the violating free surface flow in dam-break problems with high accuracy.

Another important issue to be considered is that the capability of two conventional free surface simulation models when fluids collide with fixed or moving solid bodies. A study was performed by Sasson et al. (2015) to investigate the effect of water waves on collisions with solid surfaces using VOF and SPH methods. Which was later expanded to compare SPH and RANS methods in the simulation of free surface flow in a slamming model. By comparing numerical results with experimental data, It was found that both methods are capable of slamming modeling, however, the RANS method predicts slightly better acceleration values before the acceleration peak. Containing some disadvantages, the main advantage of SPH in comparison with VOF is that fractions of SPH transport theirs own physical

properties, therefore it simulates free surface flow complicities effectively. The best numerical answer in the study was obtained from the RANS method by selecting a small CFL number, which indicates the fact that the results of the VOF method are strongly dependent on the size of the generated cells and time step value. The results of the study can be seen in Figure 2.6.

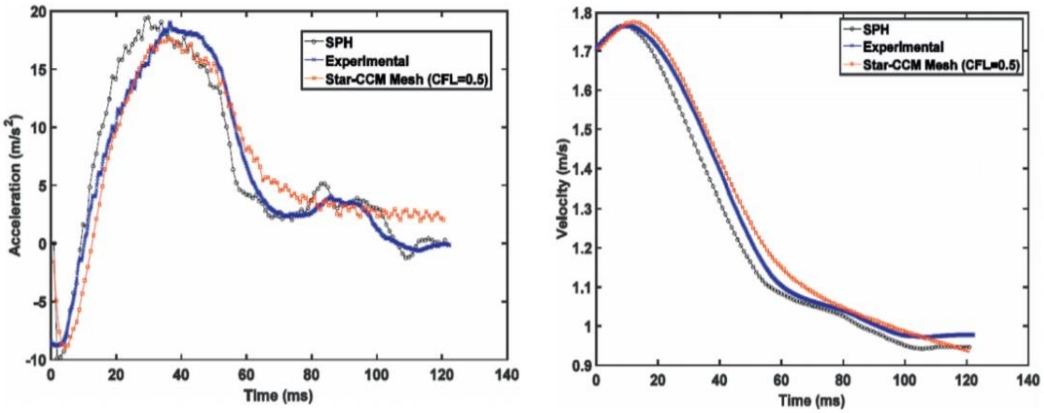

a) Acceleration time history b) Velocity time history

Figure 2.6. Comparison of RANS and SPH methods with the experimental study reprinted from Sasson et al., (2016). P. 127

With all that said, both VOF and SPH methods can accurately simulate free surface flow, under certain conditions. However, according to the second purpose of this research, which is to simulate the failure mechanism of a concrete dam, finite element method must be used to obtain the stresses applied to the dam body during earthquake. Therefore, grid generation of the models is mandatory, which is why the VOF method is chosen. According to the mechanism behind the VOF method, if advanced meshing methods are used and appropriate time steps are selected, the VOF method can submit the acceptable numerical results. Many efforts have been made by researchers in this field, some of which are mentioned. VOF/FVM forecast and trial approval for fluid-column fall was finished by Moraga et al. (2015). Numerical outcomes gotten from open face quick location were approved with 7% precision in examination to empirical estimations. Since the results of the analyzes with the VOF method are highly dependent on the appropriate mesh, many efforts

have been made to improve grid generation. A mesh refinement method for tracking free-surface was utilized by Tate et al. (2006) and developed to dynamic mesh adaptation in 3-D SWE by Savant et al. (2018). Modifying the meshes till the solution for the measure of interest does not alter within some defined tolerance is the most critical part of making spatially-converged grids process. Additionally, a 2D Finite-Volume Eulerian-Lagrangian method on an unstructured grid for free-surface flows was developed by Hu et al. (2017) and was expanded to three-dimensional unstructured mesh in the case of flood propagation by Zhang and Feng (2017). This study presented a 3D model for flooding has been presented, which can be applied to various kinds of flooding.

2.2 Methodology in Numerical Investigation

From the literature review, the gap of lacking a powerful method in efficiently treating with free surface complicities was detected, which is essential to gain the exact quantity of time-dependent discharge due to dam breach. During the most recent decades expanding consideration is focused on the figuring strategies in the case of flow with free-surface, that exist in many of hydraulic engineering issues like Dam-Break. Free surface flow can be defined as two immiscible fluids separated by sharp interfaces, mostly water, and air in hydraulic engineering problems, which continuously alter with time. Admittedly free-surface flow hydrodynamic is not fully known yet because of the flow discontinuities, air entrapments, turbulence effects, etc. Numerous strategies for surface tracking are introduced in the literature. Generally, there are three known numerical approaches for tracking free surfaces containing: 1. Lagrangian, 2. Eulerian and 3. Arbitrary Lagrangian-Eulerian description. To properly model free surface, three vital features are needed for the chosen method involving: 1. a scheme for presenting form and situation of face, 2. an algorithm to develop the time-dependent form and situation of face 3.a proper boundary condition for the face.

Various numerical simulation programs are under scrutiny to locate the best procedure to numerically recreate complex free-surface and effects issues. Because of the above-mentioned complexities of free surface flow, all the numerical approaches need kinds of simplification of equations to get converged results. A prevalent way of simplification of existing equations is using of VOF method. This method divides the domain into smaller cells, which are known as grids. Then the properties of the fluid for each cell are gained by the averaging process. One of the important properties of the fluid is the value of F, which presents the location of the free surface. The value of F is a number between one and zero that one is the cell full of water and zero is the air cell, therefore the grids on the free surface must contain a fraction less than one and more than zero quantity for the F value (see Fig. 2.2). As mentioned in this method the properties of fluid flow are gained by averaging process and this averaging can be time, ensemble, spatial, etc., depending on the governing equations and physics of the problem. Based on all that has been said, a framework that uses the VOF method is selected to simulate the failure of the dam.

2.2.1 Introduction to GMO model

After selecting the appropriate method for simulating the free surface flow, it is time to select a suitable method for simulating water and solids interaction. Because the case of dam failure is a two-phase issue including solids separated from the dam body and the outlet water from the reservoir. FLOW-3D software uses the General Moving Object (GMO) model to simulate a fluid interaction with a moving solid body by defining two coefficients including friction and restitution. A GMO is a rigid body with any kind of motion that is either user-prescribed or dynamically coupled with fluid flow. It can have six degrees of freedom or motion constraints such as a fixed axis/point. Prescribed forces and torques can be applied on a GMO under coupled motion. This model allows multiple rigid bodies under independent motion types as well as rigid body interactions including collisions

and continuous contact. The model is robust, efficient, and powerful and is the only one of its kind in commercial computational fluid dynamics software. One of the strengths of the GMO model is the simultaneous simulation of 500 solids immersed in water, each of which can have different shapes and physical properties. Therefore, FLOW 3D can be a good choice as a CFD to simulate the failure of the dam, because the dam's body can be divided into a large number of GMO parts at the time of failure.

2.2.2 Introduction to FLOW-3D

The numerical model will be based on general Reynolds-Averaged Navier–Stokes (RANS) equations with Renormalization Group (RNG) turbulent closure model by using the volume of fluid technique. The GMO model developed in fluid dynamics (CFD) code FLOW-3D will be applied to simulate the motion of solid blocks coupled with the surrounding water. In this study, the sharp interface method will be used to simulate viscously incompressible interacting with moving solid boundaries. The sharp interface method tracks the boundary by identifying the control volumes in a cartesian grid that are cut by the immersed boundary. Consequently, when a simulation of flow with moving boundaries is attempted the irregular shape of cut cells results in a need for complicated interpolation to approximate fluxes.

FLOW-3D has been using its unique FAVOR technique to describe geometric objects in a computational domain with concepts of area fraction (AF) and volume fraction (VF) in rectangular meshes. The VF is defined as the ratio of the open volume to the total volume in a mesh cell, and three AFs (AFR, AFB, AFT) are defined respectively at the three cell faces in the increasing cell-index direction as the ratio of the open area to the total area. The FAVOR technique deals with complex geometries by introducing the effects of AF and VF into the conservation equations.

Equations of motion for the rigid body will be solved for coupled motion. Area and volume fractions will be used to represent the objects in the fixed-grid at every time

step to describe the time-variation of object locations and orientations. Continuity and momentum equations for fluid and scalar transport equations are modified to account for the effects of object motion. The continuity equation is modified with the addition of a source term to account for the effect of moving objects on fluid. The wall shear terms in the momentum equations are also modified accordingly. Hydraulic, gravitational, environmental, and control forces and torques are calculated, and equations of motion for the rigid body are solved explicitly for translational and rotational velocities for each moving object under a coupled motion. Two categories of moving objects are allowed in multiple GMO systems comprising prescribed motion and fully coupled motion, which under each of them, an object can move with six DOF or rotate about a fixed axis or a fixed point. For a GMO with coupled motion, inertia parameters must be given fully in the input file since no physically meaningful default values are available. There are two options for entering inertial data. The first option is to give the total mass, the coordinates of the mass center in the space, and the moment of inertia tensor about the center of mass. The second option is to provide only the mass density of the moving object. In the second case, the object must first be within the computational range so that the total mass, the location of the initial mass center, and the moment of inertia tensor in the preprocessor can be calculated based on the assumption of uniform density. If there are multiple GMOs, each GMO can have its own specific inertia data. For GMOs with prescribed motion, the input of inertial data is not required but if provided, the residual control force and torque are calculated by the program.

2.2.3 Road Map in Numerical Analysis

Up to this point in the study, according to the researches cited in the literature and the requirements for simulating the model of dam failure, FLOW-3D software is selected due to its two advantages including using: 1.VOF methods to simulate free surface flow 2. GMO for simulation of fluid interaction with moving objects and collision of moving solid bodies.

In general, the purpose of this study is to obtain the flow rate due to dam failure. For this purpose, the failure mechanism of the dam should be simulated in full detail. Due to the complexity of the issue, it is necessary to first ensure the capability of the selected software in the field of dam failure simulation. For this purpose, in the first part of the analysis, which is presented in the third chapter of the thesis, the ability of FLOW-3D to calculate water pressure near moving solids will be examined. Generally, in order to properly simulate the failure mechanism of the dam, the pressure inside the cracks created by the earthquake in the body of the dam should be obtained correctly and with high accuracy. Additionally, the movement of solid pieces separated from the main body during the failure process is directly related to the water pressure near them. The obtained results from the numerical analysis will be verified with experimental data to ensure the accuracy of the captured pressure values inside cracks. After learning about the pressure distribution within the cracks created in the dam body and getting insight about the important parameters needed to accurately capture it, such as time step value and VOF cells size, in the second part of the study, which will be presented in the fourth chapter of the thesis, the motion of separated solid body from the dam body due to the earthquake will be examined. In other words, first, the motion of a single solid body due to seismic, hydrostatic, and hydrodynamic forces is investigated, and after validation of different motion histories using various experimental and numerical methods, the model will be extended to include more fragments resulting from the failure of the dam. In summary, the third part of the thesis, which includes simulation of pressure inside cracks during an earthquake, is used to verify the VOF method, and the fourth chapter of the thesis, which includes the study of different motion types of solid objects due to the earthquake, is used to verify the GMO method in the scope of dam failure study. Finally, in the fifth chapter of the thesis, using the results and information obtained from the third and fourth chapters, models for the dam failure mechanism will be presented in sudden and gradual forms. Lastly, the summary of the results will be presented in the sixth chapter of the thesis.

Admittedly, the availability of a computer with a minimum of 16 GB RAM and Intel Core i7 CPU is compulsory for implementing this research. As mentioned, the result's accuracy of VOF techniques is highly influenced by effective grid generation. This detailed meshing would increase the simulation time extremely, Therefore, a computer with high processing power is required to perform this study.

CHAPTER 3

PRESSURE DEVELOPMENT INSPECTION INSIDE THE CRACKS CREATED BY EARTHQUAKE

3.1 Inspection of Pressure Distribution Inside the Crack Using Finite Volume Technique

3.1.1 Introduction

Due to the issues mentioned in the previous chapters and due to the complexity of the dam failure problem before entering the main topic, VOF and GMO methods should be verified in the subject under study. Given that it is not possible to simulate the failure of a concrete dam experimentally, which will be explained in detail in the following sections, the main issue should be divided into smaller sections or sub-sections to verify the results in these sub-sections and thus the general answer of the model for breaking the concrete dam can be ensured. Therefore, the current chapter is done to verify the VOF method. The most important factor involved in dam failure is the ability of the VOF method to simulate the pressure inside the cracks created in the body due to the earthquake because the mechanism of the dam failure due to the earthquake starts from cracking of the body and the expansion of these cracks is directly related to pressure distribution inside them, besides, the movement of solid blocks separated from the main body is affected by water pressure near them.

To inspect pressure development inside of the crack a CFD model is built using a slice of the crack zone in a dam's body. The pressure value in the crack mouth is kept in constant value and the walls in two sides of the crack are oscillated with defined crack mouth displacement and different frequency to inspect the pressure variation with time inside of it. The study indicates that by increasing the distance from the crack mouth, the pressure values in the crack area are increased and the

maximum pressure value is captured in fluid stagnation point or end of the crack. From frequency analysis, by reduction of frequency in the constant amplitude of oscillations the overall pressure value is decreased. Additionally, sudden jumps and falls in pressure value especially in simulations with high frequencies reveals the occurrence of cavitation. In fact, in the opening cycles of the crack, the pressure is reduced and by reaching the vapor pressure the water begins to chang phase to vapor. The validity of the utilized method was verified by the experimental test results of Javanmardi et al. (2005) journal article.

3.1.2 Test Case Definition

Crack propagation in the upstream face of the concrete gravity dams is a complex problem affected on the global scale by reservoir-structure interaction and on the local scale with crack mouth effects and in-crack fluid pressures. Estimation of dynamic crack pressures within a crack is a very challenging problem, requiring the simulation of movement of fluid within the crack due to crack opening/closing, cavitation-reversion to air bubbles, and the consequences of pressure increase due to increasing pressures. During an earthquake, reservoir water enters an open crack with moving walls and propagating crack tips forming complex boundary conditions. The closing of the crack leads to water pushing out, while the opening of the crack may lead to water rushing in at the mouth of the crack and loss of pressure and cavitation within the crack. This process is also cyclic as a consequence of the earthquake load on the mass concrete with complexity further increased by initial conditions dependent on initial cracking or pre-existing cracking on gravity dams and load conditions.

Reservoir-dam interaction and crack propagation within a concrete dam are already complex research topics without considering fluid-crack interaction on a cracked concrete mass. Detailed coverage of the developments on these issues can be found in Løkke & Chopra, (2019), and Shi, (2003), respectively, and fall out of the scope of this work. The interest in fluid flow within a propagating crack has been initiated

by concerns over dam safety by structural engineers. As a consequence of the complexity of the problem as well as the experimental challenges, it poses, only a handful of studies have been conducted for investigation of this phenomenon. On the existing system, monitoring of pore water pressures are conducted with the static pressures in mind mostly for the purpose of detecting unwanted infiltrations to the system. Given the difficulties in experiments and the real-life monitoring, realistic computational simulations verified by the few experiments are the only way in which to assess the importance of crack fluid pressure on gravity dam monoliths' behavior. The primary goal of this study is to demonstrate the capability of the finite volume technique in simulating and predicting this complex behavior using the results of a benchmark test (Javanmardi, Léger, & Tinawi, 2005) as a case study. The pressure variation vs. time in a given crack as measured in Javanmardi et al. (2005) is simulated by modeling the experiment setup and conditions. The effect of boundary conditions and cell sizes on the analysis results are investigated considering the computational time/processing capabilities.

3.1.3 High-Frequency Testing and CFD Modeling

3.1.3.1 Test Information

A range of experiments were conducted by Javanmardi et. al. (2005) in order to investigate the crack fluid pressure in cracks with dynamic moving boundaries similar to the conditions for earthquake loading of gravity dams with reservoir. The complex experimental setup for these tests is given in Figure 3.1. A plain concrete block (0.15m × 0.55m × 1.5m) with a pre-formed crack was tested on a shaking table for a range of sinusoidal motions with different frequencies and amplitudes. To simulate the reservoir conditions, a water tank (0.15m × 0.2m × 0.3m), placed at the opening of the pre-formed 0.55m long-crack, was pressurized by the air compressor to keep the pressure level constant in the crack mouth. Piezometers were installed along the crack at 0.00, 0.09, 0.18, 0.27, and 0.36 meters from the crack mouth to

record the fluid pressure within the crack during the opening-closing cycles imposed on the block. The relative displacements on the crack were monitored using LVDTs installed on the cracks. The testing on pre-existing crack was conducted for a 10 seconds duration in two phases: first, the initial crack mouth opening was increased to a maximum value, followed by a reduction to a non-zero quantity representing residual opening. The tests were repeated on the same specimen with a maximum crack opening of 0.2-2 mm and at different shaking frequencies (2, 5, and 10Hz) representing seismic loading conditions.

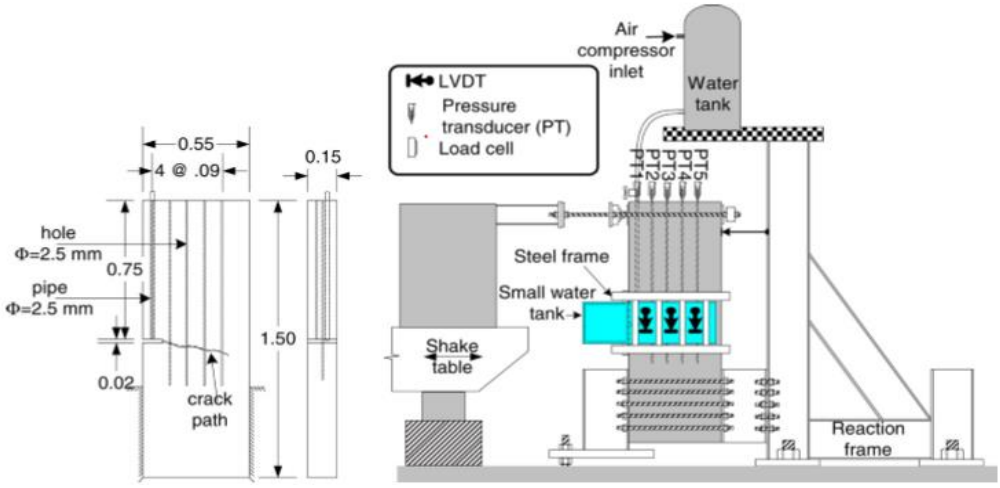

Figure 3.1. Experimental test case setup reprinted from Javanmardi et al. (2005). p. 4.

3.1.3.2 CFD Model Generation

The CFD model of the test setup can be seen in Figure 3.2. The crack zone of the dam prototype was modeled in SOLIDWORKS and imported to Flow-3D as an STL file. The solid block is free to rotate around the fixed point D. The flow domain within the crack boundaries was divided into rectangular cells under the finite volume approach in Flow3D. Different cell sizes were utilized in the study, starting from 8mm and reducing its size until 0.5mm to achieve convergence of pressure

values for all the desired locations. The boundary condition at the top of the model was defined as a zero-gradient condition corresponding to zero velocity constraint normal to the boundary. The right and bottom boundaries were set as stationary walls with no slip/no penetration conditions. A wave absorbing layer was placed at the left boundary to prevent wave reflection from the wall. The reservoir side of the crack was pressurized at a constant level at the crack mouth in accordance with the test setup.

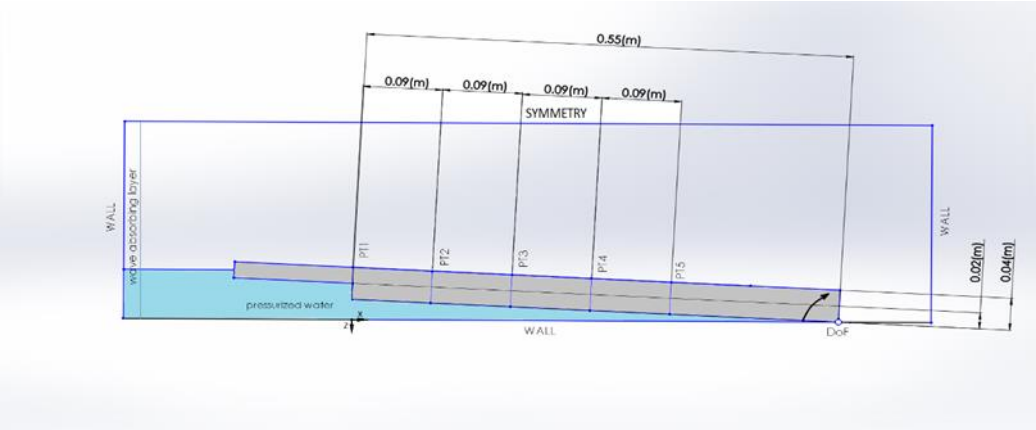

Figure 3.2. One degree of freedom CFD model

3.1.3.3 CFD Using FLOW 3D

Finite volume solutions of flow problems involve the division of the flow domain into rectangular cells and then numerically approximating the equation terms by using pressure and velocity averaging in each cell block. A summary of the basic theory underlying the software FLOW-3D is given below.

3.1.3.3.1 Basic Theory

Fluid motion equations consisting of continuity and momentum equation in three dimensions, i.e. the Navier-Stokes equations, are solved to determine the fluid

behavior in FLOW-3D. The continuity equation and the momentum equation in terms of $\vec{V}$, the velocity components in three directions, are given in (Eq.3.1) and (Eq.3.2). The total derivative is then written as (Eq.3.3),

$$\nabla\vec{V} = 0 \tag{3.1}$$

$$\rho\frac{D\vec{V}}{Dt} = \nabla p + \rho\vec{g} + \mu\nabla^2\vec{V} \tag{3.2}$$

$$\rho\frac{D\vec{V}}{Dt} = \left[\frac{DV}{Dt} + (V.\nabla)V\right] \tag{3.3}$$

where ρ, μ, and p represent the density, viscosity, and pressure of the fluid, respectively.

3.1.3.3.2 The Volume of Fluid Technique

The tracking of the free surface is the most challenging part of CFD simulations for hydraulic structures because of the discontinuity of the fluid properties like velocity, pressure, and density in that boundary. In FLOW-3D, the free surface is considered as the external boundary of a fluid, and it is tracked using the Volume of Fluid (VOF) technique. The VOF consists of three main components: the definition of the VOF function, the solution of the VOF transport equation, and setting the boundary conditions at the free surface. In this study, one viscous incompressible fluid with a free surface and sharp interface was defined to simulate the fluid behavior under the renormalized group (RNG) turbulent model with no-slip boundary condition.

3.1.3.3.3 Cavitation Tracking

As mentioned, in the opening cycle, cavitation can occur within the crack fluid due to the reduction of pressure in the crack. It can also happen at the start of opening or the end of the closing cycles due to the high velocity of the fluid (and the accompanying pressure reduction) with water going inside or outside of the crack. In this study, an empirical model within FLOW-3D, appropriate for use in inertial

cavitation, was used for the tracking of cavitation within the crack. Cavitation is controlled by the production rate $C_{production}$ and dissipation rate $C_{dissipation}$ as given in Eq.3.4. The cavitation and dissipation rates are calculated by Eq.3.5 and Eq.3.6,

$$\frac{D_{V_c}}{D_t} = C_{production} - C_{dissipation} \tag{3.4}$$

$$C_{production} = C_e \frac{E_{turb}}{\sigma} \rho_l \rho_v \sqrt{\frac{2(p_c - p)}{3\rho_l}} (1 - f_c) \tag{3.5}$$

$$C_{dissipation} = C_c \frac{E_{turb}}{\sigma} {\rho_l}^2 \sqrt{\frac{2(p - p_c)}{3\rho_l}} (f_c) \tag{3.6}$$

where V_c, C_e, C_c, E_{turb}, σ, ρ_l, ρ_v, p, p_c and f_c are the representative volume fraction of cavitation, coefficient of evaporation, coefficient of condensation, turbulent kinetic energy (in the laminar case is considered to be equal to 10% of total kinetic energy), coefficient of surface tension, liquid density, vapor density, fluid pressure, cavitation pressure, and cavitation mass fraction, respectively. In the scope of this study, the active void opening model with coefficients of surface tension, production, and dissipation of cavitation respectively equal to 0.073, 0.02, and 0.01 were utilized. The density of bubbles was assumed as 1.02 kg/m^3.

3.1.3.3.4 General Moving Objects Method

The rigid body motion is simulated using the general moving objects (GMO) model (Wei, 2006). In this model, the motion of the body can be coupled to the fluid flow or prescribed for each particle. Volume and area fractions in a rectangular grid are calculated to describe the object's motion at each time step, additionally, equations of motion are solved to gain rotational and translational velocities for objects under motion. In order to capture the interaction of the particle with the fluid, source terms are put on the continuity equation to represent the impact of moving rigid bodies and the tangential velocity of the moving particle boundaries is presented in shear stress terms in the momentum equation. GMO models can utilize an explicit or implicit

approach for interaction. The explicit method was used for time stepping in this study.

3.1.4 Analysis and Benchmark Test Comparisons

A range of simulations were conducted to replicate the results of the experiment. The solid object representing the upper wall of the crack was set to oscillate at 0.024 rad amplitude at 10 Hz frequency in the simulation for a duration of 10 seconds. The initial crack mouth opening was 1.0 mm for the modeled experiment while the maximum crack mouth opening was 1.43mm. The surface roughness of the moving crack wall was assumed as 0.0005 mm. The pressure was kept at 200 KPa at the crack mouth through the simulation. The pressure values are shown in accordance with the experimental results; when focusing on the pressure increase during the cyclic portion of the test was required, pressure values were reported as “dynamic” values obtained by subtracting the static crack mouth pressure from the obtained quantities in the crack.

3.1.4.1 Frequency Analysis

The fluid behavior in the crack was first investigated for different frequencies of loading using a grid size of 8mm. The results of the analyses for loading frequencies of 10,5 and 2 Hz, obtained at locations corresponding to piezometers PT1, PT2, and PT3 from the experiment, are shown below. The reduction of frequency led to a reduction in the fluid pressure in the crack. The sudden jumps and falls in the pressure graphs show the model captures the occurrence of cavitation in the crack and corresponding local explosions.

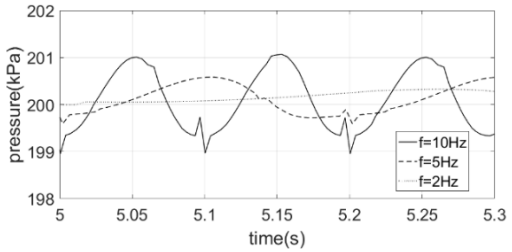

a) Pressure variation with time in PT1

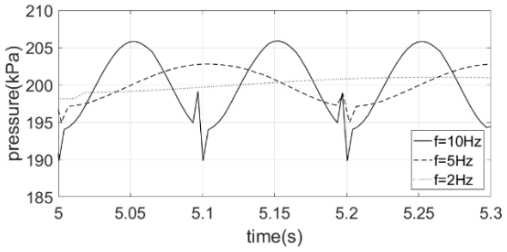

b) Pressure variation with time in PT2

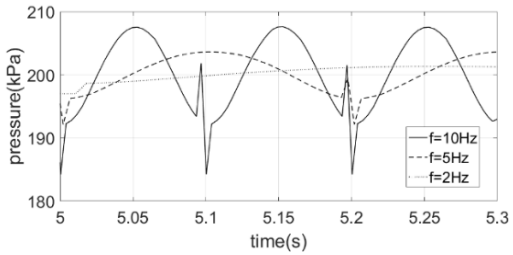

c) Pressure variation with time in PT3

Figure 3.3. Effects of frequency variation in the pressure value

The comparison of the pressure at all piezometer locations for the same loading rate is given in Figure 3.4. The pressure in the crack increased concerning the distance from the crack mouth. The change in PT1, at the crack mouth, was minimal as expected. For this mesh size, the pressure values captured were much lower than the experimental values. The crack mouth opening of 1.43mm corresponds to 1.2, 0.96, 0.73, 0.49mm movement at PT2, PT3, PT4, and PT5 piezometer locations. A grid size of 8mm led to a much smaller prediction of pressures. As the cell size was much larger than the crack opening in these locations, the averaging technique is biased towards zero (or atmospheric pressure depending on pressure reference value definition) value at nodes containing the value returning smaller pressure values for the fluid in the cell. Capturing of the pressure variation inside of the crack needs high precision in controlling the grid and time step size. Smaller cell sizes were used in the next part of the study to catch the pressure variation inside of the crack.

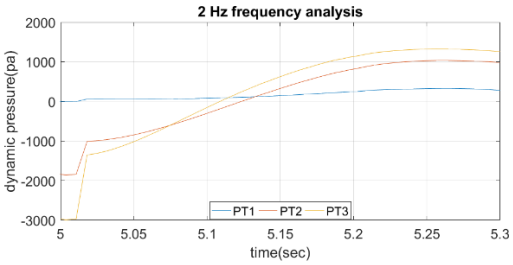

a) Dynamic pressure with 2Hz frequency

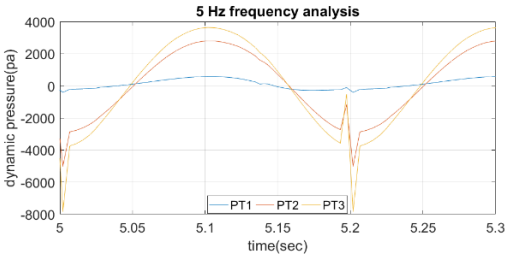

b) Dynamic pressure with 5Hz frequency

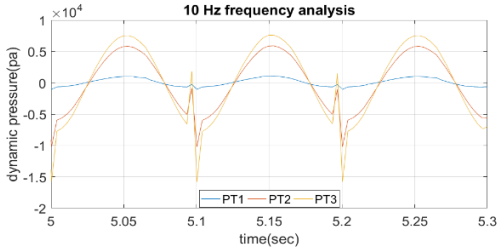

c) Dynamic pressure with 10Hz frequency

Figure 3.4. Pressure distribution inside crack with loading frequencies of 2, 5, and 10 Hz

3.1.4.2 The Effects of Grid Size and Time Step On Crack Pressure

The effect of grid size is shown in Figure 3.5 for the pressure values at PT4 and PT5 between 5 and 5.3 seconds for the loading with 10Hz frequency. The form of the response was obtained similarly for different grid sizes with the resolution of the reading increasing with the reduced grid size. The computational time increased by 8.12, 14 times for the 2,1, and 0.5mm grid sizes, respectively, compared to the time spent for the 8mm grid. The analysis with the smallest grid size took almost a month on an Intel(R) Core(TM) i7-8700CPU @ 3.2GHz computer with 16GB RAM.

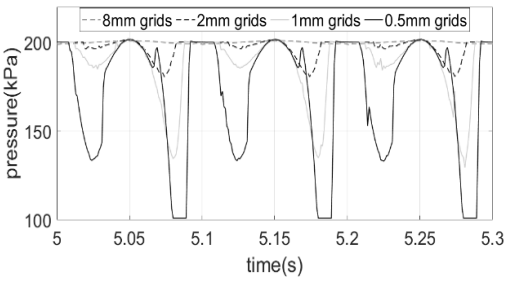

a) Grid size analysis in PT1

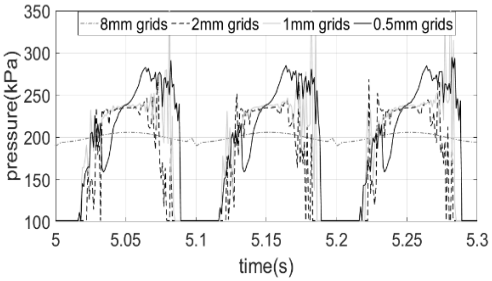

b) Grid size analysis in PT2

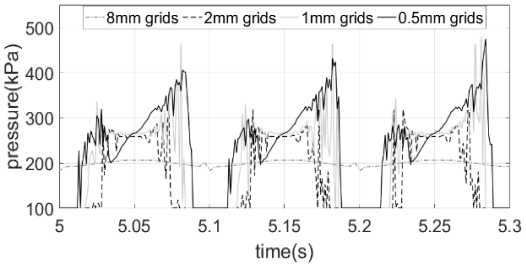

c) Grid size analysis in PT3

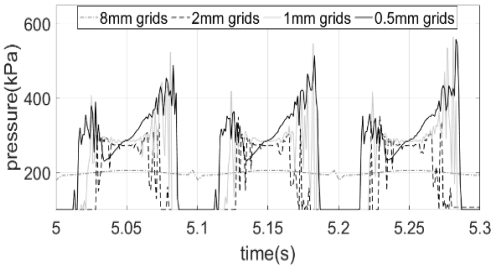

d) Grid size analysis in PT4

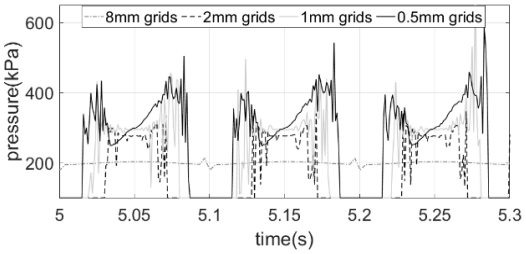

e) Grid size analysis in PT5

Figure 3.5. Grid size effects on captured pressure values

The detailed capture of the response also showed the time variation of the pressure especially near the beginning of the start and end of the pulses. The models were able to capture the very high-frequency oscillations within a very small time. A more reliable estimate of the pressure at the given location can be obtained by compressing this data in the time domain which can be conducted using re-sampling or moving average filters. The pressure values recorded at PT4 and PT5, at the original sampling period (0.00005sec), and resampled at 0.001 seconds are shown in Figure 3.6.a and b. The resulting time series using averaging on a backward window of 20

points is shown in Figure 3.6.c and d. The use of a central moving average filter with 10 data points yielded very similar results. The moving average filters reduced the high-frequency oscillations in the data showing a clear pulse-type response for the pressure values as expected.

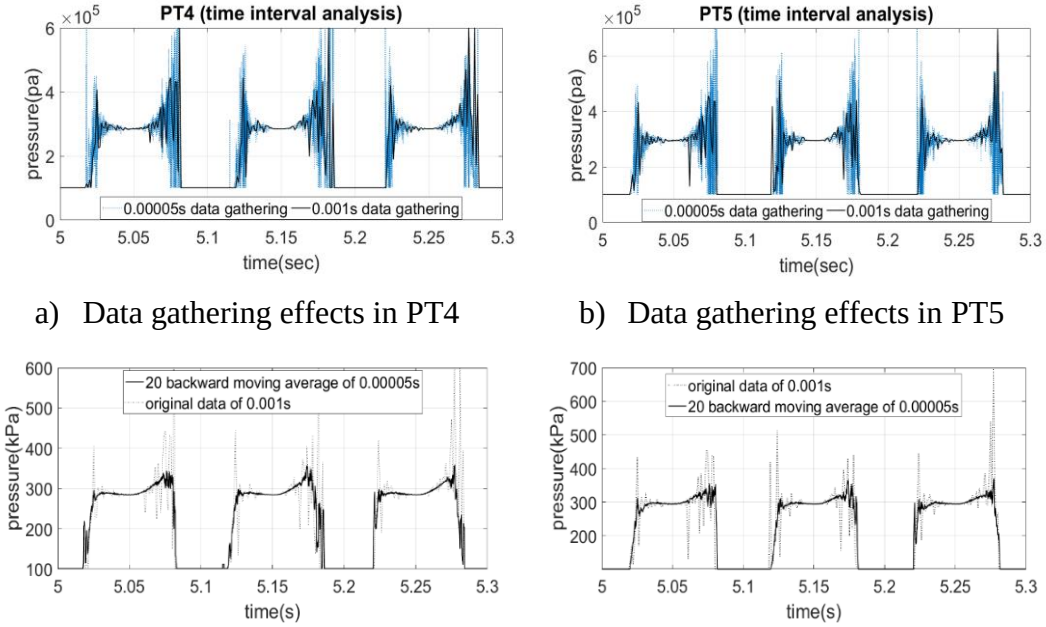

a) Data gathering effects in PT4

b) Data gathering effects in PT5

c) Time averaging effects in PT4

d) Time averaging effects in PT5

Figure 3.6. Time step and data gathering time interval size effects on captured pressure values

3.1.4.3 Detailed Inspection of Crack Pressures for 10Hz Loading Frequency

For the final set of analyses, the grid size was chosen as 0.5-1 mm with a maximum allowable time step of 0.0005 seconds. Additionally, the minimum reachable pressure value was defined as 1atm in the model in order to avoid negative pressure values due to phase change. The corresponding pressure values obtained at the piezometer locations are shown in Figure 3.7 for the first 5 seconds of the loading direction in which a steady-state of pressure variation was obtained in the crack. The

highest pressure in the fluid in the crack was obtained at PT5 in accordance with the benchmark, which can be considered as a stagnation point at the end of the crack.

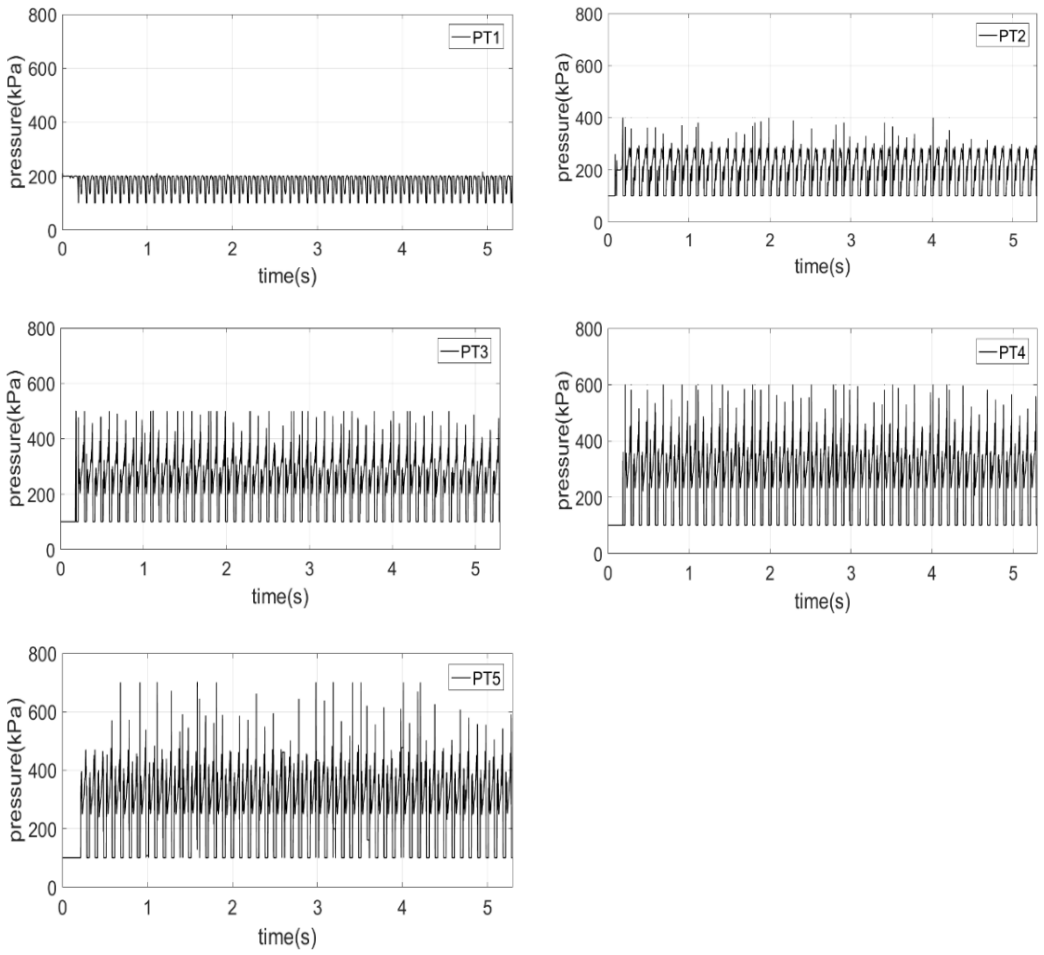

Figure 3.7. Pressure variation with time in 5.3 seconds

The pressure values within the crack are investigated in more detail for a single pulse between 5.2 and 5.3 seconds in Figure 3.8.a. By decreasing the cell size and the time step increment, small oscillations in the pressure-time graph were captured showing the response moving away from a perfect sine wave if looked in detail. By moving inside of the crack in the downstream direction both the pressure values and its oscillation due to cavitation bubbles explosion were increased and the maximum pressure value was captured at the end of the crack or PT5. PT1 is located in crack mouth outside of it, therefore due to the existence of pressurized water in that region,

at the starting of the simulation hydrostatic pressure level is observed, which is the maximum pressure level in PT1 due to stagnation of water. Over time, the water in PT1 starts to move either inside or outside of the crack, and its stagnation condition is lost, therefore the pressure value is reduced in the opening and closing cycles of the crack. Generally, PT1 pressure reduction from the constant pressure level of the reservoir is the result of fluid local motion.

Last but not least, the horizontal portions of the graphs showing atmospheric pressure in each piezometer show the emptying of the crack at that location with water moving in the up or downstream directions away from the cell. As given in Figure 3.8, the deeper into the crack, the more pronounced the movement of crack fluid becomes. From the dynamic pressure analysis of PT2 (Fig. 3.8.b), 5.157s can be considered as the starting time of the crack closing cycle in the shown pulse. During the cycle, the pressure value was increased and the maximum value was captured at 5.183s or ¼ T. The closing cycle was proceeded by a reduction of pressure until 5.21s (½ T). During the period of pressure reduction in the closing cycle, the water was pushed out of the crack, therefore the pressure value was reduced due to velocity increment. Starting from the end of the closing cycle in the pulse, during the opening cycle, a reduction in the pressure value was observed due to the penetration of water into the empty crack with high velocity. The minimum pressure value was captured at 5.235s or ¾ T, in which the crack was almost filled with water. Afterward, due to the reduction of water velocity, the pressure value was increased and the cycle was completed in 2.257s or 0.1s from the start of the pulse.

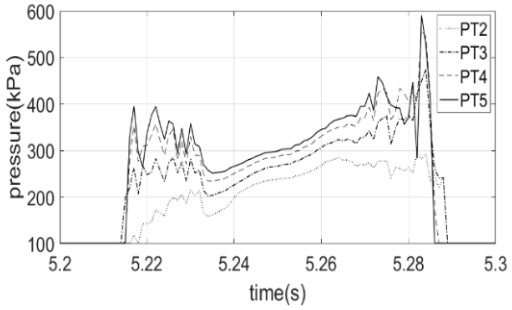

a) Pressure values in a cycle

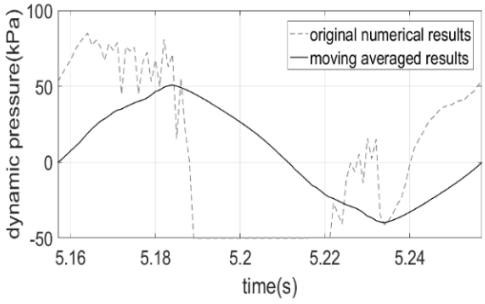

b) Dynamic pressure variation in PT2

Figure 3.8. Detailed analysis of pressure distribution

The results from the analyses are compared to the results from the benchmark test (Javanmardi, et. al. 2005) in this section. As the sensors used in the experiments were not able to capture the occurrence of cavitation reliably, outlier data were eliminated while presenting the test results (Javanmardi, 2003). The experimental data was obtained at 0.001-second sampling while the numerical results obtained in this study could be obtained with a considerably lower period at 1e-5 to 1e-7 seconds. Consequently, to compare the simulation results to the experimental counterparts, high-frequency oscillations were removed from the data using moving average filtering with 30 and 40 points (Fig. 3.9). Moreover, the piezometer used in the experiment had a fixed dimension of 2.5mm, which in essence corresponded to the recovery of pressure values at an average area within this scale.

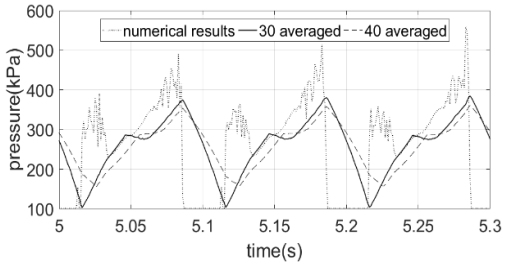

a) Data averaging effects in PT4

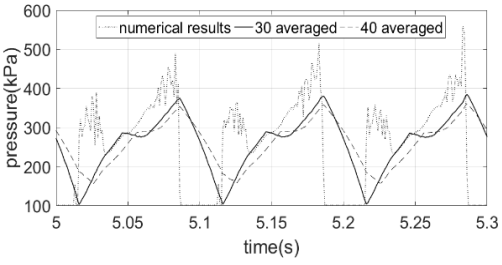

b) Data averaging effects in PT5

Figure 3.9. Moving average filtering of points PT4 and PT5

The pressure values for PT2 and PT3 are compared to their experiment values by using the afore mentioned averaging techniques in Figure 3.10. for the simulations with a grid size of 1mm. for the simulations with a grid size of 1mm. The numerical results are very close to the experimental counterparts for PT2 and PT3. For PT4 and PT5, the captured pressure values are somewhat less than the test. Refining the grid size further to 0.5mm, the higher pressure values in PT4 and PT5 are captured as shown in Figure 3.11.

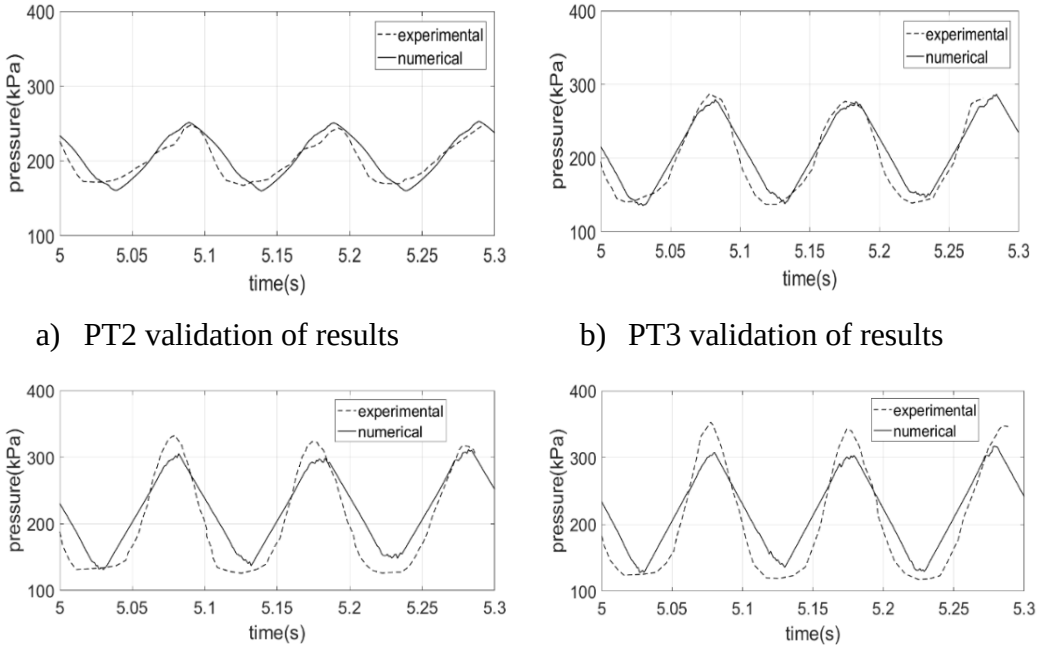

a) PT2 validation of results

b) PT3 validation of results

c) PT4 validation of results

d) PT5 validation of results

Figure 3.10. Verification of results with experimental data for PT2, PT3, PT4, and PT5 locations

At a grid size of 0.5mm, the analysis undertaken required a time increment as low as 1e-7 seconds leading to very high-frequency data capturing, the cavitation in greater detail compared to the simplification due to the sampling in the experiment. In contrast to the experiment, a two-stage pulse was obtained in PT4 and PT5 locations with a peak slightly higher than the peak of the sine pulse reported. (see Fig. 3.11)

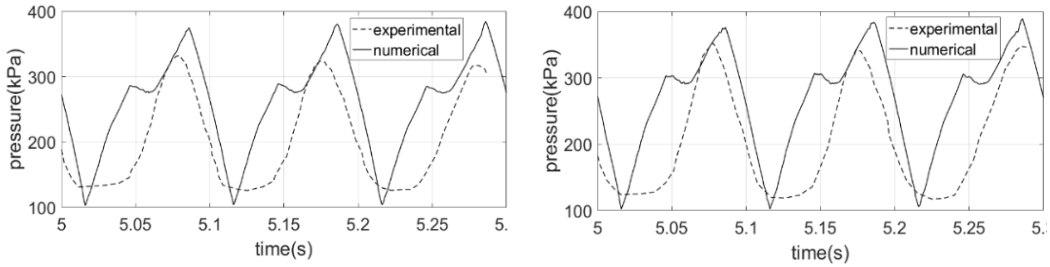

a) PT4 validation of results (0.20mm max opening)

b) PT5 validation of results (0.14mm max opening)

Figure 3.11. Verification of results with experimental data for PT4 and PT5

3.1.5 Conclusion

A CFD model is developed to inspect pressure variation with time in the crack area at the time of the earthquake and the earthquake is simulated as a sinusoidal wave with normalized corresponding frequency and magnitude. In order to avoid excessive analysis, just the crack area of the dam by considering constant pressure value in its mouth is utilized.

First of all, the study reveals that the water can penetrate to the crack and partially saturate it during the simulated earthquake, additionally in the constant magnitude of an earthquake by increasing oscillations' frequency, the pressure value is increased in the crack zone.

Second, by going through the crack in the downstream direction, the pressure values are increased and the maximum pressure value is captured at the end of the crack or PT5 with a sufficient value for the propagation of it, additionally, the occurence of cavitation is seen at starting of opening and ending of closing cycles, which are grown by moving toward the crack end as well as increasing frequency of oscillations.

Last but not least, by FLOW-3D commercial code, coincidence results with experimental data are captured for pressure variation with time, therefore the

program is applicable in any similar case of study, which deals with capturing of fluid properties in narrow cracks among moving objects.

3.2 Inspection of Pressure Distribution Inside the Crack Using Finite Element Technique

In the scope of this section, in order to gain stress values on crack walls, the new model is generated utilizing two solid blocks consisting of an upper crack wall block with prescribed motion and a constant lower wall block. The method that can be utilized under FLOW 3D commercial code to achieve stress and strain values is known as FSI (Fluid-Structure Interaction) method. Because this model is not applicable to GMO (moving object), the down wall of the crack is considered as an individual constant block to analyze stress values on its surface. The top block that is GMO, is oscillating with the magnitude of 14mm/s and frequency of 10Hz with an initial crack mouth opening (CMOD) value of 1.2mm. (see Fig. 3.12)

Figure 3.12. FSI model-Finite element model to investigate the stresses created by the earthquake in the lower part of the crack body

3.2.1 FSI Model

The Fluid-Structure Interaction (FSI) model is based on solving the fully coupled solid dynamics and fluid flow within FLOW-3D and it solves elastic stresses within solid components. The approach used for this model is unlike any other model in FLOW-3D. A conforming and unstructured finite element (FE) grid, which deforms along with the solid is used in this approach despite the other models of FLOW 3D that utilize structured finite difference mesh. This is because solving the solid

mechanics equations is far more convenient and accurate with a conforming FE mesh than with a non-conforming finite difference mesh. The standard FLOW-3D mesh is used to generate the new finite-element (FE) mesh for solid components. Throughout the bulk of the solid regions, the standard hexahedral mesh is used without alteration. At the boundaries of the solid regions, the nearest node points are moved onto the surface of the solid region along the normal to the surface and nearby nodes can be eliminated or merged with neighbors. Elements away from the interface always have 8 nodes and due to the merging of nodes near the solid interface, elements at the surface can have 7, 6, 5, or even 4 nodes.

3.2.1.1 Finite Element Method

FSI solve the standard equation of motion in solid regions (Eq. 3.7):

$$\rho \frac{d^2 x}{dt^2} = \nabla \cdot \sigma + \rho b \qquad (3.7)$$

In equation 3.7, ρ, x, σ, and b are respectively representative of the density of the solid, coordinate of a point, Cauchy stress tensor, and the body force vector. The Cauchy stress tensor for the current time level, σ^{n+1}, is computed from the linear Hookean model for each time-step increment:

$$\sigma^{n+1} = \sigma^n + \left(K - {}^2/_3\, G\right) \mathrm{tr}(E) + 2GE \qquad (3.8)$$

In equation 3.8, K, G and tr(E) are the bulk, shear moduli, and the trace of the strain tensor E and is the sum of its diagonal components, respectively. Equation 3.7 comprises a three-dimensional partial differential equation, solved during each time-step, whose unknowns are x^{n+1}. $\sigma^{n+1}$are computed directly from x^n and earlier time level values of σ in equation 3.8. The finite element method (FEM) uses the method of weighted residuals to solve the equations.

3.2.1.2 CFD Model Generation

2.3. CFD Model Generation

In the generated CFD simulation one fluid model with a free surface is utilized to inspect the pressure variation inside of the crack utilizing renormalized group (RNG) turbulence model with no-slip wall boundary condition. The model is consisting two blocks, of which the upper part is a GMO and the down one is the FSI block. The GMO block or upper wall of the crack is oscillating with magnitude and frequency of 14mm/s and 10Hz from 1.2mm with initial crack mouth opening utilizing explicit fluid-object coupling solver. The FSI block or down wall of the crack with unstructured hexahedron finite element grids is consistent in its location. The density, Young modulus, and Poison ratio of concrete are considered to be equal to 2400 kg/m^3, 2.85 Gpa, and 0.15. The crack is initially filled with water and is pressurized at the level of 200 Kpa. The data gathering time interval is selected equal to 0.001s which is the same as the benchmark test.

3.2.2 Grid Size Effects Analysis

In Figure 3.13 the effects of grid size value in reliably capturing of pressure variation inside the crack, due to the base excitation are presented. According to the analyzes, by reducing the size of the utilized cells in the model, in addition to increasing the range of pressure change inside the crack, sudden jumps in the pressure distribution due to cavitation are increased. More precisely, according to the mechanism behind the VOF technique, which is based on the averaging of fluid properties within cells, when using large cells, averaging is done with the empty part of the cell, which reduces the range of pressure change.

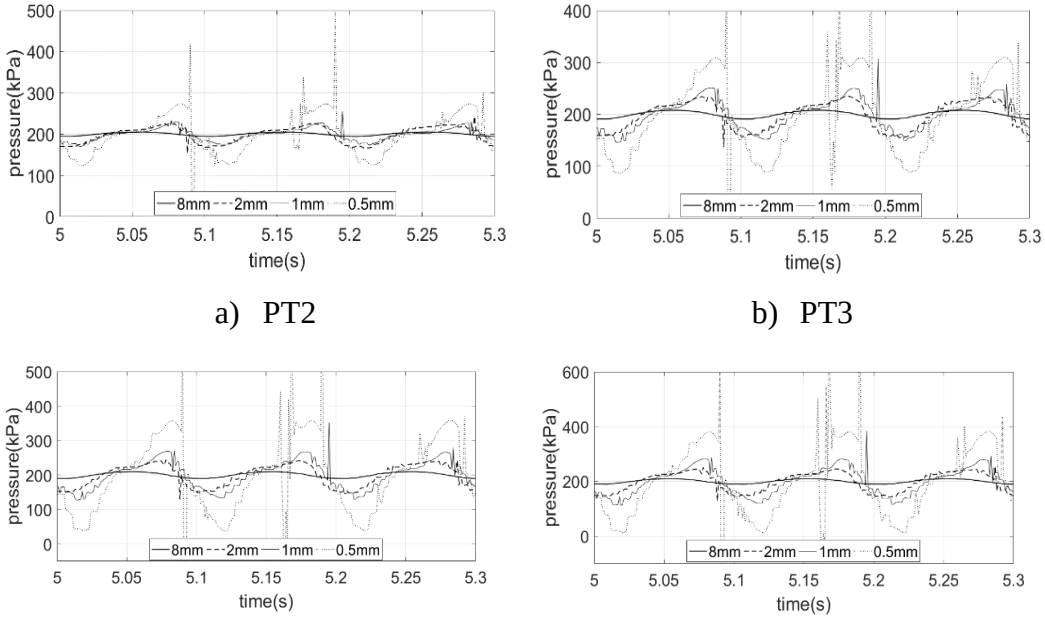

a) PT2 b) PT3

c) PT4 d) PT5

Figure 3.13. Grid size effect on capturing of pressure value

3.2.3 Time Step Analysis

In Figure 3.14 the effects of time step value in reliably capturing of pressure variation inside the crack, due to the base excitation are presented.

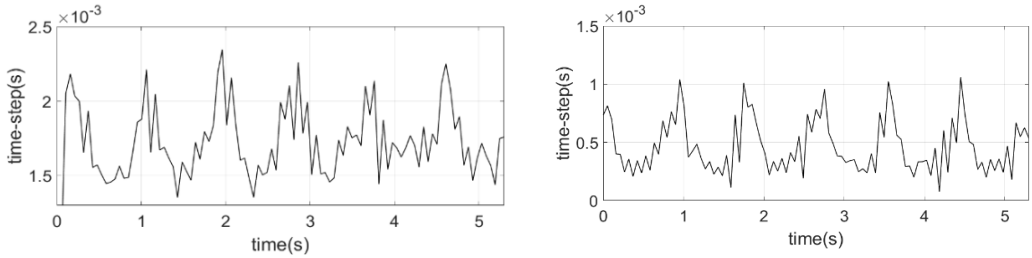

a) 8mm grid size b) 2mm grid size

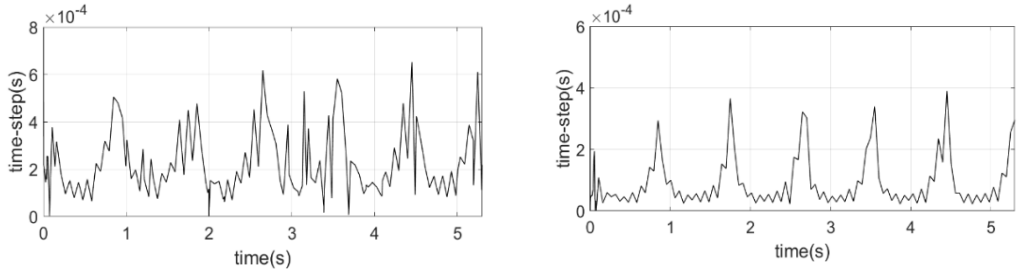

c) 1mm grid size d) 0.5mm grid size

Figure 3.14. Timestep value effects on capturing of the pressure value

From the analysis the important point to mention is that; in the case of simulating the CFD model in the presence of base excitation, besides controlling grid size convergence, the time step value should be defined by numerical trial and error. From table 3.1, by decreasing cell size smaller time step value is needed to capture pressure value in an acceptable range, therefore maximum allowable time step value should be defined to the program. In general, the software has the ability to determine the appropriate amount of time step size using the CFL number so that the pressure convergence is achieved. However, in cases dealing with earthquakes, given that earthquakes have high frequencies, defining a maximum time step of about 1E-4 s is necessary for the program to reduce it from the set value until it reaches an acceptable value. If the maximum time step of the simulation is not set due to repeated pressure divergence, the simulation will stop. In addition, a value less than one hundred times the set maximum time step must be specified for the time step of collecting the results.

Table 3.1 Time step vs. cell size

cell size	8mm	2mm	1mm	0.5mm
minimum(dt)	1.35193E-03	7.66015E-05	1.07904E-07	3.6586E-09

3.2.4 Pressure distribution Inside the Crack

In order to inspect the pressure distribution inside of the crack, two times are selected as maximum (5.08s) and minimum (5.02s) pressure distribution times. It should be mentioned that in the following graph, P1, PT2, PT3, PT4, and PT5 are respectively located on 0, 0.09, 0.18, 0.27, and 0.36m from the crack mouth.

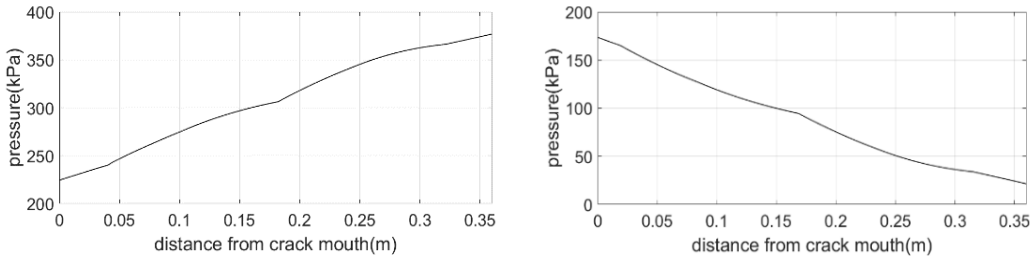

a) Maximum pressure distribution(t=5.08s)

b) Minimum pressure distribution(t=5.02s)

Figure 3.15. Peak pressure variations vs. distance from crack mouth

3.2.5 Stress Analysis Inside the Crack

By utilizing the Finite Element Method, the most vulnerable zone inside of the crack is detected as few millimeters before its ending, where the water will be in static condition. In Figure 3.16 the stress values in the finite element grids of the down crack wall can be seen at t=5s.

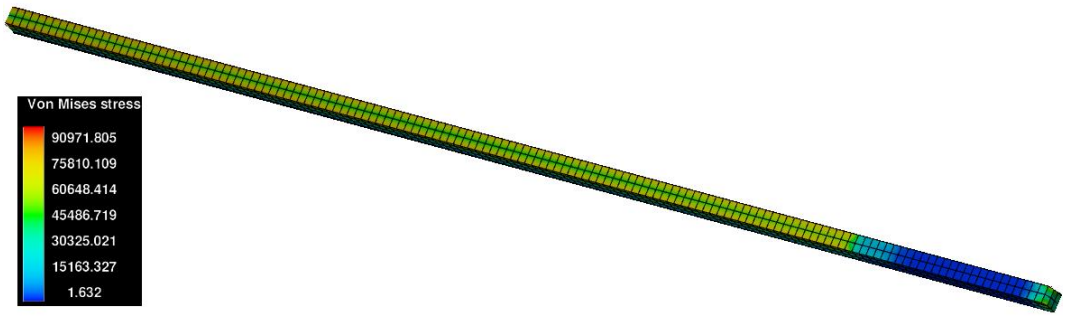

a) Von Mises stress

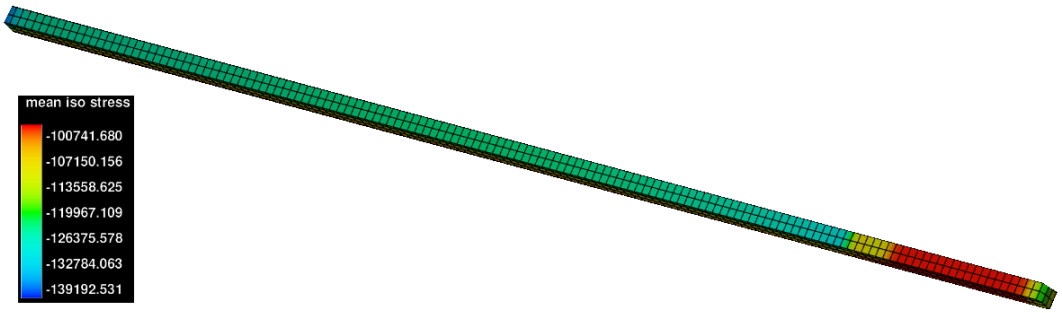

b) Mean iso stress

Figure 3.16. Stress analysis inside the crack

3.2.6 Numerical and Experimental Results

In the test case the sensors were not able to capture negative pressure values and the minimum achievable pressure value tracked by piezometers was atmospheric pressure. However, in numerical analysis the reference pressure was considered equal to zero, therfore to compare the numerical and experimental results, , the atmospheric pressure should be devoted to the captured values of pressure below 101kPa.

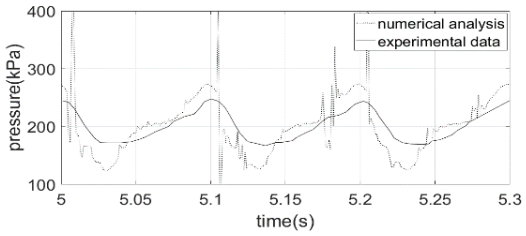

a) PT2

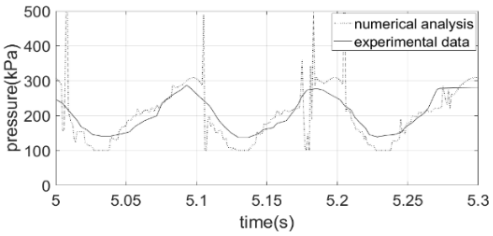

b) PT3

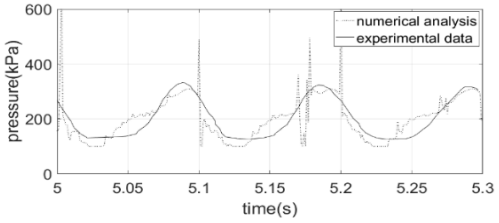

c) PT4

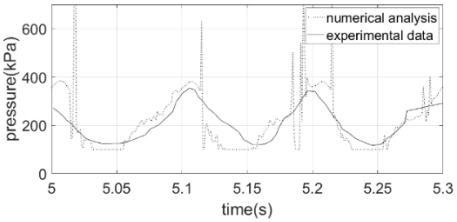

d) PT5

Figure 3.17. Comparison of numerical and experimental results of Javanmardi et al. (2005), without removing cavitation from numerical results

3.2.7 Validation of Results

Because despite the experimental test case in the numerical analysis the occurrence of cavitation was captured, which can be seen in Figure 3.17 as high rises and falls from sinusoidal pressure variation with time, to make the experimental and numerical data comparable, moving average filtering should be used. In this analysis 30 back-warded averaging is applied.

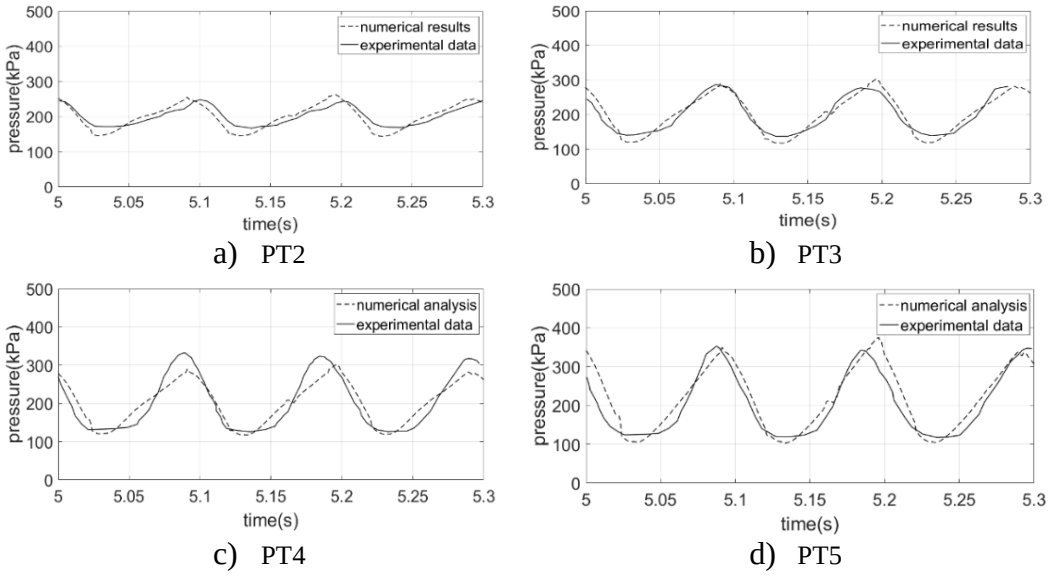

a) PT2 b) PT3

c) PT4 d) PT5

Figure 3.18. Validation of the filtered numerical results with experimental data of Javanmardi et al. (2005)

3.3 Crack Characteristics Effects on Inside-Crack Pressure Variation

In this part of the study, crack characteristics comprising crack length and crack opening effects on the pressure variation during the earthquake are inspected. In order to inspect pressure values inside of the crack, the body is rotating around its bottom-right corner with defined magnitude and frequency. Maximum time step

value and data gathering time interval are considered to be equal to 0.005s, additionally, the cell sizes are equal to 0.002m. (see Fig. 3.19)

a) Crack length = 1m

b) Crack length = 2m

c) Crack length = 4m

d) Crack length = 8m

Figure 3.19. CFD model- Increase crack length by keeping all the involved parameters constant

The desired locations inside of the crack to inspect pressure values in different crack lengths and openings are 0, 0.25, 0.5, 0.75, and 1m from the crack mouth that are named as L1, L2, L3, and L4 respectively. Lastly, the X-min boundary condition is stagnation pressure at the level of 200 kPa and the other boundaries are the wall. In the following study, the friction value and density of the body are considered to be equal to 1 and 2400 kg/m^3. The point to be mentioned here is; to minimize cavitation effects, the water region is considered as a tank and the crack is initially filled with water.

3.3.1 Crack length effects (Constant CMOD)

In this section, by keeping CMOD as the constant value, the crack length is increased to inspect its effects on pressure values in desired locations inside of the crack. In the initial model that can be seen in Figure 3.19.a, the effective crack length is equal

to 1 m, which the body is rotating around its bottom right corner (joint b) with the angular velocity magnitude of 0.01 rad/s and frequency of 10Hz. In order to make the CMOD independent of crack length, the velocity of the crack opening part of the body (joint a) is kept constant by increasing crack length. Therefore proportional to crack length increment the angular velocity of the body is decreased. Note that the minimum crack opening value is 1mm.

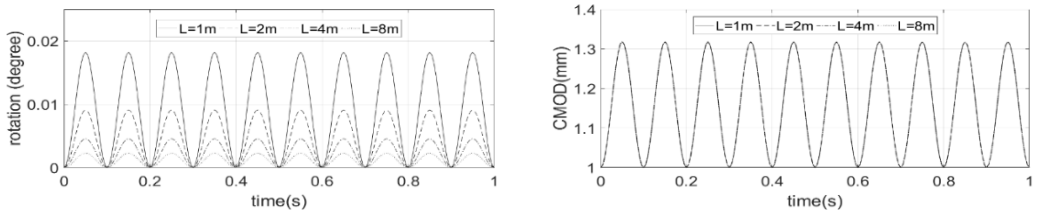

a) Rotation comparison of cases b) CMOD comparison of cases

Figure 3.20. Constant CMOD- crack length effects

Comparison of pressure values in the desired location inside the crack comprising L1, L2, L3, L4, and L5 that are located respectively at 0, 0.25, 0.5, 0.75, and 1m from the crack mouth are presented in Figure 3.21. From the analysis by increasing the crack length with the constant CMOD the pressure variation increased.

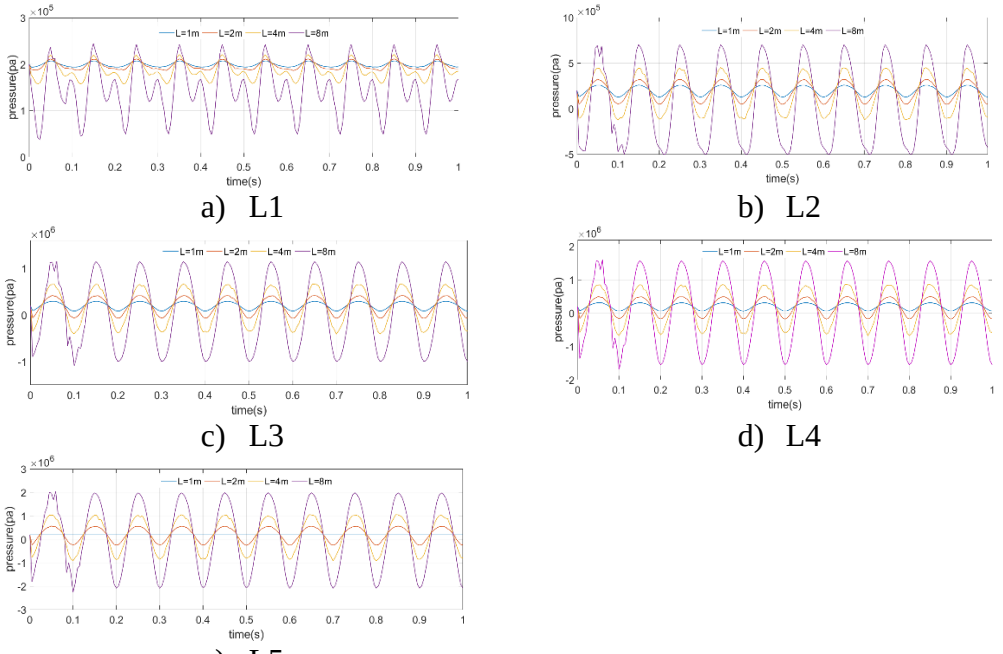

a) L1 b) L2

c) L3 d) L4

e) L5

Figure 3.21. Crack length effects on pressure distribution in the cracked area

3.3.2 Crack Opening Effects (Constant Length)

Keeping the crack length constant at the value of 1m, the crack mouth is opened to inspect its effects on the pressure variation in the desired location. The utilized model for this analysis is presented in Figure 3.19.a. In order to increase CMOD, the angular velocity (ω) around joint b is increased from 0.01rad/s to 0.015, 0.02 and 0.25rad/s. (see Fig. 22)

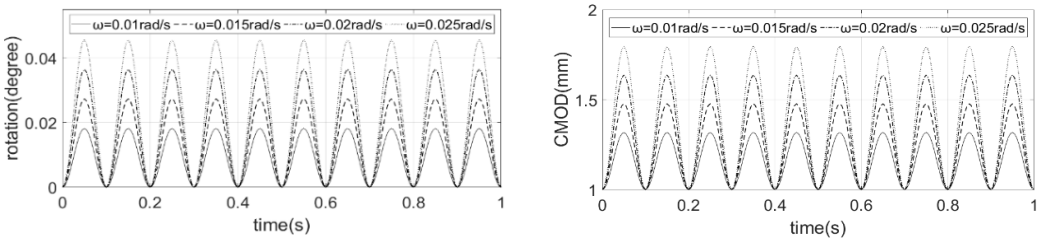

a) Rotation comparison of cases b) CMOD comparison of cases

Figure 3.22. Constant crack length- CMOD effects

Comparison of pressure values in the desired location inside of the crack comprising L1, L2, L3, L4, and L5 that are located respectively at 0, 0.25, 0.5, 0.75, and 1m from the crack mouth are presented in Figure 3.23. From the analysis by increasing the crack opening value with the constant length of 1m, the pressure variation increased.

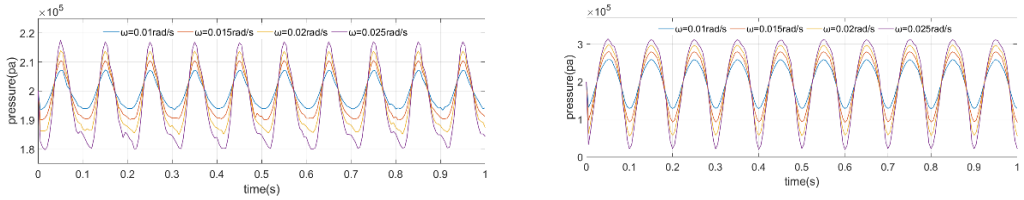

a) L1 b) L2

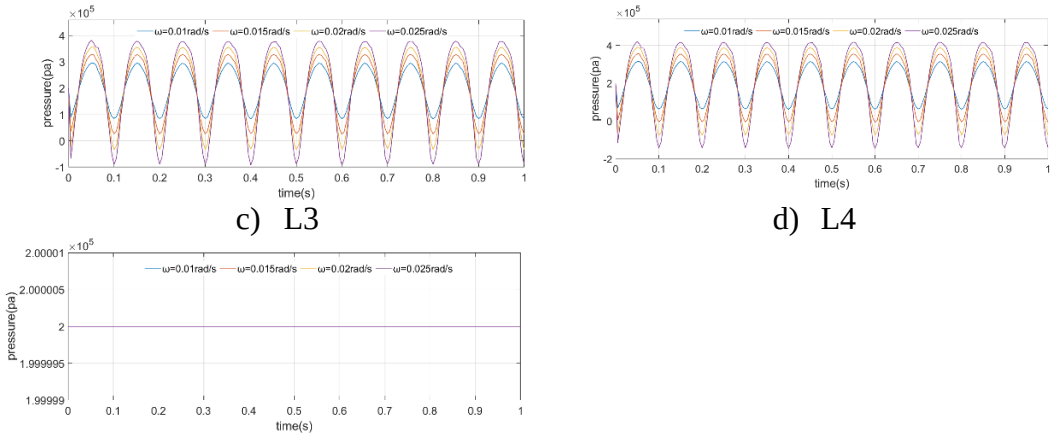

c) L3 d) L4

e) L5

Figure 3.23. Crack opening effects on pressure distribution in the cracked area

3.3.3 Crack Size Effects (Constant Angular Velocity)

Lastly, the effects of crack size increasing on the value of pressure variation are inspected. To increase crack size in the constant value of angular velocity equal to 0.01rad/s the crack length is increased from 1m to 2, 4, and 8 meters, as the results the CMOD values are automatically increased respectively 2, 4, and 8 times proportional to the crack lengths.

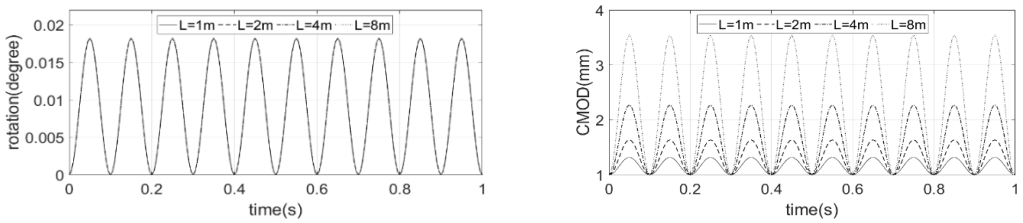

a) Rotation comparison of cases b) CMOD comparison of cases

Figure 3.24. Constant angular velocity- crack size effects

Comparison of pressure values in the desired location inside of the crack comprising L1, L2, L3, L4, and L5 that are located respectively at 0, 0.25, 0.5, 0.75, and 1m from the crack mouth are presented in Figure 3.25. From the analysis by increasing the crack size in the constant angular velocity of 0.01rad/s, the pressure variation increased.

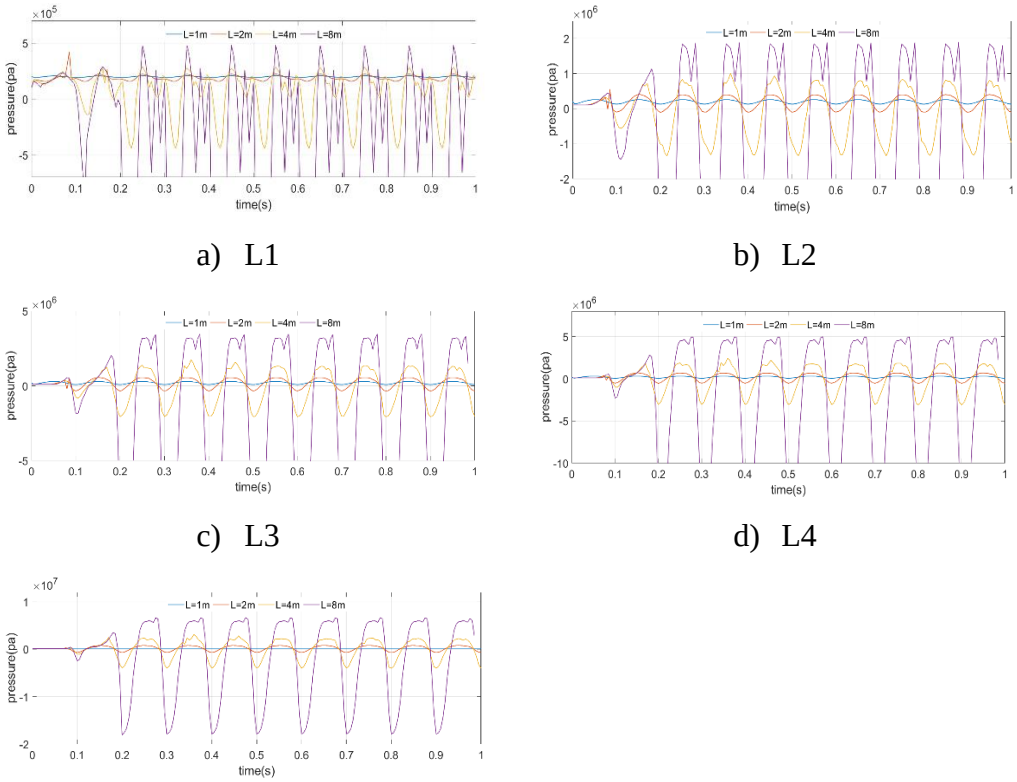

a) L1 b) L2

c) L3 d) L4

e) L5

Figure 3.25. Crack size effects on pressure distribution in the cracked area

An important conclusion to be noted is that: Due to the fact that as the size of the cracks increases, the pressure distribution within them changes, it is not possible to model the failure of the concrete dam with the scaled laboratory model.

3.3.4 Initially Empty or Full Crack Effects

In this section, the effect of the initial fullness or emptiness of the crack is investigated. The grid size is 8mm, which is very coarse to capture the exact values of pressure, therefore this part is not valid from a quantitative point of view. Below the pressure distribution inside of the crack for a corresponding time to the maximum and minimum pressure values are presented. From the comparison of pressure distribution in PT2 and PT3, again it is approved that by increasing the distance from the crack mouth the inside crack pressure value is increased.

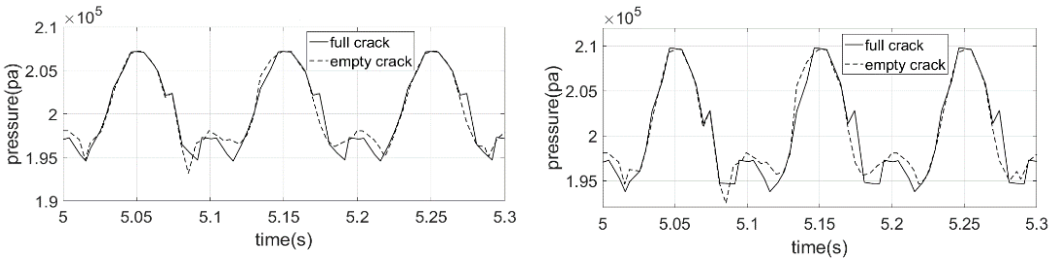

a) PT2 b) PT3

Figure 3.26. Effect of the initial fullness or emptiness of the crack in the steady-state case

To detail inspect the difference of the simulations with initially empty and full of water cracks, dynamic pressure variation with time in the initiation of the simulations for PT2 and PT3 are presented.

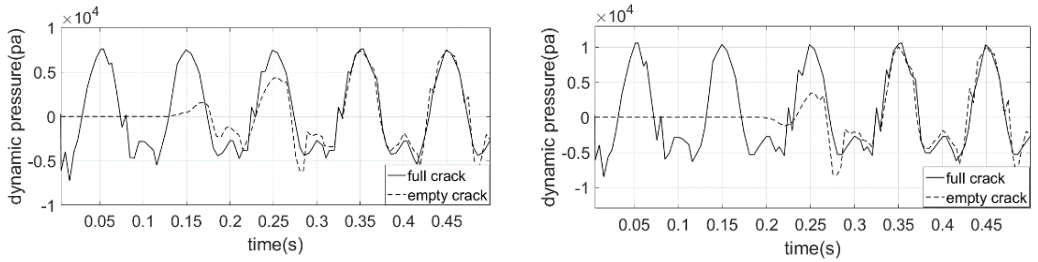

a) PT2 b) PT3

Figure 3.27. Effect of the initial fullness or emptiness of the crack in the transition case

From Figure 3.27, however, being the crack initially empty of water can effects the initial captured values of pressure, after reaching the semi-steady state condition the captured values for pressure will be the same as initially full of water crack. For the case of study after around 0.3s semi-steady state condition is reached. The other results that can be inferred from the figures are that the water would reach PT2 and PT3 after 0.15s and 0.2s respectively. The effects of hydrostatic and hydrodynamic forces of water on the movement of the Koyna dam upper part with different crack shapes are further discussed in Appendix C.

CHAPTER 4

SINGLE BLOCK MOTION INSPECTION DURING EARTHQUAKE BASE EXCITATION

4.1 Investigating the Motion of Koyna Dam's Cracked Top Part

After ensuring the ability of the VOF method to simulate water pressure near moving solid objects, the next step is to ensure the ability of the GMO method to accurately simulate the motion of rigid bodies under the combination of hydro and seismic forces. Since the force of an earthquake enters the objects in different directions and with magnitude and frequencies that change with time, the objects will experience a complex motion. Besides, in the case of dam failure, along with the seismic force, the hydrostatic and hydrodynamic forces of water also affect the body. Given all that has been said, before entering into the main problem which is to predict the failure of a dam due to an earthquake, the ability of the GMO method to simulate the movement of objects under the influence of the composition of the mentioned forces, should be ensured. In this part of the study, various verifications of the motion of objects under the influence of earthquake and water forces will be presented using experimental and numerical results. The next purpose of this section is to get an insight into the motion of a single rigid body under the influence of mentioned forces to develop it for a dam failure model that involves a large number of these solid pieces moving with water.

In the current study, simulated damaged Koyna dam during the 1967 earthquake consisting of two moving rigid objects as top block and base one is utilized. To avoid impacts of base part mass in the motion of the top part in collision time, the corresponding velocity fields to the vertical and horizontal acceleration of earthquakes are applied to the base part to inspect the motion of the top one in three degrees of freedom. Effects of Coulomb's law of friction and Stronge's energetic

restitution coefficients values are inspected in three hypothetical cracked Koyna dam cases consisting of horizontal, upstream sloped, and downstream sloped crack. Maximum and minimum displacement of the top part is seen respectively in downstream and upstream sloped crack cases due to hydrodynamic and hydrostatic effects of the reservoir. It is revealed that an increase in restitution and friction coefficients from zero to one, respectively cause increasing and decreasing of the upper part displacements, however by more increase of friction coefficient value from 1, any direct relationship between motion of top part and friction coefficient value is not detected that is due to the change of the type of movement from sliding type to rock-sliding one.

4.1.1 Introduction

During the earthquake of magnitude 6.5 on December 11, 1967, Koyna Dam was damaged significantly at the location of slope change on dam monoliths and at the base. The formation of the continuous crack along the monolith from the upstream to the downstream face can be considered as the starting of a dam breach mechanism if coupled with a strong enough shaking for causing instability. Stability in sliding and overturning of the independent monolith under inertial and hydraulic forces is a complex issue affected primarily by crack and block geometry and boundary conditions. The crack shape is an important factor for the displacement of separated blocks because of hydro-forces comprised of hydrostatic, uplift, drag, and buoyancy forces acting on the solid particles. Extra complexity is brought to the issue due to the collision of solid blocks and their interaction with the surrounding water. Seismic safety of a damaged dam monolith from a viewpoint of the breach, during an earthquake event, is hence a complex research topic because of the solid-fluid interactions and the extra nonlinearity of free-surface flow.

In order to investigate the seismic behavior of dam/reservoir systems, several experimental studies were conducted with the primary goal of predicting the crack shapes during earthquakes and investigate the effective factors (Mridha et al., 2014,

Nuss et al., 2012, Hall et al., 1998). The massive size of these structures and the corresponding scaling requirement limits the number of these attempts. A detailed investigation of the effective factors in experimental studies is also not straightforward as in the experiments there are utmost 2 specimens (usually one) and the difficulty in instrumenting, testing, and monitoring of a large set up in a laboratory even without considering the large size reservoir that should be included in the setup. These tests do not provide a clear insight into the collapse problem as the primary focus is on crack positioning and propagation. Consideration of seismic safety requires an insight into the behavior of the system after the formation of such a crack severing a block from the main system. The size and complexity of the problem, therefore, requires analytical investigation of the complex reservoir/monolith interaction problem for the possibility of breaching, defined by sliding and overturning of the severed monolith on top of the intact part of the dam.

A comprehensive study on the behavior of a damaged dam monolith is conducted using a finite volume technique with the goal of identifying the primary factors affecting the collapse behavior of the severed monolith. The case study of Koyna Dam was selected following the literature for comparison as well as validation with the former studies. In this study, first, the effect of the crack orientation was considered: the motion of the severed block over three idealized flat cracks in horizontal, upstream sloped, and downstream sloped orientations. Next, the effect of important parameters defining the sliding and rocking of the block, the coefficients of restitution and friction were investigated. The main goal of this study is to demonstrate the capability of the finite volume technique in simulating and predicting the interactive behavior of water and solid blocks using the results of a benchmark test (Pekau et. al., 2004) as a case study.

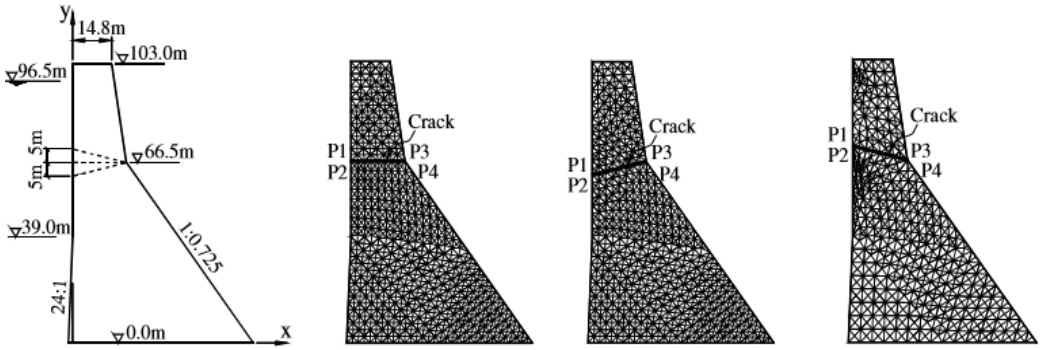

a) Crack Models reprinted from "Pekau & Yuzhu, (2004). P. 5.

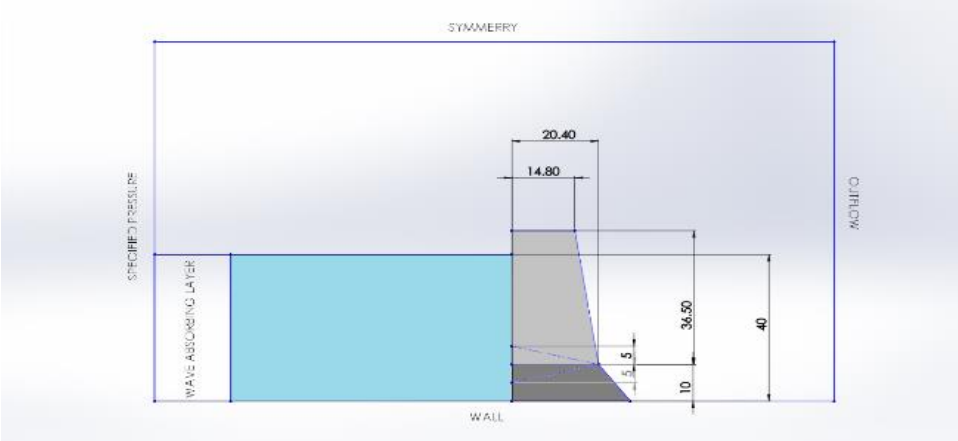

b) CFD model-generated by SOLIDWORKS

Figure 4.1. Cracked dam models

In the benchmark test whole the Koyna dam was simulated utilizing the distinct element method. Under the method, the body of the dam was divided into deformable triangular blocks, that were connected by joints with normal, shear springs and dashpots. The model of the benchmark test is provided in Figure 4.1.a.

4.1.1.1 CFD Model Generation

The CFD model consisting of two rigid bodies, with the top block resting on the base was generated in SOLID WORKS and imported to FLOW 3D as an STL file. Vertical and horizontal velocity time series were prescribed to the base letting the top block displace in three degrees of freedom. FLOW 3D uses finite volume grids,

therefore the flow domain is divided into rectangular cells within the mesh planes. In the model $Z_{maximum}$ or top boundary condition was set as a symmetry plane applying zero velocity condition normal to the boundary. The bottom boundary ($Z_{minimum}$, $Y_{maximum}$, $Y_{minimum}$) was set as a stationary wall with the no-slip condition. A stagnation boundary was defined at the left boundary of the model: the velocity upstream from the boundary was zero keeping the reservoir at a constant level. A wave absorbing layer was also placed here at the far end of the reservoir to prevent wave reflection from the boundary. For the right-hand boundary, exit flow was enabled. The static reservoir condition was assumed as the initial condition.

4.1.1.2 Basic Theory

Computational Fluid Dynamics (CFD) is a solution of the fluid flow governing equations comprising conservation of mass, momentum, and energy in three directions. Finite volume solutions of flow problems involve the division of the flow domain into rectangular cells and then numerically approximating the equations of motion by using pressure and velocity averaging in each cell block.

The fluid flow governing equations are discretized and solved using numerical methods. In hydraulic structures, as heat transfer is usually ignored, fluid motion equations consisting of continuity and momentum equations in three dimensions, i.e. the Navier-Stokes equations, are solved to determine the fluid behavior.

Continuity equation:

$$\nabla . \vec{V} = 0 \tag{4.1}$$

Momentum equations:

$$\rho\frac{D\vec{V}}{Dt} = \nabla p + \rho\vec{g} + \mu\nabla^2\vec{V} \tag{4.2}$$

in which is total or material derivative and is equal to:

$$\rho\frac{D\vec{V}}{Dt} = \left[\frac{DV}{Dt} + (V.\nabla)V\right] \tag{4.3}$$

In the above-mentioned equations, ρ, μ, and p respectively represent the density, viscosity, and pressure of the fluid. Additionally, $\vec{V}$ is the velocity vector in three directions.

The tracking of the free surface is the most challenging part of CFD simulations for hydraulic structures because of the discontinuity of the fluid properties like velocity, pressure, and density in that boundary. In FLOW-3D, the free surface is considered as a fluid external boundary, and it is tracked using the Volume of Fluid technique. The VOF consists of three main components, which are, the definition of the volume of fluid function, solution of the VOF transport equation, and setting the boundary conditions at the free surface. There are two main types of fluid interfaces: a sharp interface and a diffuse interface. In this study, one viscous incompressible fluid with a free surface or sharp interface is defined to the program to let it simulate the fluid behavior under the laminar model with no-slip wall shear boundary conditions. A free surface is an example of a sharp interface used in one-fluid flows with void regions.

The rigid body motion is simulated using the general moving objects (GMO) model (Wei, 2006). In this model, the motion of the body can be coupled to the fluid flow or prescribed for each block. Volume and area fractions in a rectangular grid are calculated to describe the object's motion at each time step, additionally, equations of motion are solved to gain rotational and translational velocities for objects under motion. In order to capture the interaction of the solid with the fluid, source terms are put on the continuity equation to represent the impact of moving rigid bodies and the tangential velocity of the moving object boundaries is presented in shear stress terms in the momentum equation.

Friction and restitution are treated by Coulomb law and Stronge's restitution coefficient, respectively, in FLOW 3D. The Coulomb law compares the friction resistance due to normal force (dp) to the resultant of tangential forces in 1 and 2 (tangential) directions as given in Eq. 4.4. In the case of sliding, the change in forces

in tangential directions is expressed by Eq. 4.5 The basics of Coulomb law of friction is utilizing by FLOW 3D:

$$\sqrt{(dp_1)^2 + (dp_2)^2} < \mu\, dp \quad \text{if} \quad v_1^2 + v_2^2 = 0 \tag{4.4}$$

$$dp_i = -\frac{\mu v_i}{\sqrt{v_1^2+v_2^2}} dp \quad i=1,2 \quad \text{if} \quad v_1^2 + v_2^2 > 0 \tag{4.5}$$

In these equations v_i, p_i, and μ are respectively representatives of the relative velocity of contact points, impulse of the contact force at the i[th] tangential direction, and the coefficient of friction.

Impact in the normal direction is simulated using Stronge's restitution coefficient (e):

$$e^2 = -\frac{w_3(P_f)-w_3(P_C)}{w_3(P_C)} \tag{4.6}$$

where w_3 represents the work done by impulse forces, P_C and P_f, representing the normal impulse in compression and the total impulse during the collision, respectively.

GMO models can utilize an explicit or implicit time-stepping algorithm for interaction. The implicit method iteratively calculates the fluid and solid motion at each time step using velocity and force data of the current time step, while the explicit method uses the data of the previous time step to obtain the current time step values. In this study, the implicit method was preferred given the higher precision required in the simulation of the behavior of the severed block.

4.1.2 Analysis and Benchmark Test Comparisons

The base motion was prescribed in the form of horizontal and vertical velocities by numerical integration of the recorded Koyna ground accelerations for the event of December 11, 1967, with peak horizontal and vertical accelerations of 0.49 g and 0.34 g's, respectively. In the vertical direction, data are calculated in MATLAB using

1000 data points for each component in 10 seconds. Two 500 data points each corresponding to 5 seconds of motion were provided to the program for simulation of 10 seconds of ground motion due to the FLOW 3D limitation of importable input data (see Fig. 4.2). The analysis was conducted in two parts consisting of 0 to 5 seconds of the earthquake with defined initial conditions and 5-10 seconds with restart from the conditions of the 5th second of the previous interval. Various earthquake simulation methods in the CFD model are discussed in Appendix B.

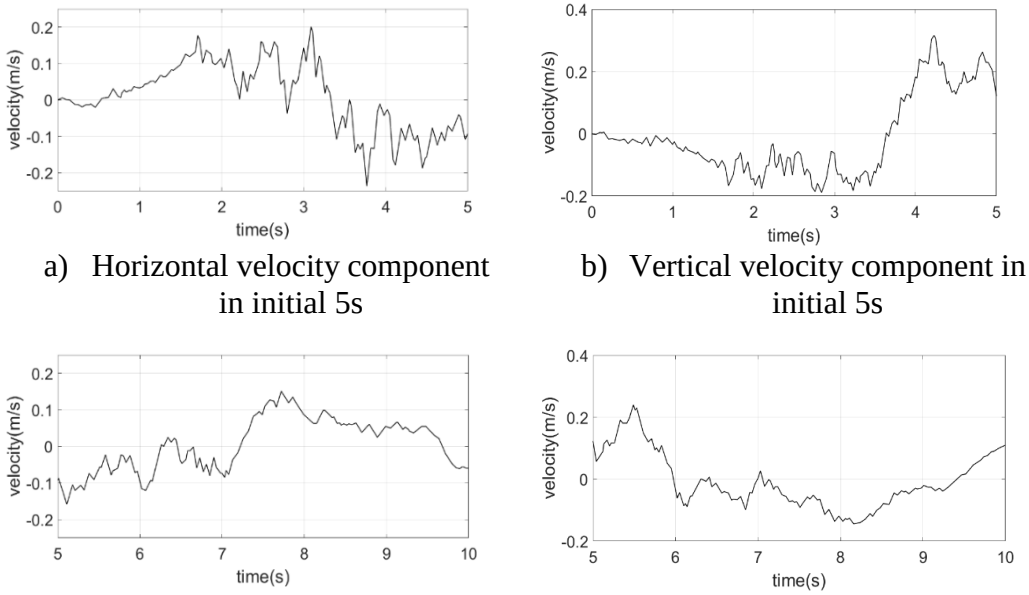

a) Horizontal velocity component in initial 5s

b) Vertical velocity component in initial 5s

c) Horizontal velocity component in the last 5s

d) Vertical velocity component in the last 5s

Figure 4.2. Applied velocity to base part

For the models, the surface roughness of the rigid bodies was assumed as 1mm. Collision properties were changed to inspect their effects on the motion of the top part. The maximum time step was defined as 5e-5 seconds. The minimum time step, initially defined at 1e-7 seconds had to be reduced to 1e-9 seconds to achieve convergence in some cases.

4.1.3 Restitution Analysis

One of the main objectives of the study is to inspect the effect of friction and restitution coefficients in the motion of the top part. To this end, first, the effect of the coefficient of restitution on the behavior was investigated by varying e between 0 to 1 while keeping the friction coefficient constant at 0. The friction coefficient was selected lower than realistic conditions in order to keep the top block in a pure sliding-type motion while evaluating the effect of the impact.

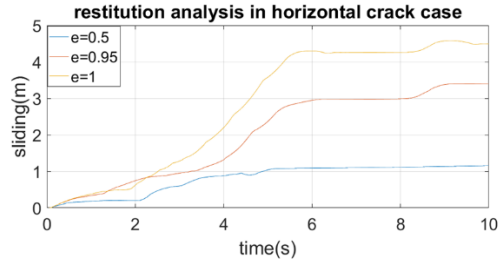

a) Horizontal crack

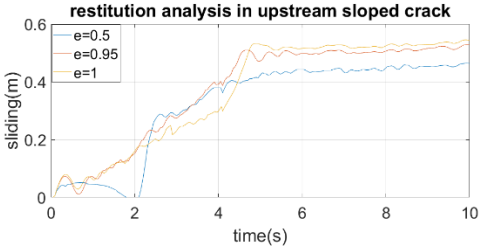

b) Upstream sloped crack

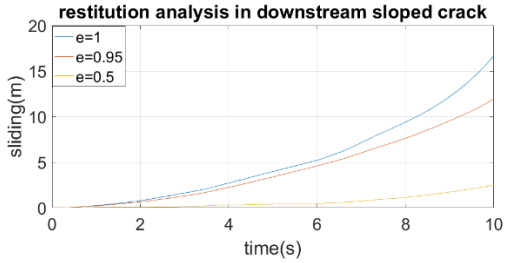

c) Downstream sloped crack

Figure 4.3. The effect of restitution coefficient on top block sliding

For the pure sliding motion, for all crack orientations, the increase in the coefficient of restitution yielded more permanent deformations in the downstream direction. The permanent forces effective on the top during the drift phase, defined as a full separation of the top block from the base, define the extent of the motion. Retaining more energy during impacts led to more drifting time and corresponding permanent deformations. The maximum permanent sliding of the top block, in this case, was directly proportional to the retained energy of the block and the restitution coefficient for the horizontal and downstream sloped cases as given in Figure 4.4.a. The effect

is more amplified for the downstream sloped crack as the reservoir force in the downstream direction increases the relative drift times between each impact. In this case, for an upstream sloped crack, the balancing effect of the reservoir in limiting the permanent deformations is also clearly observed with a minimized effect of the restitution coefficient on permanent deformations after shaking.

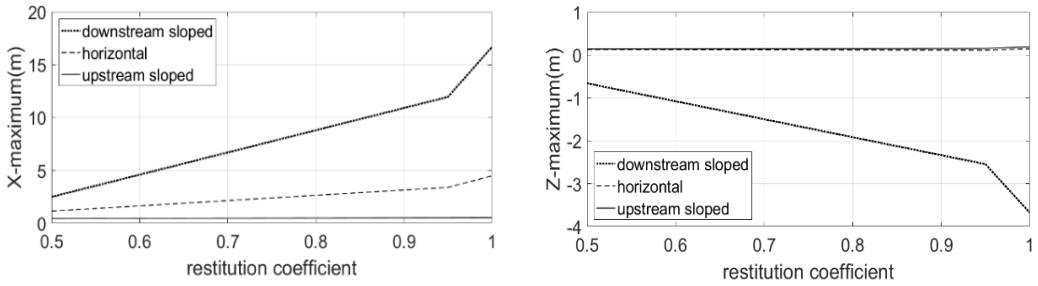

a) Maximum horizontal displacement

b) Maximum vertical displacement

Figure 4.4. Three cases of crack maximum displacements

The top part absolute displacement in the horizontal crack case was inspected to evaluate the effects of restitution coefficient value on drifting of the top block. Increasing the restitution coefficient led the top block to drift more. Total drifting time for restitution coefficients of 0.5, 0.95, and 1 were respectively captured equal to 1.63s, 4.28s, and 6.04s. The mentioned time is equal to almost zero and 10s for upstream and downstream sloped crack respectively.

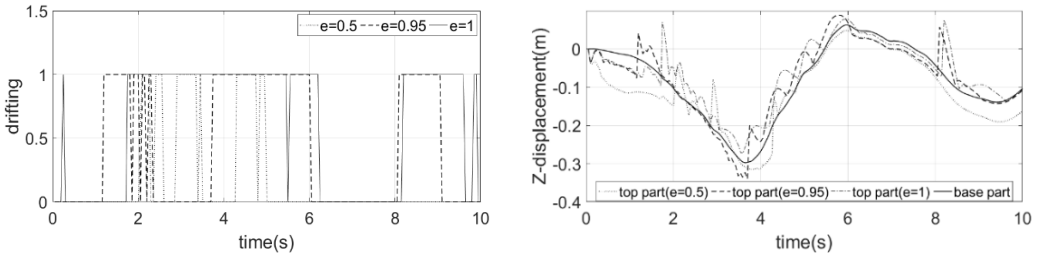

a) Drifting time

b) Absolute upward displacement

Figure 4.5 Restitution coefficient effects on upward displacement

4.1.4 Friction Analysis

The effect of the coefficient of friction was investigated next for realistic friction coefficients between 1-1.3 while keeping the coefficient of restitution at 0.95. The time history of the sliding of the top block for these cases are provided in Figure 4.6. The results of the analyses show the effect of the friction coefficient, varying with a realistic bound between 1-1.3 which can be obtained between wet/rough concrete surface contact, is very small for upstream sloped and the horizontal crack.

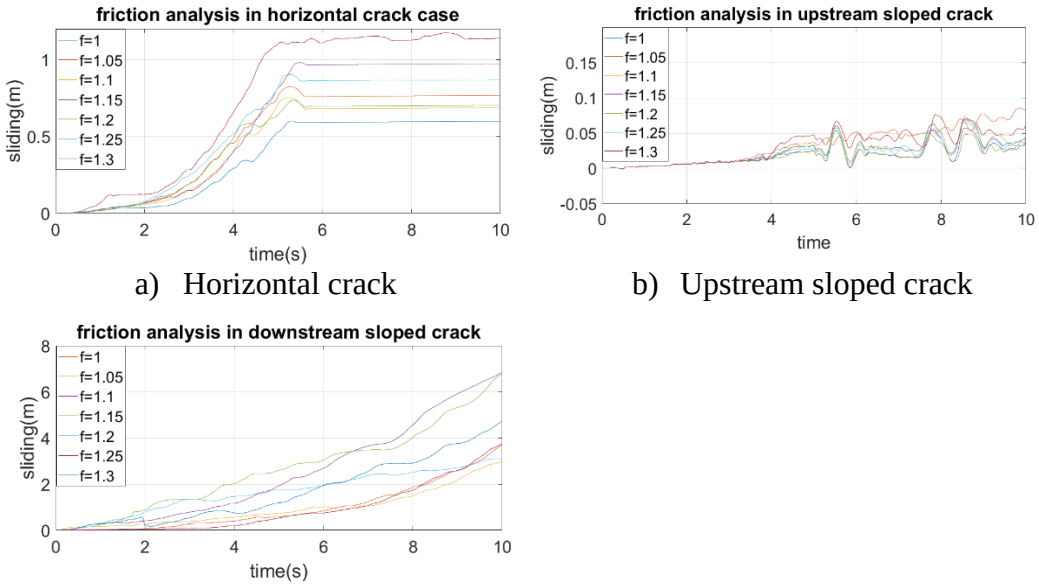

a) Horizontal crack

b) Upstream sloped crack

c) Downstream sloped crack

Figure 4.6. Friction coefficient effects on the motion of top Part

A direct effect of friction is very hard to infer for all crack cases given the very complex contact-drift-sliding solution of the top block. The variation of the sliding with respect to the coefficient of friction was highest for the downstream sloped crack with a maximum 50.11% difference w.r.t. mean value. The corresponding values for the horizontal crack was 39.30%. As expected, the most unstable solution belongs to the downstream sloped case, with both the variance and the mean value increasing corresponding to the other solution. For this case, a breach scenario appears to be possible only for this case of cracking.

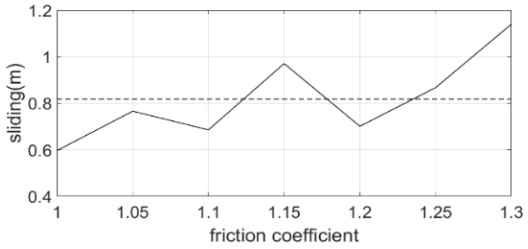

a) Horizontal crack

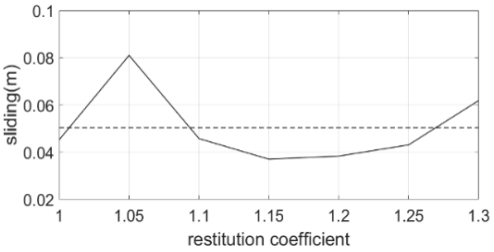

b) Upstream sloped crack

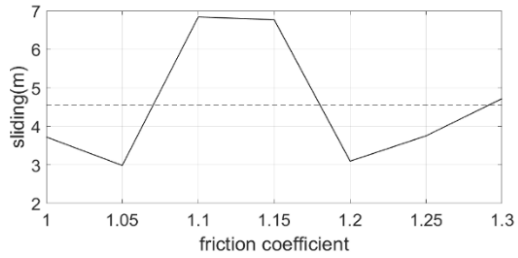

c) Downstream sloped crack

Figure 4.7. Final displacement vs. friction coefficient

4.1.5 Displacement of Top Part

The displaced shape of the top block is shown at t=5 and 10s in Figure 4.8. These analyses were conducted with friction and restitution coefficients respectively equal to 1 and 0.95. The top block is stable for horizontal and upstream slope cracks during the earthquake while drifting in the downstream sloped case.

To inspect the motion of the top part in detail the concepts of drifting, rocking, and sliding motions are defined as the displacement of the top part with respect to base one when there are respectively 0, 1, and 2 contact points between blocks. In the upstream slope case of the crack, the most dominant type of motion is rock-sliding with almost zero drifting values, however, in the horizontal crack, all type of motions consisting of sliding, rocking and drifting is visible. In the downstream sloped crack case a few centiseconds after starting of the simulation the top part was detached from its base as the results of water penetration into the crack, therefore the most dominant type of motion is drifting for the mentioned case.

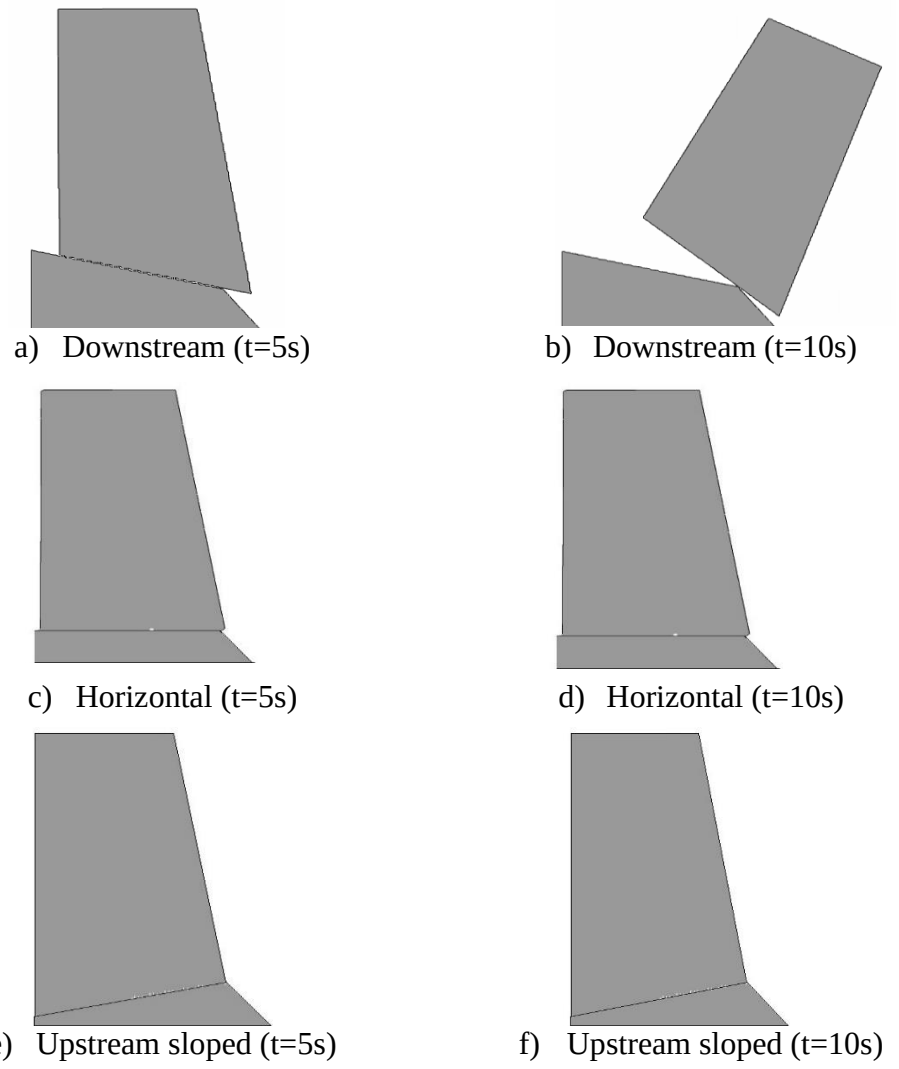

Figure 4.8. Displacement comparison of three cases of cracks

4.1.6 Results Validation

The results from the analyses were compared to the corresponding results from Pekau & Yuzhu (2004) for the friction and coefficient of restitution values of 1.0 and 0.95. The results of the aforementioned study were obtained using the distinct element method considering the full reservoir with a free surface level of 96.5m. The displacements at the bottom left corner of the top block are presented for both studies in Figure 4.9The results of the current study agree well with Pekau and Yuzhu

(2004), both in terms of the trends and the maximum permanent deformations of the top block.

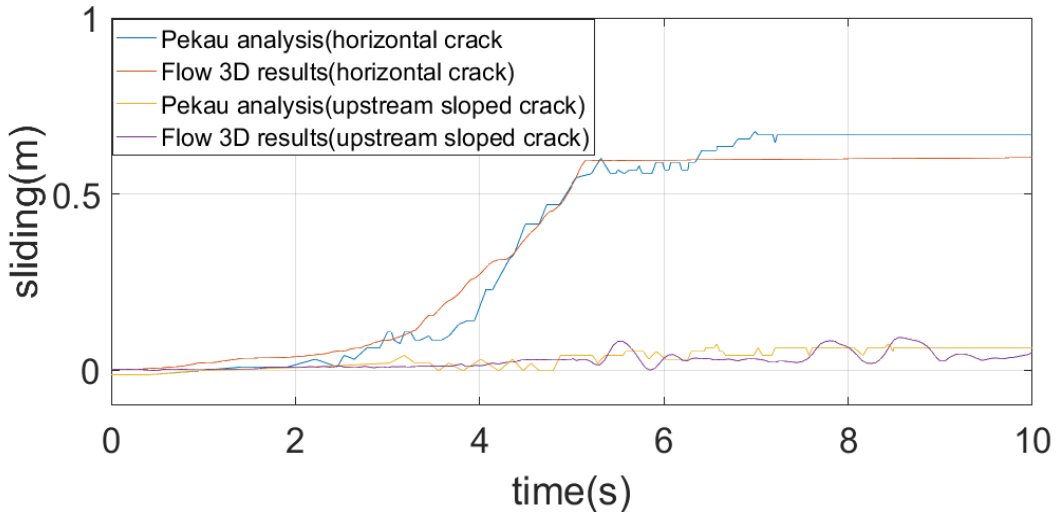

Figure 4.9. Comparison with Pekau and Yuzhu (2004)

The slight difference in the results of the two methods is due to the different formulations used by the two methods. Pekaus' methods are based on the Fineite Differential method (FDM), while FLOW 3D benefits from the Fineite Volume method (FVM).

4.1.7 Conclusion

The behavior of the severed part of a concrete gravity monolith was investigated for three different crack orientations assuming a straight crack geometry. The comparison of the permanent deformation of the top block for the three cases shows that the most dangerous shape is the downstream sloped cracks due to the possibility of the detached part falling. Much smaller permanent deformations were obtained for the horizontal and upstream sloped cases.

The motion of the detached part is highly dependent on the value of the restitution coefficient and the recovered kinetic energy after the collision directly corresponding to higher non-contact (i.e.) drift times leading to permanent deformations.

The variation of the response due to the coefficient of friction was obtained the highest for the downstream sloped case. The variation was the least for the upstream sloped case forming the most stable scenario. It is also not possible to stop a detached part from failing by increasing the friction coefficient in the model and detailed inspection of motion type is necessary.

4.2 Single Motions Validations

In this part of the study, the correctness of the simulated motion of the object is checked by numerical analysis. Therefore, the results from the Flow 3D numerical analyses will be compared to the corresponding results from Pekau and Zhu (2006).

4.2.1 Sliding Type of Motion

4.2.1.1 Sliding Motion Validation of Square Block

The low square block with sides equal to $1m^2$ in Figure 4.10.a, is subjected to the sinusoidal ground motion of Figure 4.10.b to verify the sliding feature of the proposed model with a coefficient of friction of 0.2 and restitution coefficient of 0.75.

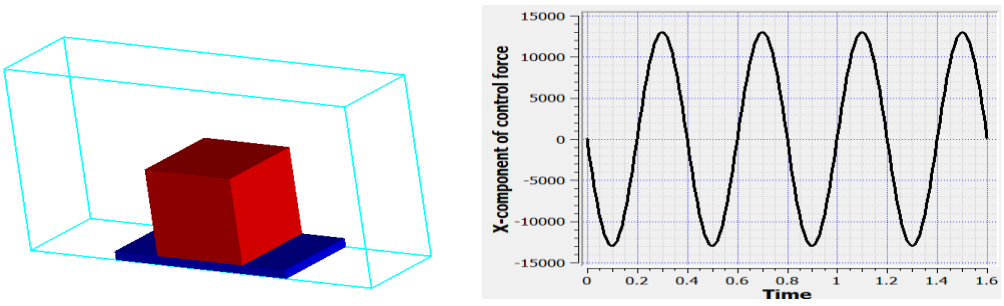

a) Low block model b) Applied force on the low block

Figure 4.10. Square block model

The validation of results with the 3DOF model developed by O. A. Pekau et al can be found in Figure 4.11.

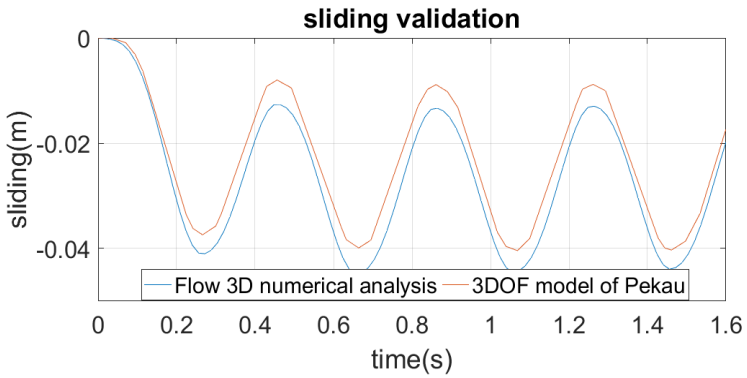

Figure 4.11. Square block sliding motion validation

The slight difference in the results of the two methods is due to the different formulations used by the two methods. Pekaus' methods are based on the Fineite Differential method (FDM), while FLOW 3D benefits from the Fineite Volume method (FVM). FDM is based upon a differential formulation of the governing equations, however FVM is based upon an integral formulation of the governing equations. In finite difference method, the partial derivatives are replaced with a series expansion representation, usually a Taylor series. The series is truncated usually after one or two terms. The more term include, the more accurate the solution. But it causes complxity and increase of nodes. In finite volume method, governing equations are integrated over a volume assuming piecewise linear variation of dependent variables. Using these integrations, you essentially balance fluxes across the boundaries of individual volumes. Therefore, by increasing the numbers of nodes in the FDM and the cells in the FVM, the results of the two methods will be closer to each other.

4.2.1.2 Sliding Motion Validation of High Block

To examine the Flow 3D GMO model reliability, the sliding of the high block on a rigid foundation will be inspected to compare with the finite element analysis of

Pekau. The block is 8x16 m standing on a rigid steel foundation with E=200 GPa and Poisson's ratio of zero. In this analysis, the coefficient of friction is considered to be equal to 0.2, and 0.9 is adapted for the restitution coefficient.

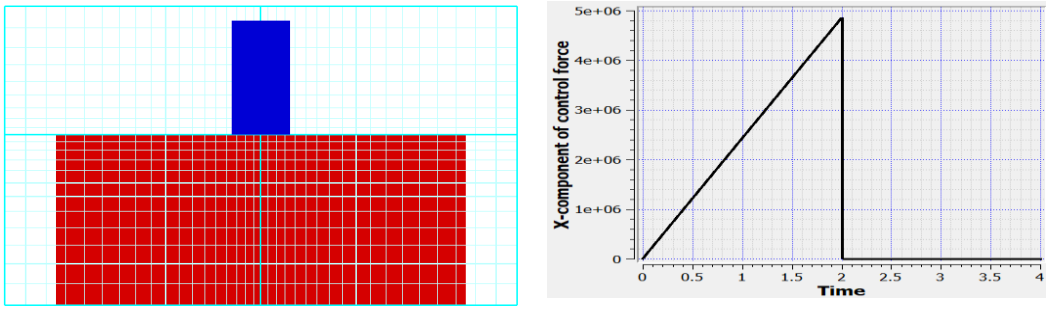

a) High block model b) Applied force on the block

Figure 4.12. High block model

Again by comparison of the numerical analysis results with the IDCE model of Pekau, the reliability of the Flow 3D-GMO model for sliding case of a moving object, is proved. The comparison can be found in Figure 4.13.

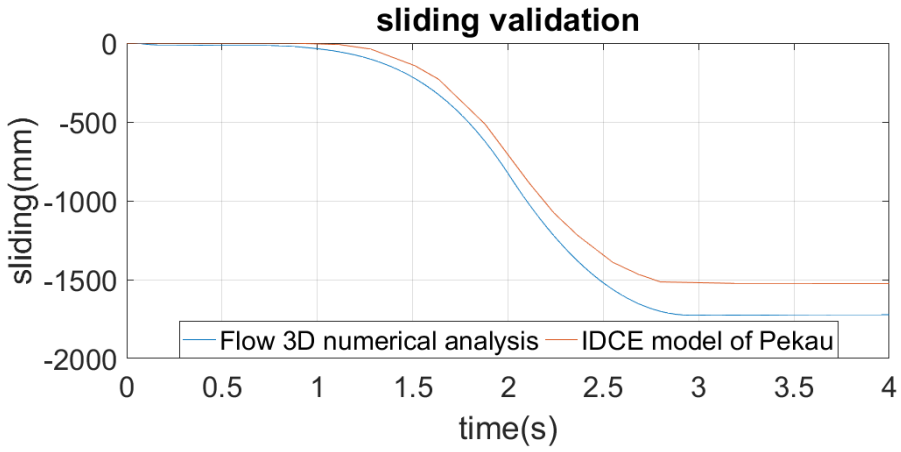

Figure 4.13. Sliding verification of the high block on the foundation

4.2.2 Dropping and Rebounding Validation

In this part to inspect GMO model capability in capturing of dropping and rebounding features of a moving object, a vertical 160mm long steel bar with a cross-

section of 1x10 mm^2 dropping from a height of 5mm above a rigid surface is tested to compare it with theoretical results. In this analysis, the coefficient of friction and restitution are respectively equal to 1 and 0.8.

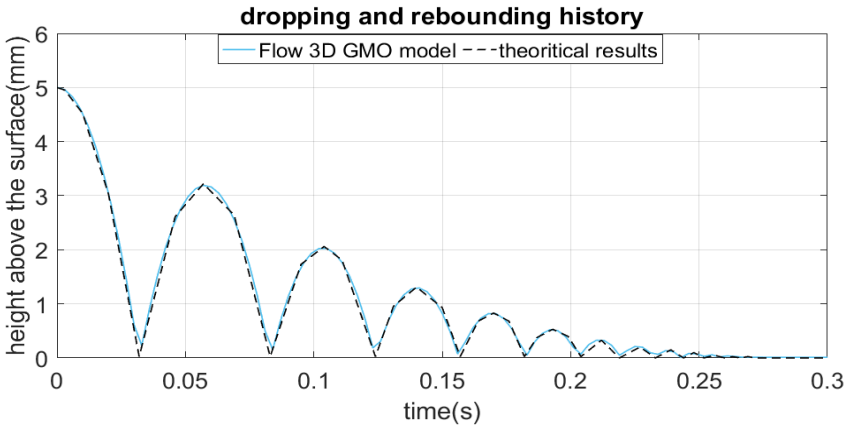

Figure 4.14. Dropping and rebounding validation

4.2.3 Rocking Type of Motion

4.2.3.1 Low Block's Rocking Validation

To study rocking and impact features of the square block in Figure 4.10.a, the mentioned block is subjected to the strong ground motion pulse of 2g. In this analysis the coefficient of friction and restitution coefficients are equal to 2 and 0.75 respectively, additionally, the utilized time step will be equal to 5E-5 s, same as Pekau analysis.

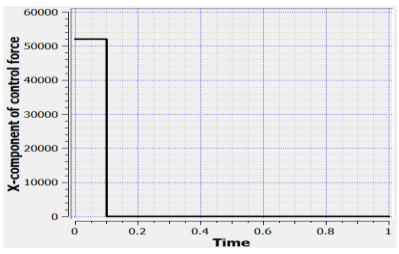

a) Applied force on the block

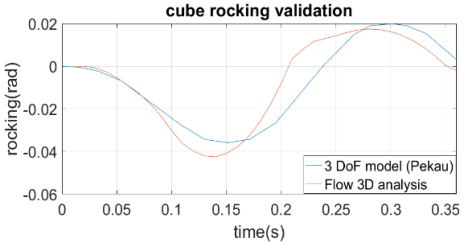

b) Results validation

Figure 4.15. Square block’s rocking motion validation

4.2.3.2 High Block’s Rocking Validation

To get an deeper insight into the issue, the high block on foundation analysis of Figure 4.12 will be repeated for the rocking case by the coefficient of friction equal to 1.2 and the restitution coefficient of 0.9. the applied force on the high block can be seen in Figure 4.16.a. Comparison of the Flow 3D-GMO model analysis with Pekau IDCE model can be found in Figure 4.16.b.

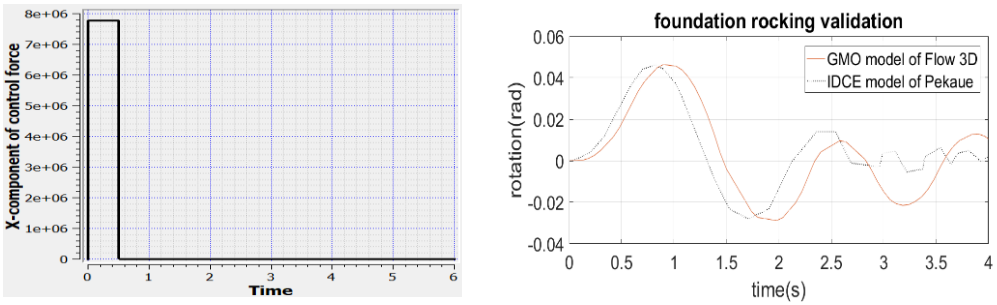

a) Applied force on the block b) Results validation

Figure 4.16. Insert figure caption here

4.2.3.3 Slender Block’s Rocking Validation

For the last analysis, a high rectangular block with a slenderness ratio of 3 was subjected to the sudden ground acceleration of 0.8g in 0.1 s. In this analysis, the coefficient of friction is equal to 1 and the restitution coefficient of 0.75 has been applied, additionally, the utilized time step is 5E-5 s same as Pekau's analysis. The comparison of the results with the 3DOF model of Pekau submitted the following results.

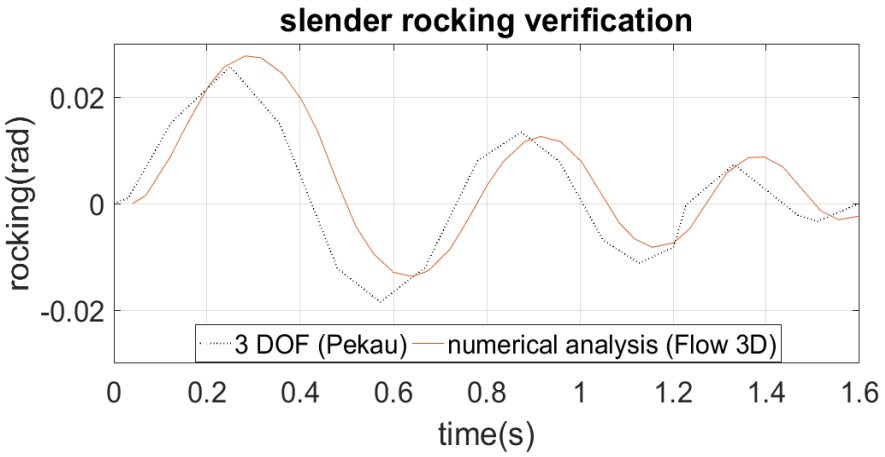

Figure 4.17. . Rocking validation of slender bar

4.2.4 The Top Part of the Cracked Koyna Dam

The top part of the cracked Koyna dam is investigated and the numerical results will be compared with the 3DOF model of Pekau ones. In the analysis coefficient of friction is equal to 1.1, also the restitution coefficient of 0.5 has been considered. Additionally, the time step size is assumed to be constant with a value of 5E-5 s during simulation time. Here it should be mentioned that the model has been considered as two blocks, and the velocity, which has been gained by numerical integration of base acceleration with 0.01 second time interval in MATLAB, has been applied to the down part or base of the dam. (see Fig. 4.18)

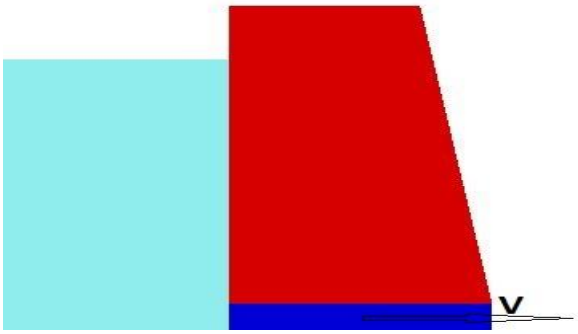

Figure 4.18. Cracked Koyna dam's CFD model

4.2.4.1 Empty Reservoir Case

In the first step, the simulation will be proceeded by considering an empty reservoir (without any hydrostatic or hydrodynamic force) then in the next part, the effects of the full reservoir will be inspected.

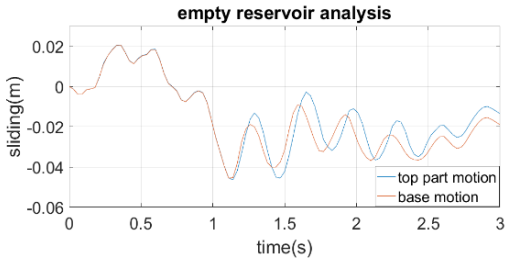

a) The motion of top and base blocks in an empty reservoir

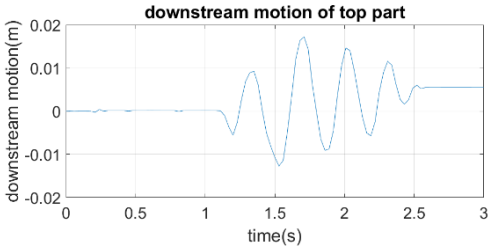

b) The downstream motion of the top block

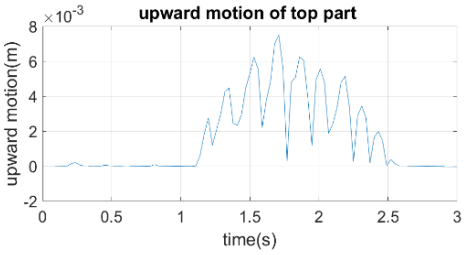

c) The upward motion of the top block

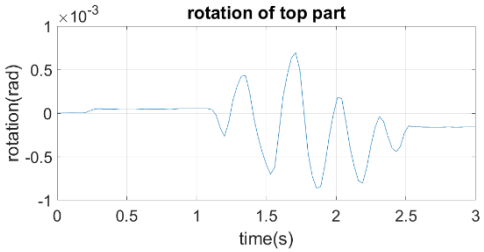

d) The rotation of the top block

Figure 4.19. Empty reservoir analysis

From figure 4.19, in the case with an empty reservoir (neglecting hydraulic forces), the top part's motion is almost the same as the base motion, which means that in the absence of water the top part will mostly fluctuate on its base with negligible detachment from it. Additionally, the relative motion of the top part in its whole degrees of freedom comprising downstream direction (X), upward direction (Z), and rotation, are presented. It can be inferred that in the case of the empty reservoir the upper part will be detached from its base just during two peak seconds of ten seconds earthquake (between 4s and 6s) and in the time between zero to four seconds and six to ten seconds, it will be oscillated sticking on the base block.

4.2.4.2 Full Reservoir Case

In this case, by filling the reservoir part of the model with water, the motion of the upper part will be inspected by considering hydrostatic and hydrodynamic forces to compare the top part motion with the empty reservoir case.

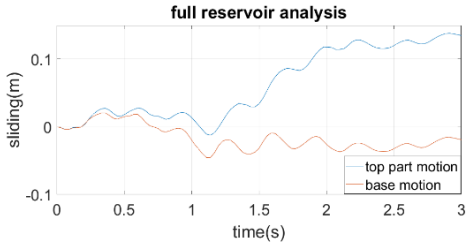

a) The motion of top and base blocks in a full reservoir

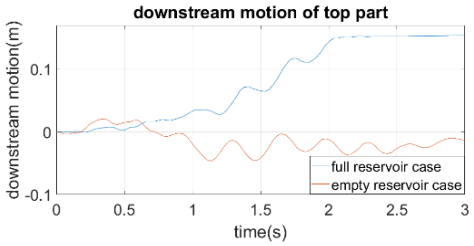

b) The downstream motion of the top block

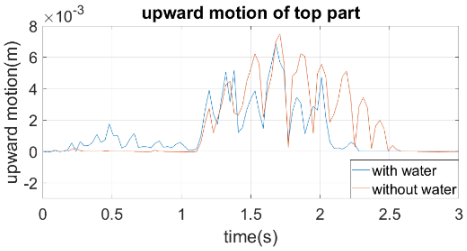

c) The upward motion of the top block

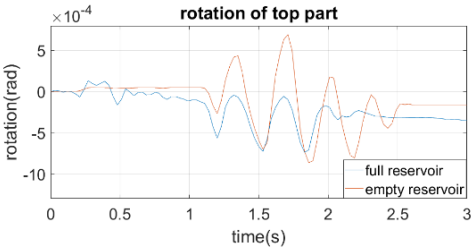

d) The rotation of the top block

Figure 4.20. Full reservoir analysis compared to empty reservoir case

From figure 4.20, again the base is smoothly sliding to the upstream direction same as the empty reservoir case, but by considering hydraulic forces, despite the empty reservoir case the top part has been detached from its base and moved to the downstream direction. Nevertheless, filling of the reservoir didn't influence the peak value of upward motion, in the case with a full reservoir, upward motion of the top part has been started and finished sooner. This phenomenon can be explained by the buoyancy force concept (uplift forces due to pressure at crack zone) that acting on the top block in the upward direction in the crack area and helps it to detach from the base sooner. Additionally, the existing water inside of the crack acts like a damper (dissipating energy) in collisions of two blocks. Therefore, the top part land on the

base block sooner in comparison with the empty reservoir case due to containing less energy. Finally, the overall rotation of the case with water is less than the empty reservoir case. As mentioned, this event is the result of existing water inside of the crack which causes the energy dissipation of the top block in collision times. The important point here to be mentioned is that however, water will increase the first rotation value because of uplift force as the result of buoyancy, retards the next rotation cycles by dissipating collision energy.

4.2.4.3 Results Validation of Cracked Koyna Dam Case

In this part the results of the full reservoir case will be validated with the Pekau 3DOF model for three cases of total sliding, drifting, and rock sliding motion. Total sliding comes from the difference of top and down part motion, additionally drifting is the value of motion when there is no contact between blocks and the rock sliding is due to existing one or two contact points.

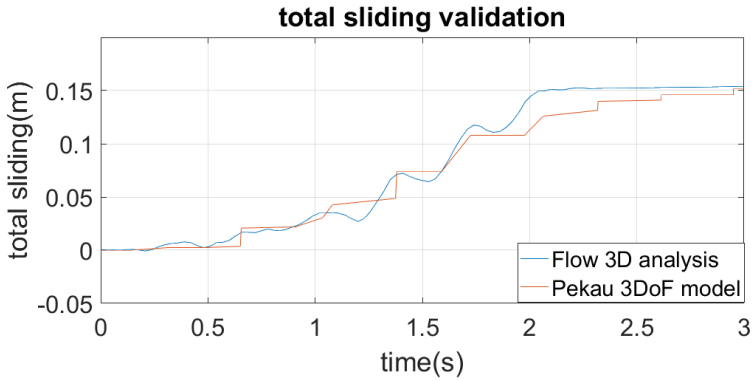

a) Total sliding validation

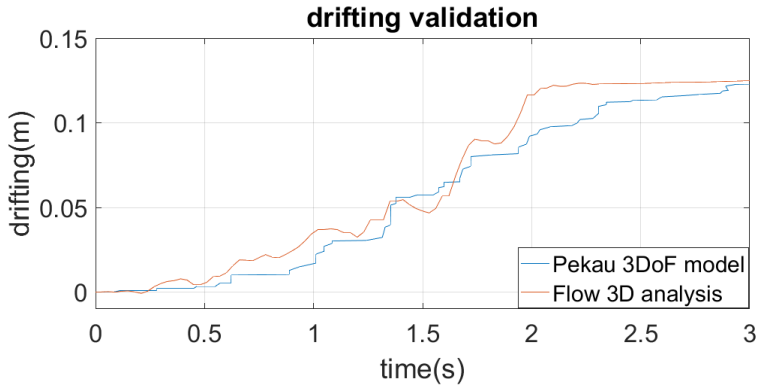

b) Drifting validation

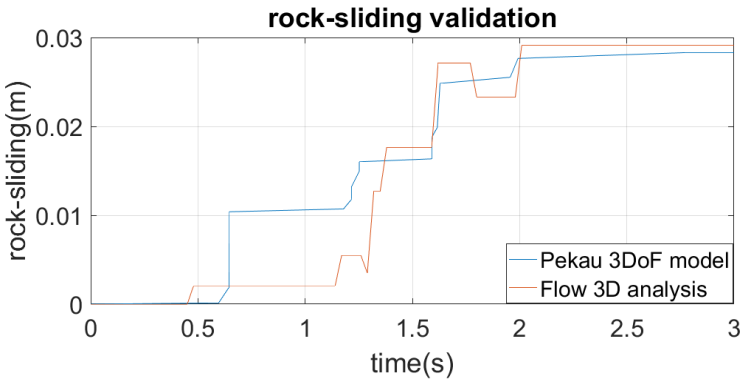

c) Rock-sliding validation

Figure 4.21. Top part motion verification in cracked Koyna dam analysis

An important point to be noted here is that a code has been developed in MATLAB software to separate the motion components from its' total value that could be found in Appendix A.

As mentioned, The difference in the results of the two methods is due to the different formulations used by the two methods. Pekaus' methods are based on the Fineite Differential method (FDM), while FLOW 3D benefits from the Fineite Volume method (FVM). In addition, due to the fact that to separate the rocking, from the motion components it is necessary to determine a tolerance value. Because FVM is able to predict the motion of objects that depend on the size of the network cells, therefore the size of the network cells must be close to zero to accurately analyze the size of the motion. In other words, the FVM cells must be small enough to act like

FDM nodes. Given that the simulation time increases sharply as the size of the cells decreases, setting a tolerance value for the rocking motion is mandatory so that if the distance between two solid objects is less than this value, the two objects are considered in contact. As mentioned, in order for this tolerance to be equal to zero, the size of the grids must be considered close to zero, which makes the simulation very difficult from time perspective. Therefore, the tolerance of the distance between two objects is defined so that the final amount of motion is correctly estimated. (see Fig. 4.21)

4.3 Discharge Analysis in Single Block Failure (Koyna Top Part)

In the scope of the following part, the discharge variation with time for three cases of crack introduced in part 4.1.1 is inspected to compare the restitution and friction coefficients effects on the value of volumetric flow rate.

4.3.1 Reservoir Size Effects on Discharge Hydrograph

Firstly, in order to inspect the reservoir size effects on the value of maximum discharge by considering constant friction and restitution coefficients respectively equal to 0.95 and 1 the reservoir size is increased in opposite of stream direction in the case of a downstream sloped case. As can be observed in figure 4.22, the reservoir size is considered to be equal to 2,3,4 and 5 times of water-free surface elevation that is equal to 55m.

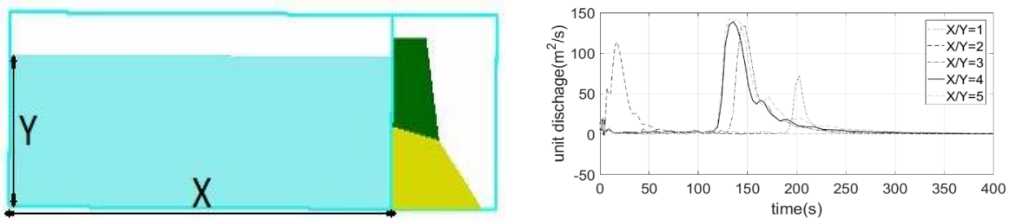

a) Reservoir characteristics b) Reservoir size effects

Figure 4.22. Reservoir size effects on maximum discharge

Considering the ratio of reservoir size (X) to free surface elevation (Y) as reservoir characteristics, it can be inferred that the reservoir size must be considered at least equal to four times of water surface elevation in order to keep the maximum discharge value and the time of capturing of its value, independent of reservoir size. In the following study to captured the discharge hydrograph, the mentioned assumption is considered for reservoir size.

4.3.2 Restitution Coefficient Effects on Discharge Hydrograph

In the scope of this part, the effects of restitution coefficients on the value of maximum flow rate and the time of capturing of this value are inspected for three cases of cracks comprising horizontal, upstream, and downstream slope. The friction coefficient for the whole of the simulations is equal to 1 and three restitution coefficients consisting of 0.5, 0.75, and 0.95 are used in the study. In this study, the far end reservoir boundary is considered as the wall to capture the complete discharge hydrograph.

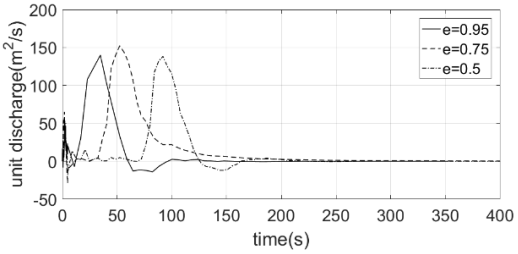

a) Horizontal crack case

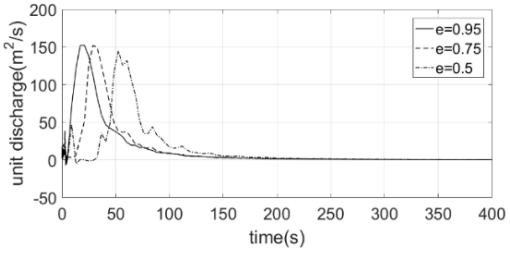

b) Downstream sloped crack case

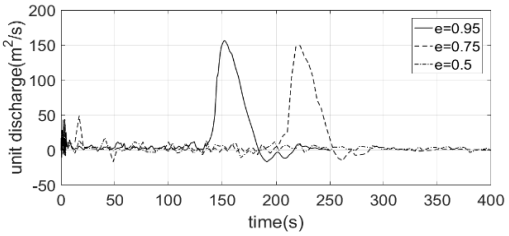

c) Upstream sloped crack case

Figure 4.23. Restitution effects on discharge hydrograph

From the analysis by increasing of restitution coefficient the top part felt sooner, therefore the fluid reached its maximum flow rate earlier (see Fig. 4.23). The point to be mentioned is that this study aims to find out the mechanism of restitution coefficient effects on falling time of the top part and to gain the exact values of discharge detailed controlling of grid size and time step values are needed that would be presented in the next parts. Lastly, the falling of the top part in the upstream sloped crack case did not happen in 400 seconds of simulation time with a 0.5 restitution coefficient. Generally, by increasing the restitution coefficient the top part would be easily drifted, and therefore it felt sooner.

4.3.3 Friction Coefficient Effects on Discharge Hydrograph

In the scope of this part, the effects of friction coefficients on the value of maximum flow rate and the time of capturing of this value are inspected for three cases of cracks comprising horizontal, upstream, and downstream-sloped. The restitution coefficient for the whole of the simulations is equal to 0.95 and three friction coefficients consisting of 0.5, 0.75, and 1 are used in the study.

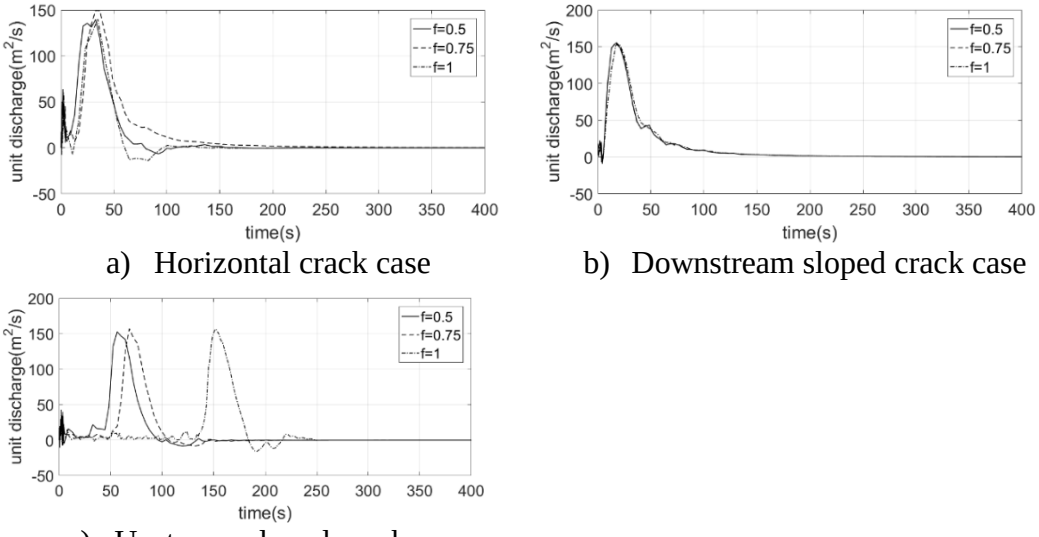

a) Horizontal crack case

b) Downstream sloped crack case

c) Upstream sloped crack case

Figure 4.24. Friction effects on discharge hydrograph (f<1)

From Figure 4.24, the time of capturing of maximum flow rate is not influenced from friction coefficient value between 0.5 to 1 in the horizontal and downstream sloped crack. However, in the upstream sloped crack case by increasing of the friction coefficient the time of capturing of maximum flow rate is postponed. It can be explained by the fact that in the upstream sloped crack the motion type is mostly sliding, however in the others drifting is the most dominant type of motion. Considering the friction coefficient range between 1 to 1.3 any relationship between the friction coefficient and the flow rate was not detected. It should be mentioned that the analysis was done by coarse grids and they are only valid for comparison. (see Fig. 4.25)

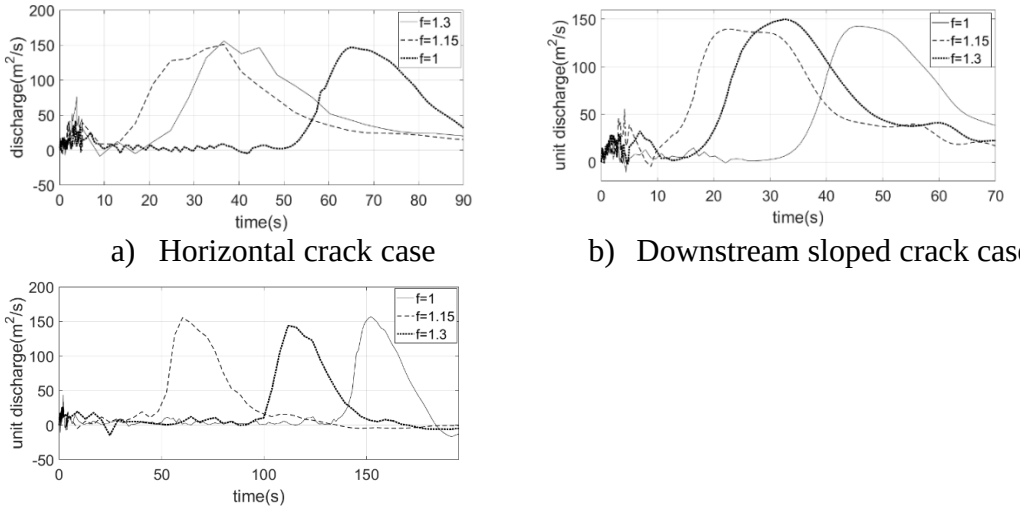

a) Horizontal crack case

b) Downstream sloped crack case

c) Upstream sloped crack case

Figure 4.25. Friction effects on discharge hydrograph (f>1)

4.3.4 Unit Discharge Value in Single Block Failure Case

This part aims to get the exact value of discharge. Therefore, by considering the constant water level in the reservoir far end boundary condition to simulate the huge size of the reservoir, the maximum discharge values are captured for three cases of crack. In the following analysis, restitution and friction coefficients are respectively considered to be equal to 0.95 and 1.

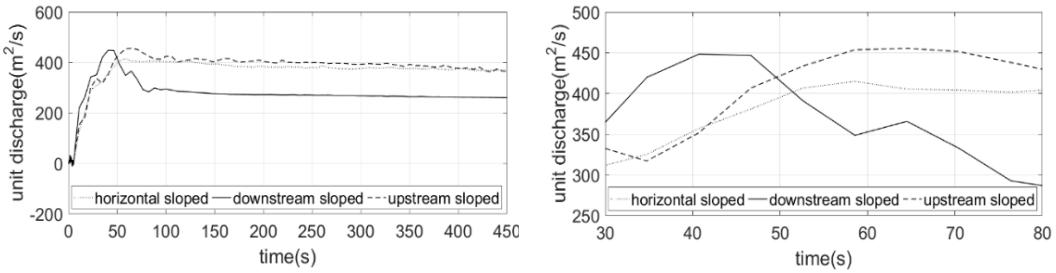

a) Three cases of cracks discharge b) The peak of the discharges

Figure 4.26. Unit discharge comparison of three crack cases

From figure 4.26, the maximum discharge values are captured respectively for upstream, downstream, and horizontal crack cases equal to 4.56E+02, 4.48E+02, and 4.15E+02 m^2/s. The time of capturing of maximum discharge values are equal to 6.45E+01, 4.07E+01, and 5.86E+01 seconds after starting of earthquake respectively for upstream, downstream, and horizontal crack cases.

CHAPTER 5

FAILURE MECHANISM INVESTIGATION OF DAM DUE TO EARTHQUAKE BASE EXCITATION

5.1 Failure Mechanism Investigation Using Concepts of Continuum Mechanics

In this part of the study, using all the analyzes of previous chapters, a model of concrete dam failure due to earthquakes that cause the dam body to crack is presented. This model includes two types of failure mechanisms. If the earthquake is strong enough to start the breaking process during its occurrence, the dam body will experience an instantaneous failure that occurs within a few seconds, and most of the body time will collapse during earthquake. The second type of failure occurs when the earthquake creates cracks in the body of the dam, but the movements transferred from the ground to the body of the dam are not sufficient to enlarge the cracks, so the dam will not collapse during the earthquake. But due to the presence of cracks that are the accumulation of stress, the body is on the verge of collapse. With the infiltration of water into the cracks created in the body of the dam as a result of the earthquake, the cracks tend to expand due to the water pressure inside them, and therefore over time, parts of the dam from which the cracks are enlarged, are separated from the standing part of the dam. This type of dam failure will occur within minutes to few hours after the earthquake base excitation, which is known as the gradual failure of the dam. In this study, both dam failure models have been investigated using VOF techniques to simulate water flow. The Koyna earthquake on the Koyna dam is investigated as a test case. Comparing the output discharge due to breaking of the dam in the case of instantaneous failure, the peak discharge was observed in 300 seconds after the earthquake, while in the model of gradual failure of the dam, this value was observed in 900 seconds after the Koyna earthquake of

magnitude 6.5 on December 11, 1967. However, this time will vary depending on the damage to the body affected by earthquakes of different strengths.

5.1.1 Introduction

During the 6.5 magnitude earthquake on December 11, 1967, the Koyna dam was severely damaged at the slope region and base part of the dam. Creating continuous cracks from upstream to downstream, if accompanied by a vibration strong enough to create instability, can be considered as the beginning of the failure mechanism. Stability in sliding and independent overturning under independent inertial and hydraulic forces is a complex issue that is primarily influenced by crack and block geometry and boundary conditions. Generally, in the breaking mechanism of the dam three cases of single block motion comprising sliding, rocking, and drifting were seen. To inspect the motion of the top part in detail the concepts of drifting, rocking, and sliding motions are defined as the displacement of the top part with respect to the base when there are respectively 0, 1, and 2 contact points between blocks (see Fig. 5.1). A comprehensive study on the integrated behavior of the damaged dam has been performed using a finite volume technique to identify the main factors affecting the collapse mechanism.

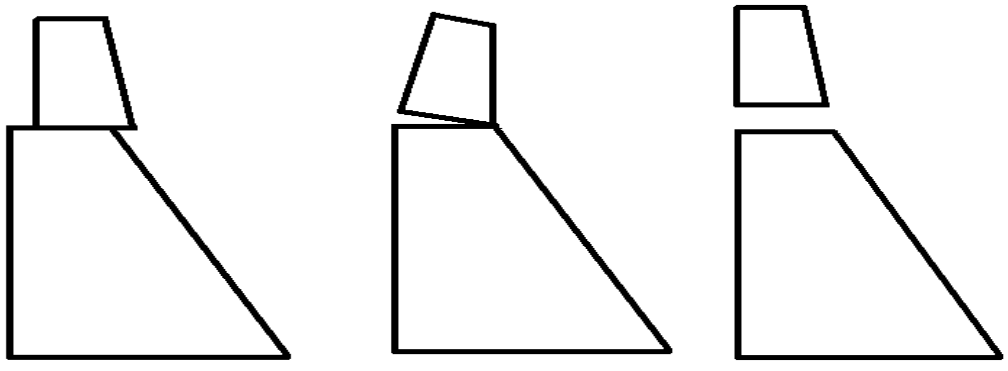

a) Pure sliding b) Pure rocking c) Pure drifting

Figure 5.1. Single block motion in pure sliding, rocking and drifting type of motions

The displacement of the detached block from the dam's body can experience compositions of the mentioned motion types. The sliding type of motion is the result of a low friction coefficient between blocks. This type of block motion is common in small earthquake magnitudes with high duration because in that case there is sufficient time for water to penetrate the crack and decrease the friction coefficients between contacting blocks by buoyancy force. The rocking of the separated block is the result of high friction coefficient and it is mostly observable in pulse base acceleration. During the occurrence of a large magnitude earthquake with a small duration, there is not sufficient time for water to penetrate totally into the crack, therefore it will stagnate somewhere before the end of the crack. Pressure distribution inside of the crack with the static pressure level of the 200kPa in the normalized earthquake with a maximum crack mouth opening of 0.4mm, crack length of 0.55m, and the oscillation frequency of 10Hz, is given at maximum and minimum pressure conditions in Figure 5.2. The figure provides the causes why the rocking process takes place.

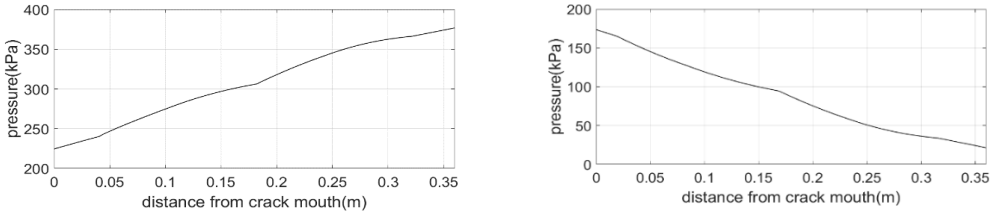

a) Maximum pressure distribution (t=5.08s)

b) Minimum pressure distribution (t=5.02s)

Figure 5.2. Pressure distribution inside of the crack

The first supporting reason for the occurrence of rocking is the pressure variation inside the crack; the maximum pressure value in the point is almost two times the corresponding value in the crack mouth opening (Fig 5.2a). The second reason is that when the pressure value at the end of the crack is reached to its maximum, the corresponding value in the crack mouth is in its' minimum range, therefore the block is prone to rock. Lastly, the drifting of the separated block is seen when the earthquake magnitude is very big that can directly overcome the cohesive forces of the construction material, which is not common in concrete structures.

5.1.1.1 CFD Model Generation

The CFD model consists of 32 cubic rigid blocks with 10m dimensions to form the Koyna Dam in two dimensions, located on a large base block, which is considered as the ground under the dam. In fact, 32 cubic blocks is the minimum number of blocks to form the Koyna dam's body in two dimensions. More precisely, the defined model is first verified with the largest block size to obtain the necessary information about the mechanisms of failure in gradual and sudden cases, then to more accurately determine the failure process, the number of blocks will be increased to achieve fixed results. It is necessary to mention that the Flow 3D has the ability to form movable blocks up to 500 pieces. Vertical and horizontal, velocity-time series of Koyna earthquake are prescribed for the base, allowing the upper blocks to be moved in three degrees of freedom. FLOW 3D as a CFD code uses a finite volume technique; therefore, the current domain in the mesh plane is divided into rectangular cells. In the vertical direction, the upper boundary condition was set to a zero-gradient condition applying zero velocity gradient normal to the boundary, and the lower boundary was set as a fixed wall with the non-slip condition. In the Y-direction both the boundaries are set to symmetrical. A stagnation boundary was defined at the left boundary in the stream direction of the model: the vertical velocity upstream from the boundary was zero keeping the reservoir at a constant level. A wave absorbing layer was also placed here at the far end of the tank to prevent the wave from reflecting from the boundary. For the right border, the outflow was activated. Static tank conditions were considered as initial conditions with a reference pressure value equal to atmospheric pressure. (see Fig. 5.3)

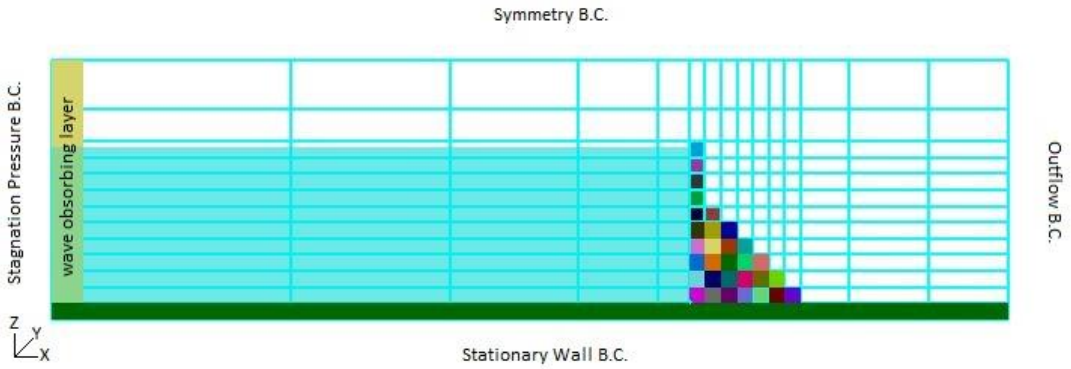

Figure 5.3. Utilized mesh planes and boundary conditions in CFD model

5.1.1.2 Finite Element Analysis of Stress on the Dam's Body

Firstly, to get an insight into the failure mechanism of the dam, finite element analysis was performed on the full reservoir Koyna dam with water surface elevation of 96.5m during the 1967 Koyna earthquake with a magnitude of 6.5, the results of which are presented in Figure 5.4. In this study, the thermal expansion coefficient, bulk, shear, young modulus, and Poison ratio of concrete are considered to be respectively equal to 1e-5 1/K, 14.7 GPa, 13.4 GPa, 30.8GPa, and 0.15.

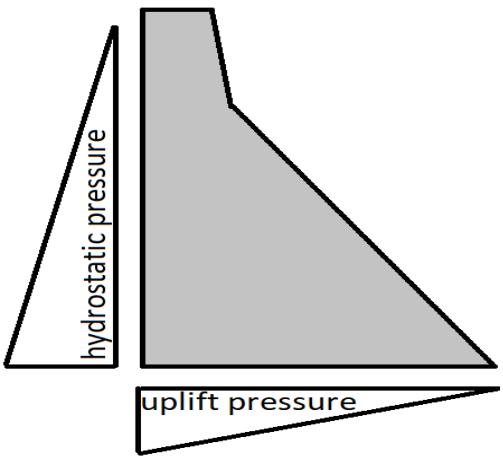

a) Prototype model in t=0s

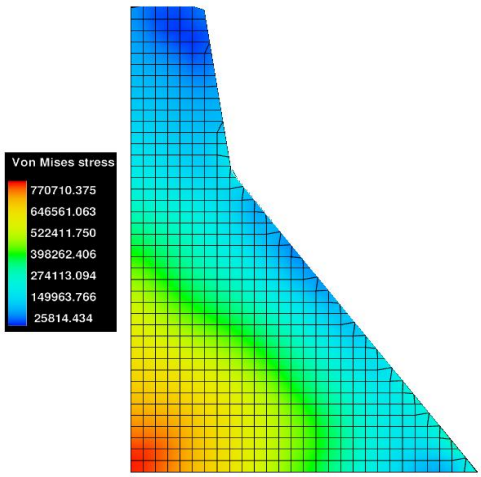

b) Stress analysis in t=0s

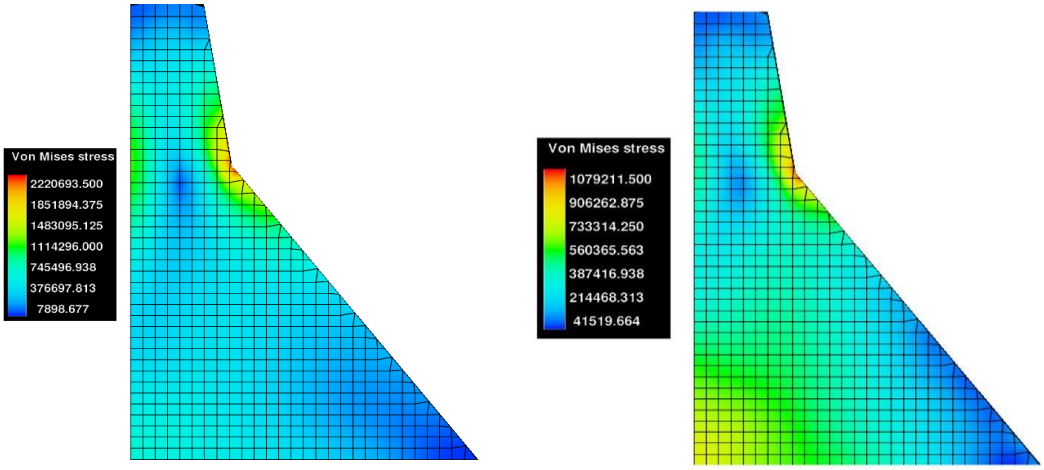

c) Stress analysis t=5s d) Stress analysis t=10s

Figure 5.4. Stress analysis on Koyna dam's body

From a stationary model that can be seen in Figure as the results of hydrostatic and uplift pressure, the most vulnerable part of the dam in the static condition is the bottom-left corner of the body. The same result is captured by finite element analysis with Flow 3D that is presented in Figure 5.4.b. Since the maximum intensity of the earthquake occurs in a period of 4 to 6 seconds from its starting, the most vulnerable part of the dam is captured at the slope changing area at t=5s. After passing the earthquake peak, both regions including slope changing location and the lower part of the dam was identified as high-risk areas to begin the process of dam failure. Generally, post-earthquake analysis on the dam body confirms the presence of cracks in the two zones of narrowed and the lower part of the dam therefore, the finite element solution is acceptable.

5.1.2 Failure Inspection

The process of breaking a concrete dam begins with the creation of cracks in the body and eventually, the expansion of these cracks ends with the complete separation of the cracked part of the dam. Due to the presence of cohesive forces between solid molecules, in the process of breaking the areas on both sides of the crack can move

in one degree of freedom before complete separation from the main body. After the completion of cracking, the separated part can move in all directions. To simulate the initiation of the dam failure due to earthquake base excitation, the blocks forming the dam, are allowed to move in only one direction. Therefore, three models can be defined for the starting of the failure process in a two-dimensional analysis. This involves moving the blocks in one of the streamwise, upward, or rotational directions, which leads to three modes of sliding, drifting, and rocking failure initiation, respectively. (Fig. 5.5)

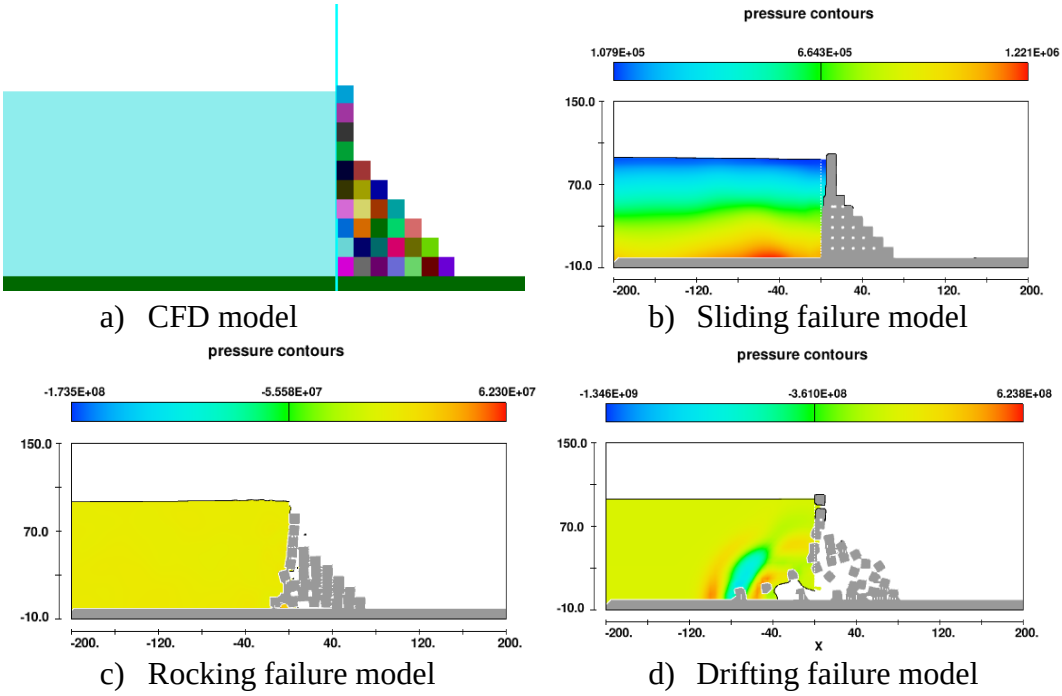

a) CFD model b) Sliding failure model

c) Rocking failure model d) Drifting failure model

Figure 5.5. Sliding, rocking, and drifting mode of dam failure initiation

5.1.2.1 Dam Failure Mechanism

Generally, the breaking of a structure initiated in the drifting mode is the result of a large magnitude energy release in a short time, similar to a bomb explosion. During an earthquake, the concrete structures rarely can experience this kind of failure because of the cohesive force among their molecules. In other words, if such an earthquake occurs, no structure will remain on the ground. Therefore, the beginning

of the failure process should be either in sliding or rocking mode. Microscopically, if the magnitude of the earthquake could cause developments of cracks in the dam body, the crack walls will oscillate during the earthquake. As a result, the pressure value inside of the crack would change due to water movement and it will be at its maximum level at the end of the crack because of the fluid stagnation. The pressure variations in different locations inside the crack due to base excitation are presented in Figure 5.6. These pressure variations inside the cracks can continue developing until the detachment of blocks from the dam's body.

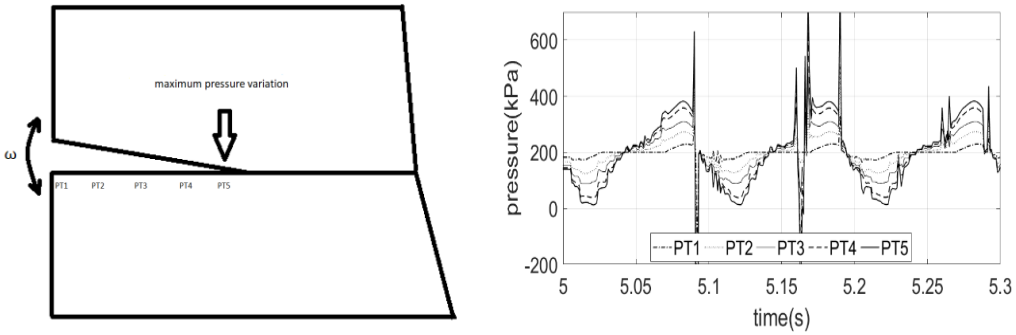

a) Crack walls motion

b) Pressure variation inside of the crack

Figure 5.6. Inside crack pressure variation

From the analysis of a single block motion that is mentioned in part one of the study, due to the pressure distribution within the cracks and due to the fact that there is still adhesion in the attached part of the crack, the crack walls can only rotate on a very small scale. Therefore, the beginning of the dam failure process during the earthquake will be in the rocking mode.

5.1.2.2 Bounding Forces Simulation

Concrete beams are designed to crack in tension rather than in compression, therefore if an earthquake force can overcome the tensile strength of concrete the cracking will happen. To simulate the cohesive force of concreate by its weight, the density of the block should be equal to or greater than tensile strength. Simply the

earthquake force is stretching the body in the opposite direction of the cohesive force of concrete to break it down.

Considering any rectangular block with the surface area of a*c and height of b contacting with other one or resting on the ground. As mentioned, to simulate the cohesive force of concrete by the weight of the block the density of the block should be increased (Fig. 5.7). If an earthquake force is larger than the tensile strength of concrete, the cracking of the body would be seen. To simulate the cracking condition, the cohesive force is substituted with the increased weight of the block as the bounding force, and the earthquake force is considered to be equal to the tensile strength of concrete multiplied by the applied surface area.

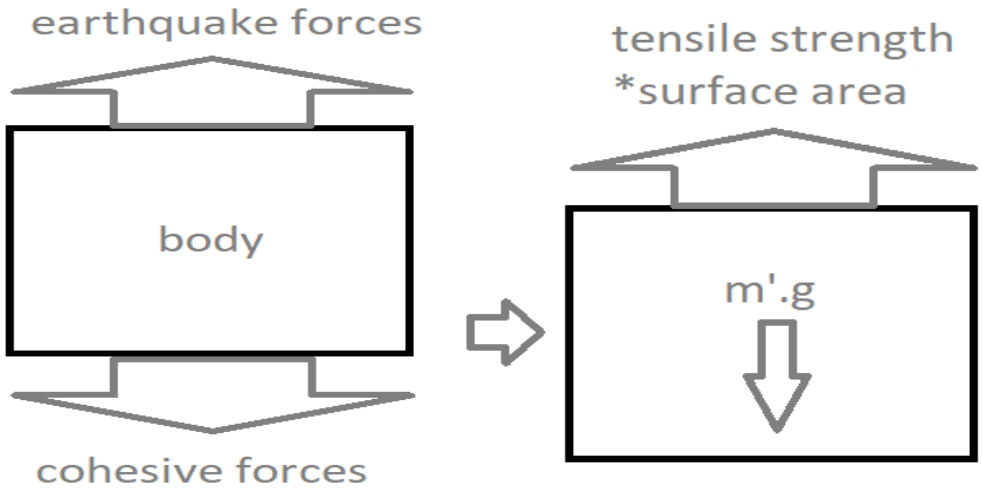

Figure 5.7. Bounding forces simulation concept

To keep the block from cracking, the increased weight should be equal or greater than the tensile strength applied on the surface area.

$$m'.g \geq T.A \rightarrow \quad (5.1)$$

$$\rho'.(a.b.c).g \geq T.(a.c) \rightarrow \quad (5.2)$$

$$\rho'.b.g \geq T \rightarrow \quad (5.3)$$

$$\rho' \geq \frac{T}{b.g} \quad (5.4)$$

Considering the most vulnerable part of Koyna dam as the slope changing area, the value of b will be equal to 40m, and if we consider tensile strength of concrete equal to 5Mpa:

$$\rho' \geq \frac{5E+6}{40*9.81} \quad \rightarrow \rho' \geq 1.3E+4 \ \frac{kg}{m^3} \tag{5.5}$$

Because tensile strength is the minimum strength of the concrete and in real cracking, the cracking area is experiencing both tension and compression the density value must be bigger than 1.3E+4.

On the other hand, according to Richard et al. (1995), the maximum recorded strength of concrete against compression is equal to 810 MPa. Similarly, since a concrete structure shows its maximum resistance to compression, adhesion force of the concrete or the weight force with increased density must be less than the compressive force, therefore:

$$m'.g \leq C.A \rightarrow \tag{5.6}$$

$$\rho' \leq \frac{C}{b.g} \rightarrow \tag{5.7}$$

$$\rho' \leq \frac{8.1E+8}{40*9.81} \quad \rightarrow \rho' \leq 2E+6 \ \frac{kg}{m^3} \tag{5.8}$$

With all that said, the acceptable range for modified density to simulate the adhesion force of concrete is between $1.3E+4$ and 2E+6 $\frac{kg}{m^3}$.

$$1.3E+4 \ \frac{kg}{m^3} \leq \rho' \leq 2E+6 \ \frac{kg}{m^3} \tag{5.9}$$

As a basic assumption, in the mentioned interval, for the sudden failure model, the value of the modified density is considered to be equal to 1E+5 $\frac{kg}{m^3}$ because the dam body is mostly in tension during the earthquake, while for the gradual dam failure model, the value of modified density is assumed to be 1E+6 $\frac{kg}{m^3}$ to simulate the

combination of tension and compression, finally, the effects of the modified weight value will be investigated for both the cases.

5.1.3 Failure During the Earthquake (Sudden Failure)

To develop the model of breaking utilizing concepts of continuum mechanics, the blocks' displacement should be considered in one degree of freedom at the initial time of breaking then they let to move in their three degrees of freedom in two-dimensional analysis. By the mentioned assumption it is possible to simulate bounding forces among the blocks by increasing their weight. If the blocks let initially move in the upward or streamwise direction the dam failure would be in drifting mode or the sliding mode, respectively. These kinds of failures are not common during the earthquake, because the blocks are stuck together and as a result of base excitation the sidewalls of the crack are in rotation around the attached part of the blocks. To simulate the breaking mechanism during earthquake it is logical to consider the blocks' motions initially as pure rocking and after the first rocking cycle of any block, it should be let to move in its three degrees of freedom. To achieve the mentioned objective, the bounding forces should be equal to the tensile strength of the concrete in the smallest contacting area among the blocks. Considering a unit volume of the concrete the density of blocks is considered to be equal to 1E+5 $\frac{kg}{m^3}$ to overcome the bonding tensile force of 5Mpa in the unit area. By increasing the density of blocks to the mentioned value all of the blocks are prevented from rotation and therefore the dam did not fail at the time of the earthquake. The important point is that after the initial rocking cycle of each block its density is returned to the regular concrete density of 2500$\frac{kg}{m^3}$.

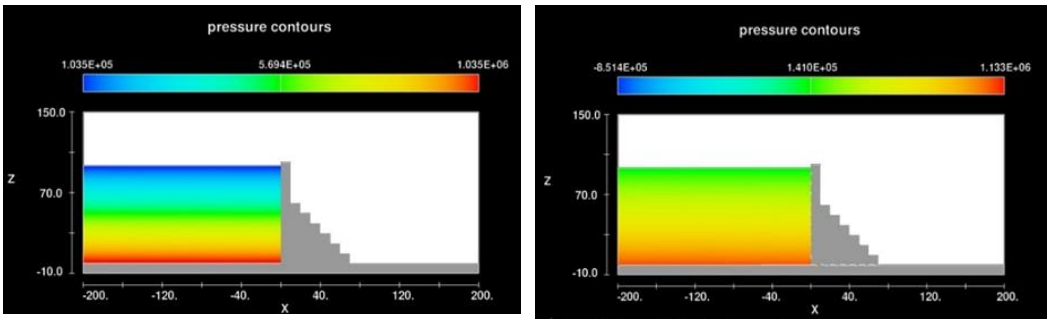

a) Body prototype before earthquake(t=0s)

b) Body deformation after earthquake(t=10s)

Figure 5.8. Failure of Koyna dam in the earthquake time

From the analysis the tensile strength is sufficient to stop the blocks from pure rocking, therefore the dam did not fail during the earthquake. By reducing the tensile strength or density of objects the fracture of the body can be simulated. Considering the tensile strength of the used material in construction 10 times smaller than concrete e. g. plaster, the modified density of the blocks in pre-breaking time should be defined as 1E+4 $\frac{kg}{m^3}$.

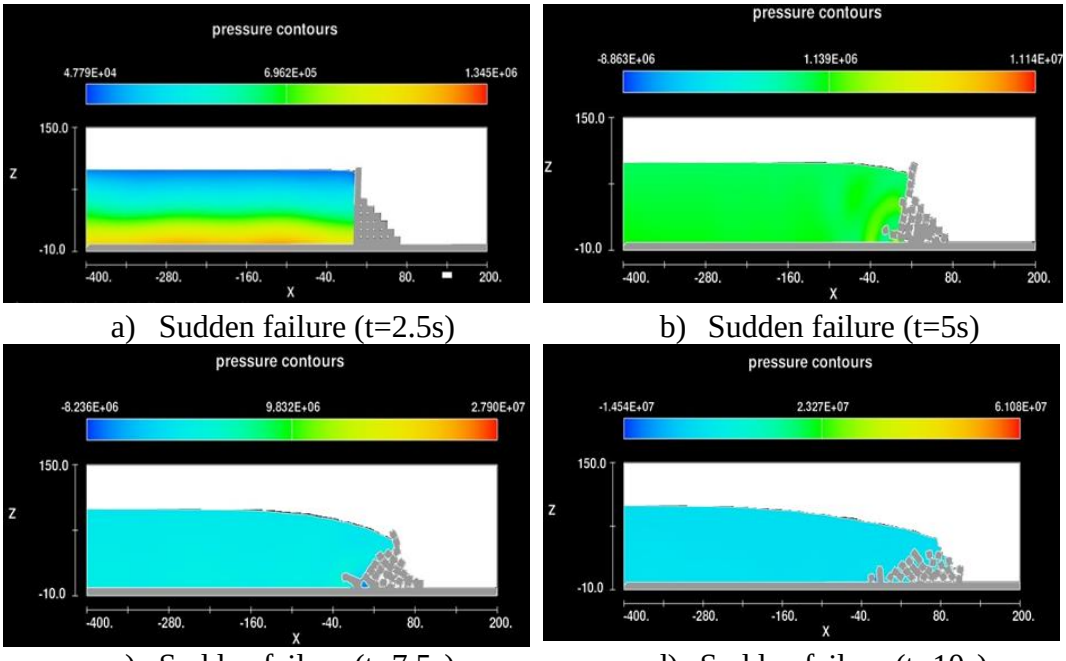

a) Sudden failure (t=2.5s)

b) Sudden failure (t=5s)

c) Sudden failure (t=7.5s)

d) Sudden failure (t=10s)

Figure 5.9. Failure of hypothetical plaster dam

5.1.3.1 Sudden Failure Inspection in General

In the scope of the following part by considering the normalized earthquake the destructivity of the earthquake in different magnitudes and frequencies of base excitation is inspected. Dams' body consisting of 32 blocks with a modified density of 1e+5 $\frac{kg}{m^3}$ is used to simulate the failure. The density of each block is returned to the original concrete density after the first rocking cycle of each one. Additionally, the coefficients of restitution and friction are considered to be equal to 0.95 and 1, respectively.

The point to mention is that in the following study the desired event is to observe the failure of a dam during the earthquake, therefore the rock sliding mode of failure is utilized. For each oscillation magnitude, the study starts from the high oscillation frequency to observe the non failure mode, then the oscillation frequency will be decreased until the dam failure occurs. The research is repeated for different frequencies by resizing the magnitude of oscillations to achieve the required magnitude value for the failure of the dam.

To avoid the effects of the base (earth) mass, the velocity fields are applied to the plate under the dam as the earth surface. As a sample, the velocity and acceleration time series of an earthquake with a velocity magnitude of 0.1 m/s and frequency of 1 Hz is given in Figure 5.10.

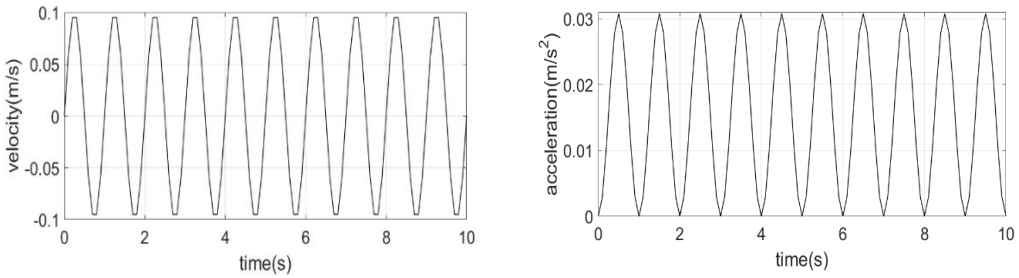

a) Velocity time history b) Acceleration time history

Figure 5.10. Normalized earthquake characteristics

5.1.3.2 Critical Frequency of Sudden Failure

Unit discharge passing through the crack is measured to identify cracking. If the discharge is amplified at a certain time this means that cracking has occurred. By decreasing the frequency of the oscillations for a given velocity amplitude, the unit discharge value increases for all the cases (Fig. 5.11). Going into the depth of the issue, sinusoidal velocity waves with an amplitude of 1 to 0.5 m/s can be destructive in frequency around 1 Hertz, however, in the amplitude between 0 to 0.5 m/s just a very high period of oscillations can cause the failure of the dam. Additionally, by increasing the amplitude of oscillations the dam is prone to fail sooner. In smaller amplitudes, the dam will not fail in sudden state, for the range of different earthquake oscillations frequency.

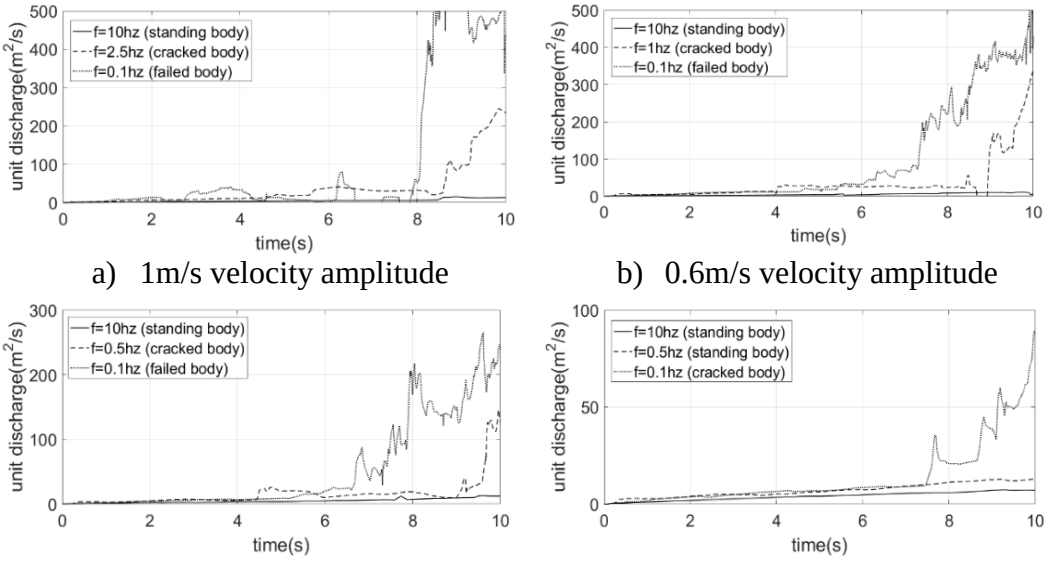

a) 1m/s velocity amplitude b) 0.6m/s velocity amplitude

c) 0.3m/s velocity amplitude d) 0.2m/s velocity amplitude

Figure 5.11. Stationary, cracking, and failure frequencies

Generally, a dam's body can experience three events during the earthquake:

1. In the case with a big frequency of oscillation and smaller amplitude than the critical ones the body will not deform; therefore, it will remain in its stationary condition with no cracking.

2. In the range of frequency and amplitude close to critical ones, the body will be cracked during the earthquake and it would break down after base excitation, therefore the failure is gradual.

3. In the case with frequency and magnitude of earthquake higher than critical ones, the body parts are detached and moved with the surrounding water and the dam's body is experiencing breaking during base excitation, this kind of failure will be a sudden break.

5.1.3.3 Analysis of Sudden Failure Initiation

In this part of the research, at any magnitude of the ground velocity wave, the largest frequency that can collapse the dam is obtained by numerical trial and error. The mentioned oscillation frequency is known as the critical frequency and any frequency less than this value at a constant velocity amplitude will cause the failure of the dam. The variation of critical frequency and failure initiation time with the velocity amplitude is given in Figure 5.12. The change of failure initiation time with the critical failure frequency is also shown in this figure.

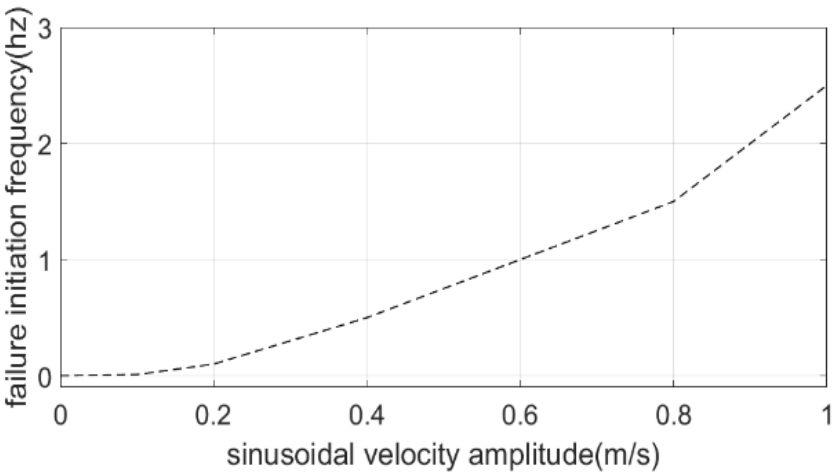

a) The critical frequency of failure vs. velocity amplitude

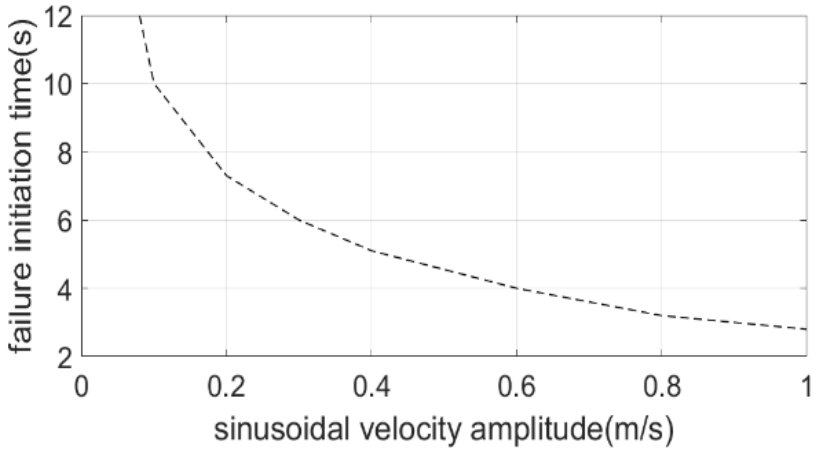

b) The failure initiation time vs. velocity amplitude

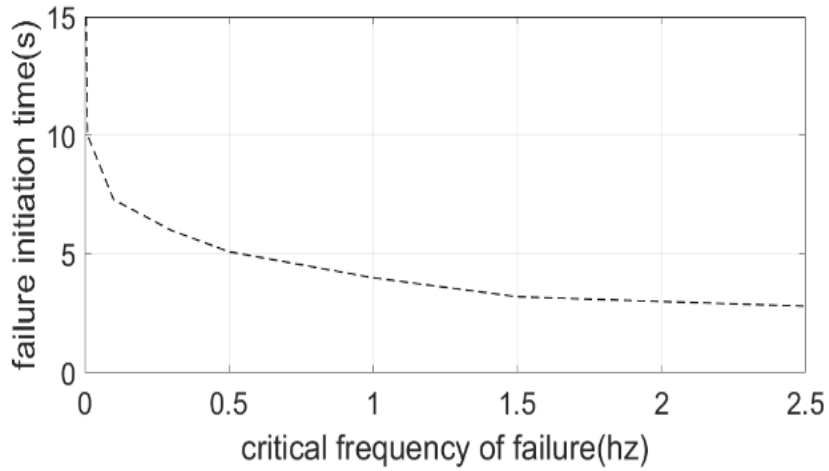

c) Critical failure time vs. critical frequency

Figure 5.12. Failure analysis using velocity concept

As can be seen from this figure, higher speeds of the base will be able to break down the dam at higher frequencies and, of course, in less time. Another important point to note is that according to Figure 5.12.c, it can be declared that before starting the failure process an earthquake with a smaller frequency of oscillation is more destructive, however, after initiation of the failure process the earthquake with a higher frequency of oscillation will break it down sooner. In other words, a higher frequency of oscillation can develop existed cracks sooner however for the initial creation of them lower oscillation frequency is more effective. To better understand

the subject, various critical acceleration waves, that can cause the formation of crack, are plotted to compare the starting time of failure in Figure 5.13.

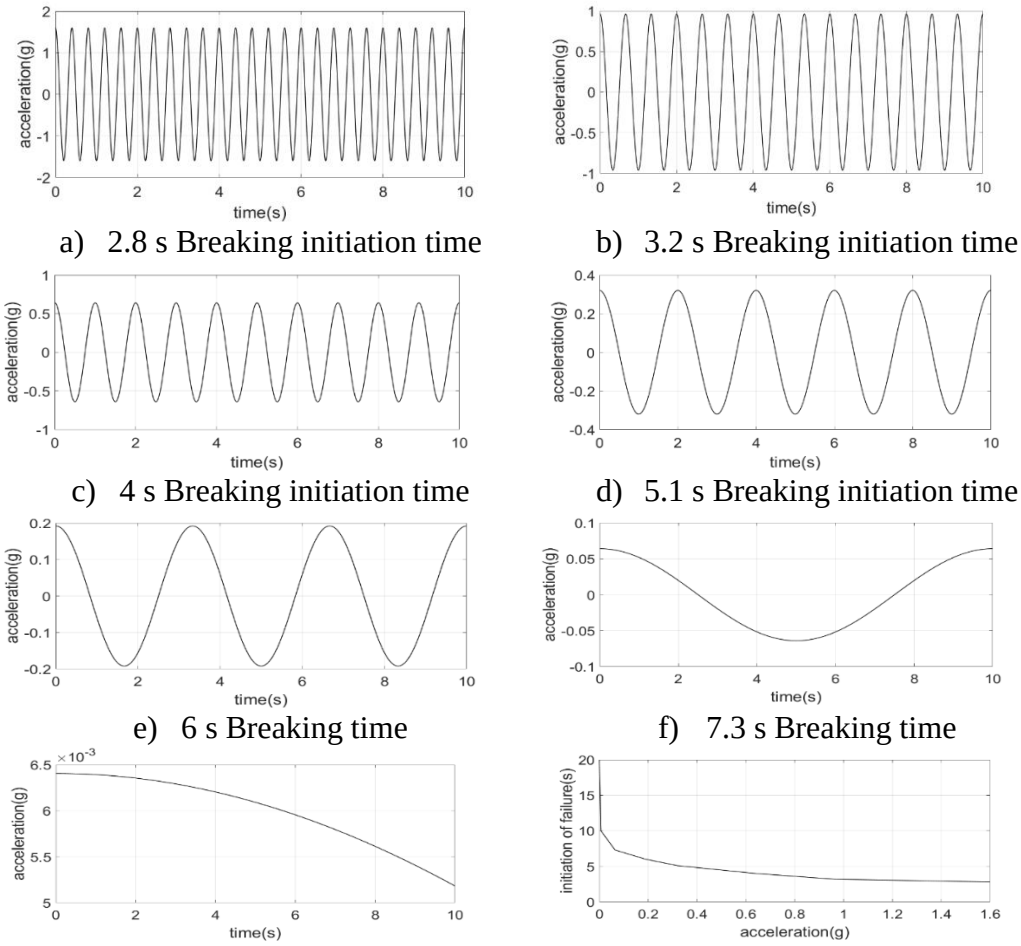

a) 2.8 s Breaking initiation time

b) 3.2 s Breaking initiation time

c) 4 s Breaking initiation time

d) 5.1 s Breaking initiation time

e) 6 s Breaking time

f) 7.3 s Breaking time

g) 10 s Breaking initiation time

h) Failure initiation time with acceleration in the critical frequency

Figure 5.13. Failure analysis using acceleration concept

From this analysis, at the higher ground accelerations, smaller periods are needed to start the failure process, while the same earthquake can break the dam in less time than earthquakes with smaller accelerations, although they have larger periods. In other words, if two earthquakes can break down a dam the one with a bigger amplitude will fail it sooner in comparison with the other that has lower amplitude, nevertheless, its period is bigger. In summary, by increasing the seismic acceleration or decreasing the oscillation frequency, hydraulic structures will be more at risk of

failure, whereas if the cracking of the structure occurs during an earthquake, higher oscillation frequencies will be able to propagate the cracks faster resulting in a sooner collapse of them.

5.1.3.4 Effects of Modified Density on Failure

As mentioned in the previous sections in this study, the adhesion force between concrete blocks has been simulated by modifying the weight of the blocks. As the density of the blocks increases, their gravitational force increases and as a result their upward motion slows down. Besides, due to the existence of friction among the blocks and the fact that the exerted friction force on an object is directly related to its weight, their movements in the downstream direction are limited too. Finally, to determine the constraint against the rotational motion, it is sufficient to consider the coefficient of friction among the blocks equal or less than one. The main reason for the pure rocking movement is the high coefficient of friction between the moving objects, which is confirmed by numerical analysis in chapter four. The pure rocking motion is observed only before the complete separation of the block from the main body. Due to the adhesion force of the concrete, there will be a very high coefficient of friction between the upstream and downstream parts of the crack. The concept of density increase to simulate the contact forces and adhesion of concrete is explained in more detail in part 5.1.2.2, where the possible density range is also given.

Although concrete structures are more prone to crack due to tension, there will be a combination of tension and compression at the contact surface of the two blocks due to the rotational movements of the walls on both sides of the crack. Thus, the effects of modified density value on failure initiation characteristics have been inspected. The important point is that after the initial rocking of each block its density is returned to concrete's regular density of $2500\frac{kg}{m^3}$.

Failure frequency values for different velocity amplitude and different block densities are given in Figure 5.14.a. It should be mentioned that in this figure the

failure frequency is the minimum value that can break down the body. In other words, for a constant velocity amplitude, any frequency smaller than the read value from Figure 5.14.a will break the dam. By assigning densities greater than 2e + 6 $\frac{kg}{m^3}$ to the blocks, dam failure is not observed in any of simulated normalized earthquakes.

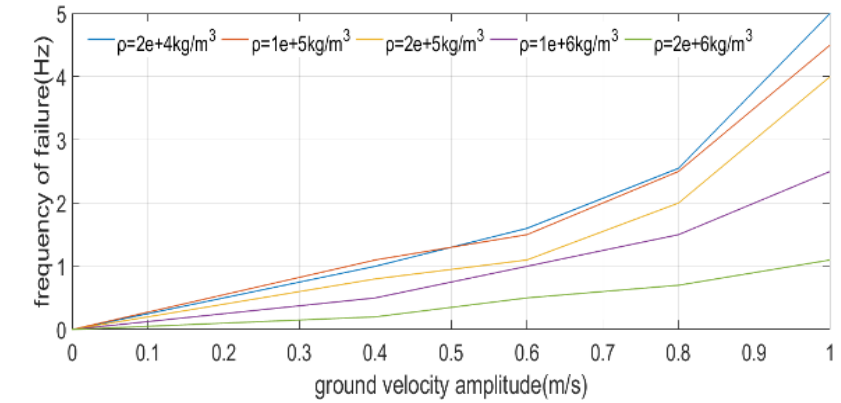

a) Density effects evaluation

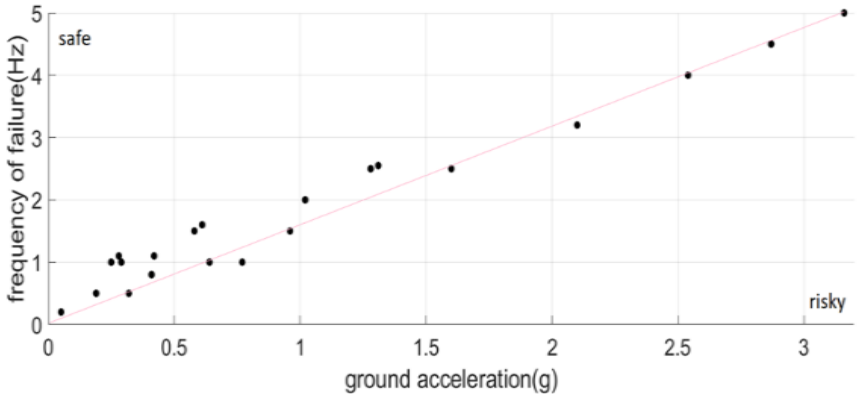

b) General model independent of the density value

Figure 5.14. Analysis of density effects on failure initiation to generate the general model of sudden failure initiation

By plotting the critical frequency at different acceleration values Figure 5.14.b is obtained. This plot comprising all the density values between 2e+4 and 2e+6 $\frac{kg}{m^3}$ where the data points seem to be in a linear trend. By drawing the trend line, any earthquake located below the line will be able to break the dam suddenly. Near the

line, cracking of the body is the most probable event, and by moving away from it upward to the left corner in the figure, the earthquake will be less dangerous.

5.1.4 Failure After the Earthquake Base Excitation (Gradual Failure)

As seen in the CFD model, the Koyna Dam did not collapse due to the 6.5 magnitude earthquake of 1967, since the bounding forces among the blocks were slightly greater than the tensile strength of the concrete, as none of the blocks show rotational motion at the increased density value. Similarly, in reality, the Koyna Dam did not collapse at the time of the 1967 earthquake, and only some cracks were observed in the slope changing and base region of the body after the earthquake. As mentioned before, during the earthquake due to the excitations of the earth, the blocks are only able to rotate before separating from the main body. However, after the earthquake, the earth returns to a static state and if cracks are created in the body during the earthquake, development of these cracks as a result of the water pressure penetrating into them will cause gradual failure of the dam. The water inside the crack tends to penetrate more to break its stagnant state, so as soon as the crack is completed, the water comes out of the static state and causes the initial movement of the separated block in a sliding type of motion. Therefore, to capture the breaking mechanism after the earthquake, the initial degree of freedom before the breaking of blocks are considered to be stream-wise sliding. In other words, after the earthquake, the body is in stationary condition and the pressure values inside of the developed crack are at a constant level of hydrostatic pressure.

If the failure takes place after the earthquake, the initial motions of blocks are limited to stream-wise sliding and after initial sliding, the blocks are let to displace in all directions. In order to achieve gradual failure of the dam, after reaching a critical value of sliding the solid objects should be allowed to freely displace. Therefore, calibration of this limiting sliding value with a realistic dam failure time should be done.

In Table 1 the first, second, third, crack formation times are given together with the complete failure time. This table is based on the critical or limit sliding value, which is defined as "streamwise moving of the block before the modified density returns to the regular concrete density". By defining different values for critical sliding, different gradual failure times will be obtained, therefore defining a single value of critical sliding is challenging due to the lack of dam failure experimental data. There are two ways to deal with this, including:

1. Define the maximum sliding recorded among the blocks just after the earthquake, as the critical or limit sliding value. In this case, the simulated model will be the fastest gradual mode of dam failure.

2. Take advantage of the fact that the gradual failure of the gravity dams takes time between 0.1 to 0.5 hours. In this case, a range for "dam failure time" will be obtained.

In this study, to simulate an example of gradual dam failure using the data in Table 1 and using the second method mentioned above, the limit sliding value equal to 0.125 meters is determined. Therefore, after sliding by 0.125 meters, the blocks are allowed to move freely in all directions at the same time as the density decreases to the actual value of concrete density. In general, the first cracks are seen in the slope changing region, Where the most stressful part of the body is during an earthquake, therefore the gradual failure process begins with the falling of the blocks located in the upper part of this area. Then, due to the increase of drag force due to the passage of water through the broken part of the dam, the blocks located at the highest unbroken part of the dam collapse. This scenario is repeated and another layer of blocks collapses from the top of the unbroken body. Eventually, cracks form from the bottom of the remaining body of the dam, causing its entire collapse.

Table 5.1 Sliding tolerance

case	limit sliding value(m)	break1(s)	break2(s)	break3(s)	failure time(s)
1	0.01	10	18	37	148
2	0.025	15	29	70	215
3	0.05	22	42	111	291
4	0.075	25	52	170	355
5	0.1	30	61	225	405
6	0.125	36	69	267	430

5.1.4.1 Gradual Failure Mechanism

In the process of gradual dam failure, during ten seconds, the earthquake creates cracks in the sloping part of the body, and with the expansion of these cracks due to the water pressure, the dam will fail after the earthquake. As shown in Figure 5.15, about 45 seconds after the start of the earthquake, the upper blocks of the sloping area are collapsed. Then, due to the drag force resulting from the overtopping of water from the broken part of the dam, respectively around 74 and 273 seconds from the beginning of the earthquake, the upper two layers of the blocks start to move and collapse. Finally, in 431 seconds, the blocks of the lower part of the dam body are moved and cause the complete failure of the dam. In the gradual failure study of the dam, the density of the blocks before separation from the main body was assumed to be 1e+6 $\frac{kg}{m^3}$ to be able to simulate the adhesion force of concrete against failure in the crack zone due to the combination of tension and compression.

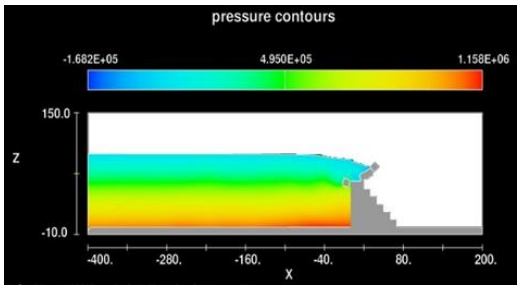

a) Gradual failure (t=45s)

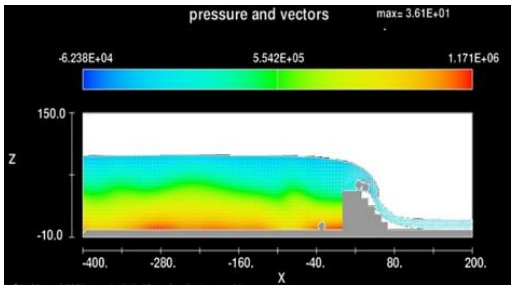

b) Gradual failure (t=74s)

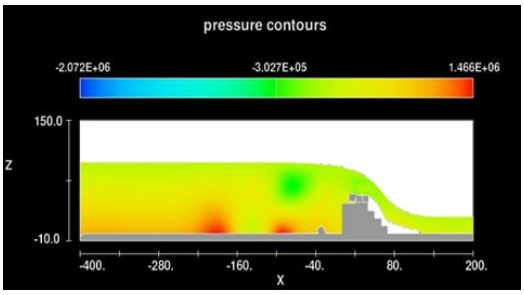

c) Gradual failure (t=273s)

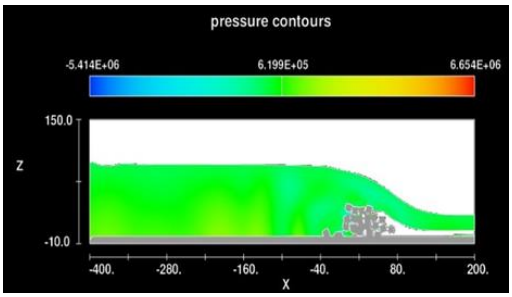

d) Gradual failure (t=431s)

Figure 5.15. Gradual failure of Koyna dam

5.1.5 Comparison of Sudden vs. Gradual Failure Hydrographs

When the water discharge values over the cracked dam after sudden breaking are compared with those after the gradual failure of the dam, similar maximum unit discharge values are observed (Fig. 5.18). The time of reaching the maximum discharge for sudden breaking is 300 seconds whereas for gradual failure the corresponding time is 900 seconds after starting of the earthquake. Besides, as shown in Figure 5.16, in contrast to the sudden failure of the dam in the gradual failure of the dam, the discharge due to dam failure increases gradually.

The final point that should be noted is that in the presented hydrographs, the outflow is recorded up to its maximum value as this value corresponds to the most dangerous state, which can have the most destructive effect at downstream of the dam. Using numerical trial and error in a two-dimensional domain, the length of the dam reservoir in streamwise was considered to be equal to four times of water surface elevation, and with a constant water level. Taking into account the above criteria, the maximum amount of discharge will not be affected by the length of the reservoir. To complete the hydrographs for an emptying reservoir after a failure, three-dimensional numerical simulations that take into account the actual size and shape of the dam reservoir are needed.

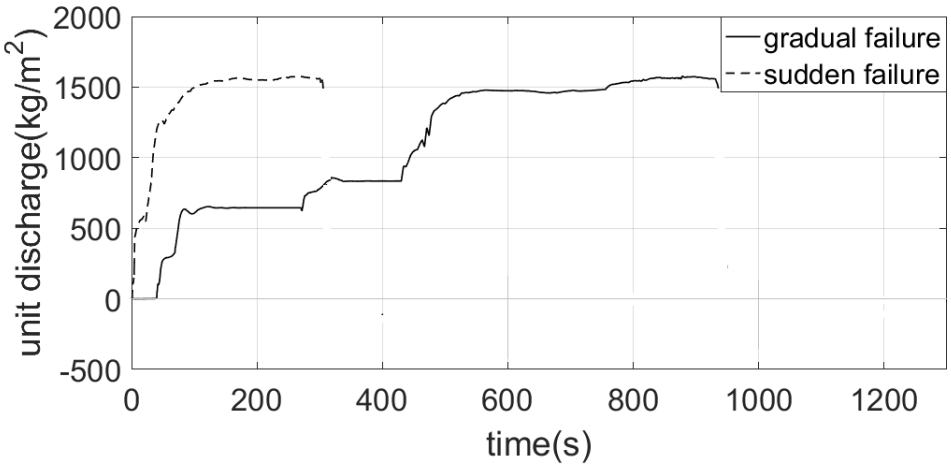

Figure 5.16. Discharge comparison of sudden and gradual cases

It should be noted that in this study only one example of gradual dam failure is given to compare with the sudden failure. Therefore, a sample of gradual failure of the dam is selected using the tolerance of block motion. In supplementary studies in the next parts, the tolerance of successive dam failures are determined according to the first failure. Thus, the first failure is determined immediately after the earthquake. In other words, the maximum recorded motion between the blocks in the flow direction after 10 seconds of the earthquake is selected as the failure tolerance, and then each block that reaches the specified amount of motion, along with reducing the density to the conventional value of concrete, is allowed to move freely in all directions. Using the mentioned mechanism, the most dangerous state of gradual failure of the dam, is simulated, which then compared with the sudden failure to get practical results.

5.1.6 Conclusion

Failure of Koyna dam because of an earthquake was selected as a test case to study dam failure mechanism using Flow 3D software and concepts of continuum mechanics. During the 6.5 magnitude earthquake on December 11, 1967, the Koyna dam was severely damaged at the slope changing region and base part of the dam.

Continuous cracks from upstream to downstream can be the beginning of a failure mechanism if accompanied by vibrations strong enough to cause instability. For this purpose, two models were defined for the failure of the dam in sudden and gradual states. During the earthquake, due to the excitations of the earth, the blocks forming the dam body are only allowed to rotate before separating from the main body because of the adhesion force of concrete in the attached parts of blocks. After the earthquake, the earth returns to a static state, and if cracks are created in the body due to the earthquake, these cracks develop due to the water pressure penetrating into the crack which will cause the gradual failure of the dam. The water inside the crack tends to penetrate more to break its stagnant state, so as soon as the crack is completed, the water comes out of the static state and causes the initial movement of the separated block in a sliding type of motion.

In general, the failure of the dam in a sudden case, which occurs, is more dangerous than the gradual failure of the dam, that occurs after the earthquake, as the maximum discharge is reached faster. In the sudden failure of the dam, the maximum discharge is reached at around 300 seconds after the earthquake, whereas for gradual failure, this time is almost three times larger.

A careful examination of the sudden failure of the dam concluded that at a constant earthquake acceleration, although with decreasing oscillation frequencies, the probability of cracking in the body of the dam increases. After cracking of the dam's body, higher oscillation frequencies will be able to break it in less time. In other words, although large oscillating periods carry a higher risk of cracking of the dam body, smaller periods propagate the resulting cracks more rapidly.

Last but not least, in the gradual failure of the dam, the failure process began from the sloping region of the body tested. By the finite element analysis, the same area of the dam has been detected to be the most vulnerable zone to cracking, which is consistent with empirical studies of Mridha et al. (2014), therefore changes are required to make this part of the dam body more strong.

5.2 Detailed Inspection of Gradual Failure Mechanism

In the previous sections, the sudden failure of the dam, which is likely to occur during an earthquake, was discussed in detail. As mentioned, this type of dam failure is observed when the cracks created in the dam body are completed before the end of the earthquake. Therefore, for its occurrence, the sum of seismic and hydraulic forces must be able to overcome the adhesion force of concrete. As discussed earlier, the sudden failure of the dam in the event of a severe earthquake.

In this part of the study, the mechanism of gradual dam failure will be examined in more detail. Unlike sudden dam failure, gradual failure occurs after the earthquake is over. Thus, the cracks created by seismic and hydraulic forces, after the earthquake and over time due to hydrostatic pressure inside these cracks, expand and cause damage to the dam. Two points must be considered in the mechanism defined for the gradual failure of the dam. First, given that the amount of displacement tolerance of blocks will be effective at the time of dam failure, so it must be accurately determined. Second, the size of the blocks and their altered density must be defined in such a way that they do not affect the failure time of the dam. In this part of the study, in order for a fixed process to take place, the displacement tolerance of the blocks is determined according to the maximum motion recorded among the blocks forming the dam, just after the earthquake. Thus, the first failure of the dam body occurs at the exact ending time of the earthquake, and then each block that reaches the specified amount of movement is allowed to detach from the main body. Using the defined mechanism, the most dangerous state of gradual failure of the dam, which reaches the maximum flow rate in the fastest possible time, is obtained, and comparing its hydrograph with sudden failure will be useful.

Also, in order to ensure that the failure process is not affected by the size of the blocks and their altered density, Koyna Dam was simulated using three models including 32, 119, and 461 cubic blocks with sizes of 10, 5, and 2.5 meters respectively. The aim of this study is to select the correct size of blocks and their modified density value. The created models can be seen in Figure 5.17.

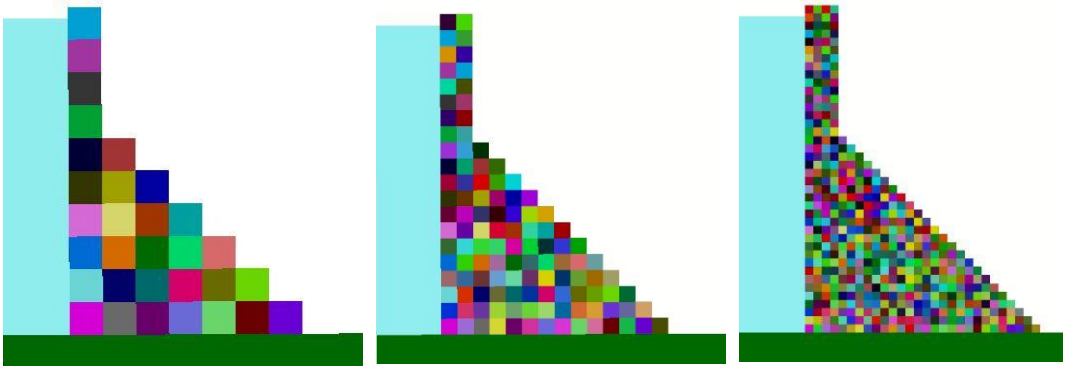

32 blocks model 119 blocks model 461 blocks model

Figure 5.17. Generated model to inspect block size effects on failure

In this part of the study, the simulation is performed for only ten seconds of the earthquake and then the maximum motion recorded between the blocks at different densities for the three models is compared. It is worth mentioning that as the number of blocks forming the dam increases, the simulation time increases dramatically. So that the simulation time of ten seconds earthquake, for the model consisting of 32 blocks was 5 hours, which was equal to 31 hours, and almost 6 days for the models including 119 and 461 blocks, respectively. Also, in the mentioned models, considering that the study of block motion due to the sum of seismic, hydrostatic, and hydrodynamic forces is desired event, the size of the dam reservoir was selected very small because the purpose of this study is not to obtain the discharge due to failure of the dam.

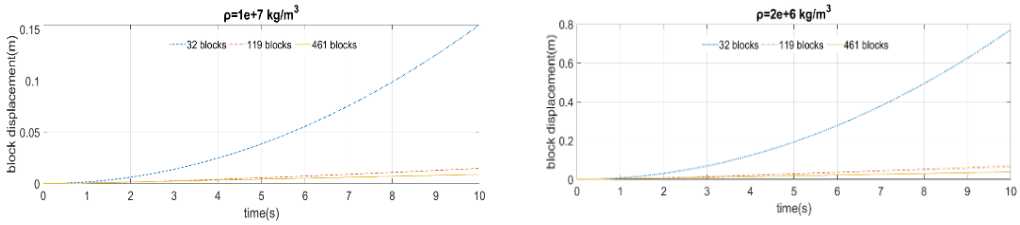

a) ρ=1e+7 kg/m^3 b) ρ=2e+6 kg/m^3

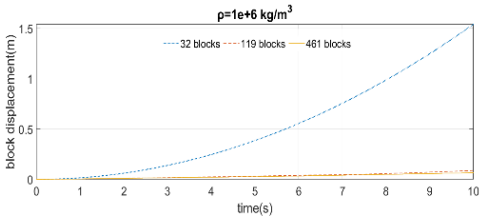

c) ρ=1e+6 kg/m^3

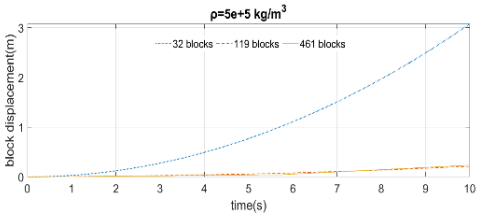

d) ρ=5e+5 kg/m^3

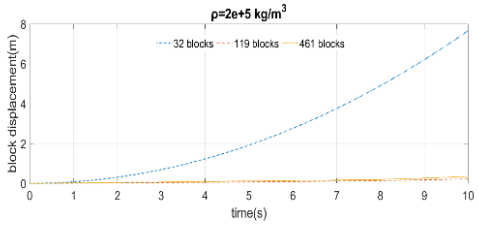

e) ρ=2e+5 kg/m^3

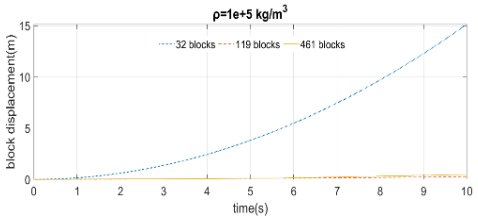

f) ρ=1e+5 kg/m^3

Figure 5.18. Maximum displacement comparison of three models

As can be seen in Figure 5.18, the size of cubic blocks equal to or less than 5 m and the modified density less than 1e+6 kg/m^3 are required to converge the results and make the failure process independent of the size and the modified density value of the blocks. It is better to point out again that the density of blocks increases in order to simulate the adhesion force of concrete, and when each block reaches a critical value of motion, while reducing its density to the actual amount of concrete, it is allowed to move freely in all directions.

5.2.1 Dam Geometry Effects on Gradual Failure Mechanism

According to the previous section, the size of the cubic blocks forming the dam is selected equal to 5 meters, and the density of blocks before their separation from the main body is considered to be equal to 1e+6 kg/m^3. In the next step, the effect of the shape of the dam body on the gradual failure process must be investigated. Due to the fact that unlike sudden failure, which increases the probability of occurrence with increasing the height of the dam, gradual failure of the dam is also possible in low-

height dams. Another reason to consider the dam smaller is that the software has the ability to simulate up to 500 moving solid objects, so in order to be able to generalize the model to three dimensions, in a two-dimensional model up to 50 blocks must be used. Therefore, the height of the dam was considered to be equal to 40 meters. In this study, 32 cubic blocks with a size of 5 meters on each side are put together in different ways to form different shapes of the dam body. It is important to note that in order to keep the hydrostatic force on the body constant, the height of the formed shapes was considered to be constant in the amount of 40 meters. The simulation lasted for 20 seconds, during which the first ten seconds of the 1967 Koyna earthquake were applied, and then the simulation continued for another ten seconds in a stationary state. (see Fig. 5.21)

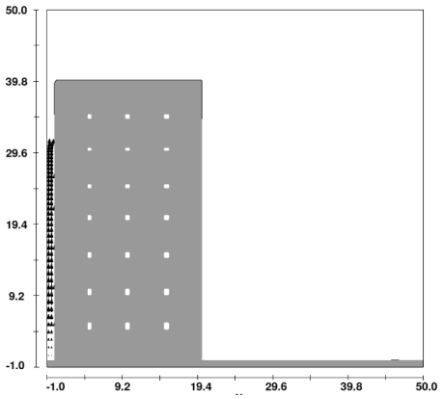

a) t=0s

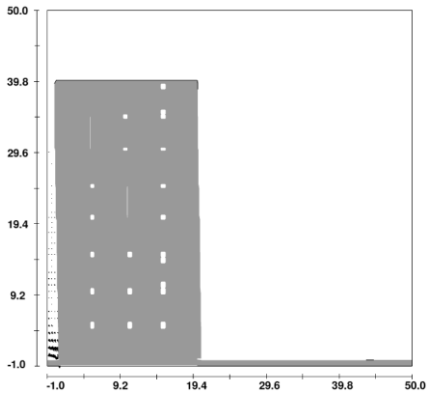

b) t=20s

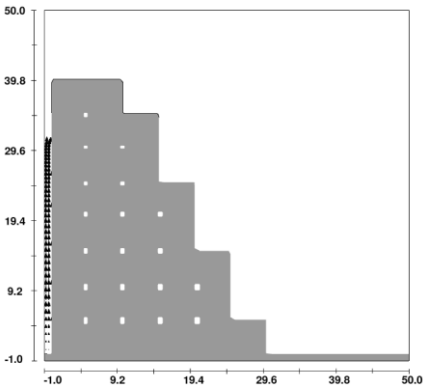

c) t=0s

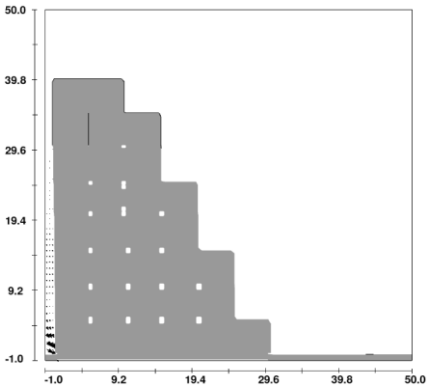

d) t=20s

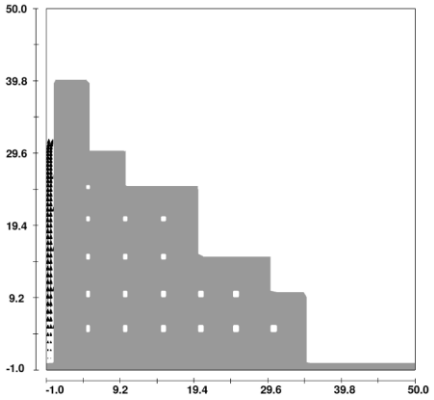

e) t=0s

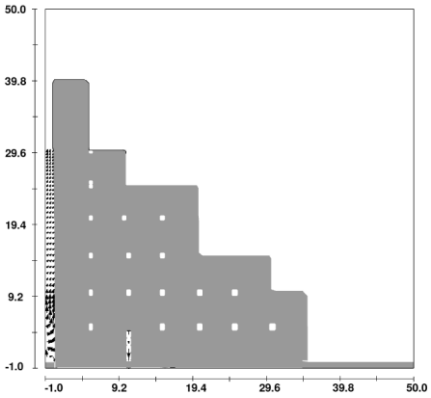

f) t=20s

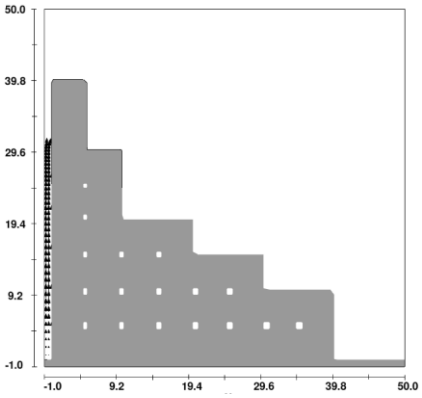

g) t=0s

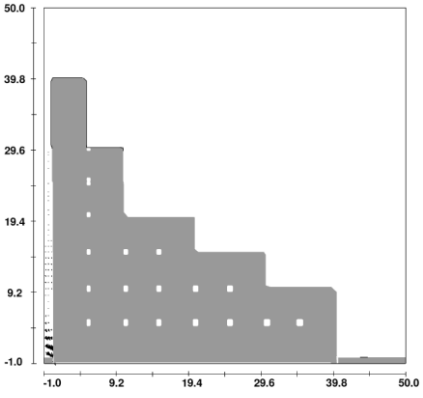

h) t=20s

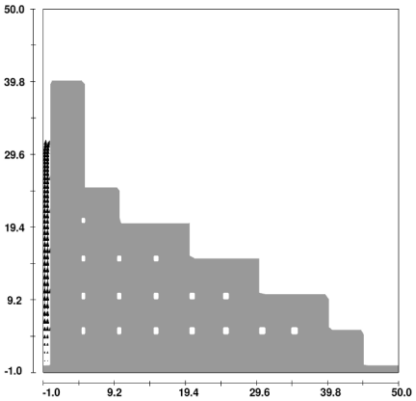

i) t=0s

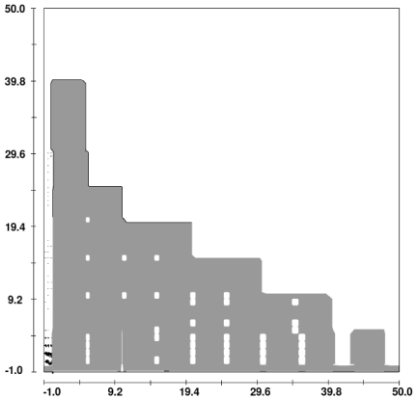

j) t=20s

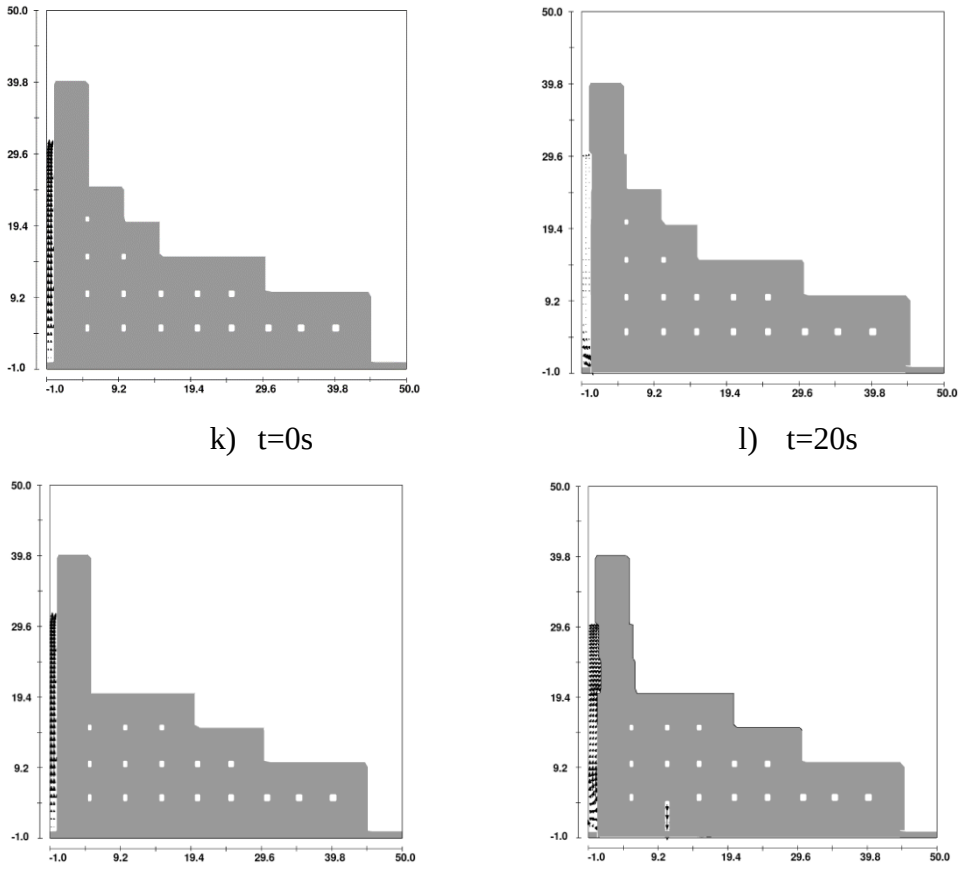

k) t=0s l) t=20s

m) t=0s n) t=20s

Figure 5.19. Effects of dam shape on gradual failure

First of all, it should be noted that many of the formed shapes cannot be the real dam body, and here they are used only to study and analyze the effect of the body shape in the process of gradual failure. As shown in Figure 5.19, the rectangular body formed in part a, begins to fail from base blocks, while by moving the upper blocks to the lower parts of the body, the dam begins to fail from different points. For example, the first failure was observed in g and k samples from a height of about 15 m and 25 m, respectively. According to the analysis performed in this section and the gradual failure of the Koyna dam, which was studied in the previous sections, it can be concluded that if there is no sudden slope change in the dam body, the lower part of the dam is at greatest risk for starting the gradual failure process. Therefore, in the continuation of the study, assuming that there is no structural problem with the

dam, the simulations for a wall with a rectangular section (Fig. 5.21.a) continue. Due to the fact that in this model, failure occurs from the bottom of the dam, it will be called "semi-gradual failure". In fact, this model is the upper part of the Koyna dam, which can be seen in Figure 5.19. Therefore, breaking this model from the bottom confirms the accuracy of studies related to the gradual failure of the Koyna dam from the slope changing area.

5.2.2 Gradual and Sudden Failure Comparison in Wall Shaped Dam

As mentioned in this part, the wall shaped dam model with a fixed thickness consisting of 32 cubic blocks with dimensions of 5 meters and the modified density of 1e+6 kg/m^3, is used to simulate the semi-gradual failure of the dam. The pre-separation density of the blocks is then reduced to 1e+4 kg/m^3 in order to simulate a sudden dam failure to compare it with a semi-gradual one. It should be noted that the assumed value for the density of the blocks is much smaller than it can simulate the adhesion force of concrete. In fact, the purpose of this section is to compare two types of failures, otherwise, a concrete dam in the shown form, will gradually collapse due to an earthquake of 6.5 magnitude. Figure 5.20 compares the two types of dam failures in different seconds.

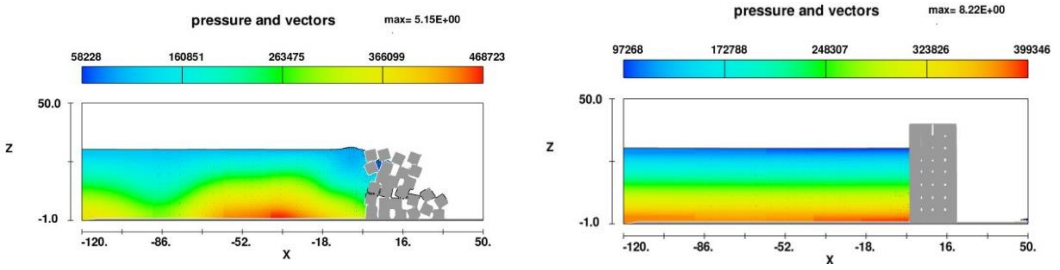

a) Sudden failure (t=10s) b) Semi-gradual failure (t=10s)

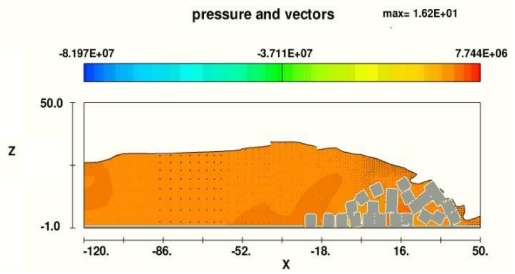

c) Sudden failure (t=20s)

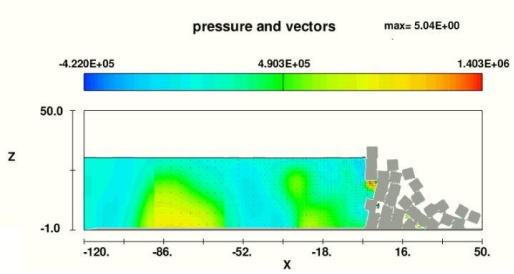

d) Semi-gradual failure (t=20s)

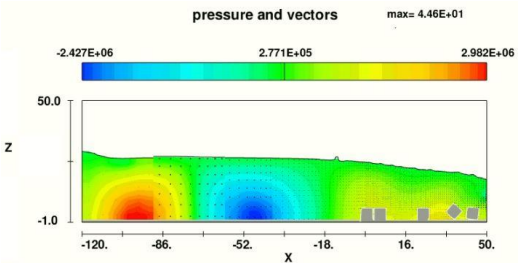

e) Sudden failure (t=100s)

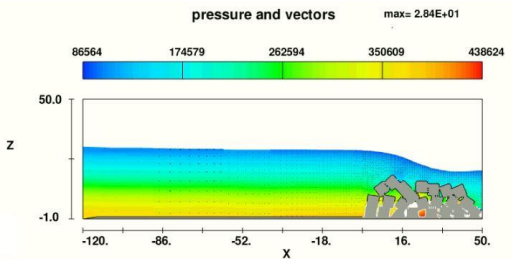

f) Semi-gradual failure (t=100s)

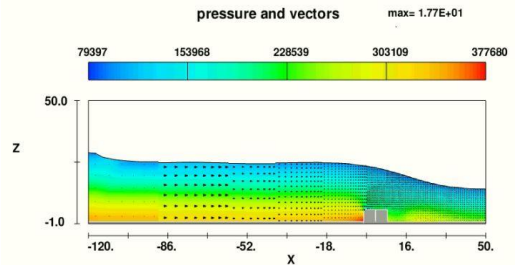

g) Sudden failure (t=200s)

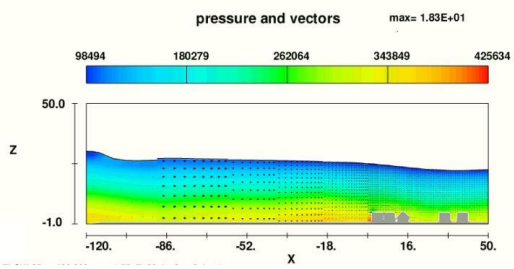

h) Semi-gradual failure (t=200s)

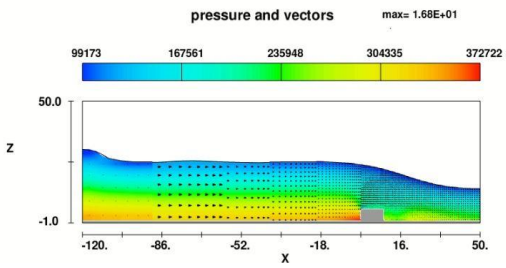

i) Sudden failure (t=400s)

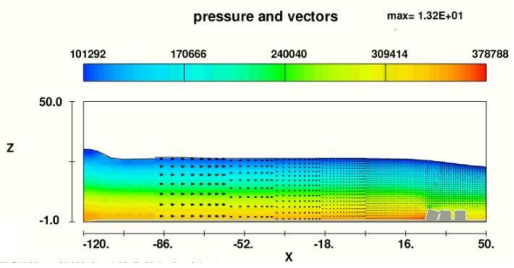

j) Semi-gradual failure (t=400s)

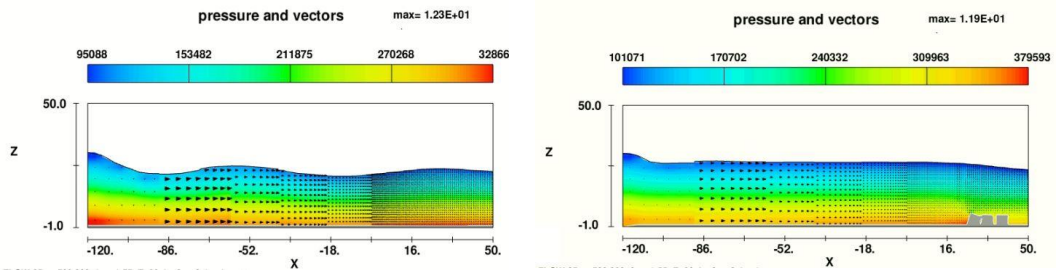

k) Sudden failure (t=500s) l) Semi-gradual failure (t=500s)

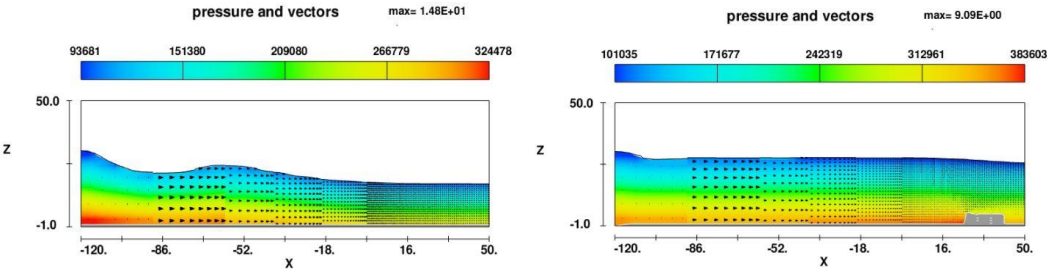

m) Sudden failure (t=1000s) n) Semi-gradual failure (t=1000s)

Figure 5.20. Comparison of semi-gradual and sudden failure

As shown in Figure 5.20, the semi-gradual failure of the dam begins at the bottom of the body, while in sudden failure, the failure begins near the free surface of the water. One hundred seconds after the start of the earthquake in the mechanism of sudden failure almost the entire dam collapsed, but in the semi-gradual failure, almost half of it remained. Finally, around 500 seconds after the start of the earthquake, the whole body collapses in a sudden failure, while in a semi-gradual failure, the blocks at the lowest part of the body never collapse.

5.2.3 Discharge Comparison of Sudden Failure Case with Semi-Gradual Failure

At the end of this part of the study, Discharge hydrographs obtained from the two failure mechanisms will be reviewed and compared. As mentioned, considering the contact forces equal to the adhesion of concrete under the effect of an earthquake of

magnitude 6.5, this dam gradually breaks. To simulate a sudden failure, the adhesion forces between the blocks were considered to be one hundred times smaller than the actual value. In fact, the sudden failure model is hypothetical and has been simulated only for comparison with semi-gradual failure. It is also important to note that the simulation model of semi-gradual failure is performed on the assumption that the first dam failure occurs at the exact moment of the end of the earthquake. In this way, the simulated gradual failure will reach the maximum discharge in the fastest possible time.

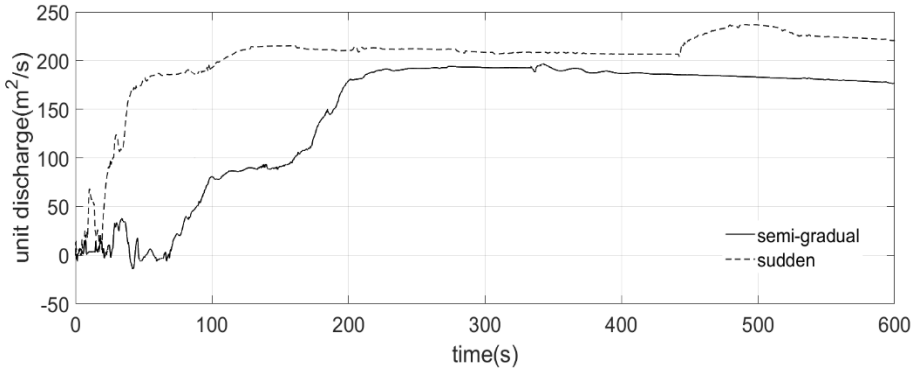

Figure 5.21. Discharge comparison of sem-gradual and sudden failure

Figure 5.21 shows the discharge hydrographs passing through each meter of the dam for both sudden and semi-gradual failure modes. As can be seen from the figure, in a sudden failure, the volume of water passing through the broken area of the body increases rapidly so that 50 seconds after the onset of the earthquake, the discharge reaches about 70% of its maximum. However, the corresponding amount of water passing for the gradual failure of the dam is observed 200 seconds after the start of the earthquake and no longer shows an increase. Similar to the gradual failure analyzes performed in the previous sections, in the semi-gradual failure, the discharge increase is step by step. In fact, this phenomenon is a positive event, because by increasing the discharge in this way, some of the fluid energy in the reservoir is dissipated, and as a result, the maximum discharge will be observed later. Another important point to note is that the difference in the maximum amount of

discharges between the two types of failure mechanisms is due to the fact that, despite sudden failure, the entire dam does not collapse in gradual failure, so its maximum discharge value is recorded about 30% less.

5.2.4 Wall Thickness Effects on Semi-Gradual Failure Mechanism

In this part of the study, the effects of dam's wall thickness on its failure mechanism will be investigated. In the previous model, by placing four cubic blocks next to each other, the thickness of the dam's wall was considered to be equal to 20 meters. In this part, by reducing the number of blocks to 3, the wall thickness is considered to be equal to 15 meters. It is important to note that other effective parameters such as dam height, reservoir water level and coefficients of friction, etc., are the same in two models, and the only different parameter between the models is the dam's wall thickness.

As mentioned in the previous sections, the purpose of this section is to compare the most dangerous state of gradual failure with the sudden failure of the dam. For this purpose, semi-gradual failure where the first blocks start moving from the bottom of the dam was selected. Also, to simulate the most dangerous case of semi-gradual failure, the first failure of the dam was considered at the moment when the earthquake stopped. In addition to previous studies, the effects of dam wall thickness are investigated to obtain the most dangerous gradual failure state. In general, the gradual failure of the dams is directly related to the shape of the dam, the quality and life of concrete, so they break in the time range between 0.1 to 0.5 hours.

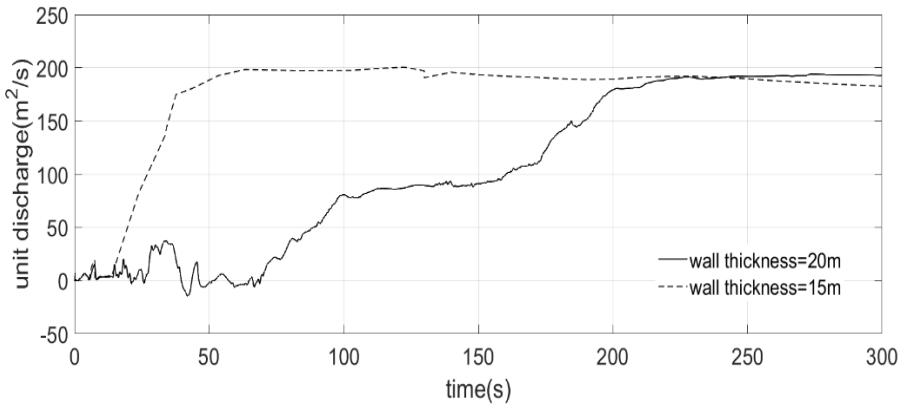

Figure 5.22. Dam wall thickness effects on gradual failure mechanism

As shown in Figure 5.22, as the wall thickness of the dam decreased from 20 m to 15 m, the dam began to break more rapidly in a semi-gradual state. Also, comparing the hydrographs of the two models, it can be concluded that unlike the semi-gradual failure of the model with a wall thickness of 20 meters, which has a step-up behavior, this behavior is not very clear in the hydrograph of the model with a wall thickness of 15 meters. In general, it can be concluded that by reducing the wall thickness, the gradual failure model becomes closer to the sudden failure model. This result was confirmed by reducing the thickness of the dam wall from 15 meters to 10 meters. Considering a model with a wall thickness of 10 meters, which includes two adjacent blocks, under a 6.5 magnitude earthquake, the dam suddenly breaks. Regarding that by reducing the wall thickness of the dam, the dam breaks suddenly, the failure model of the above simulation with a wall thickness of 15 meters is named as the critical semi-gradual failure model, which in fact will be the closest failure mechanism to sudden failure. The last important point that should be mentioned is that the difference in the maximum amount of discharges is because in the model with a wall thickness of 20 meters, the whole dam does not collapse, while in the model with a wall thickness of 15 meters, the entire dam collapses. For this reason, the maximum flow in the model with a wall thickness of 15 meters is higher than the corresponding value in the model with a wall thickness of 20 meters.

5.3 Three Dimensional Inspection of Dam Failure Mechanism

In the last part of the study, the simulated model of dam failure in the previous section, which included a dam with a wall height of 40 meters and a thickness of 15 meters, will be extended to three dimensions, taking into account the length of the dam of 100 meters. It is important to note that the model simulated in the previous section is in fact the closest gradual failure mode to the sudden failure mode, which was considered with the lowest possible wall thickness and was named critical semi-gradual failure.

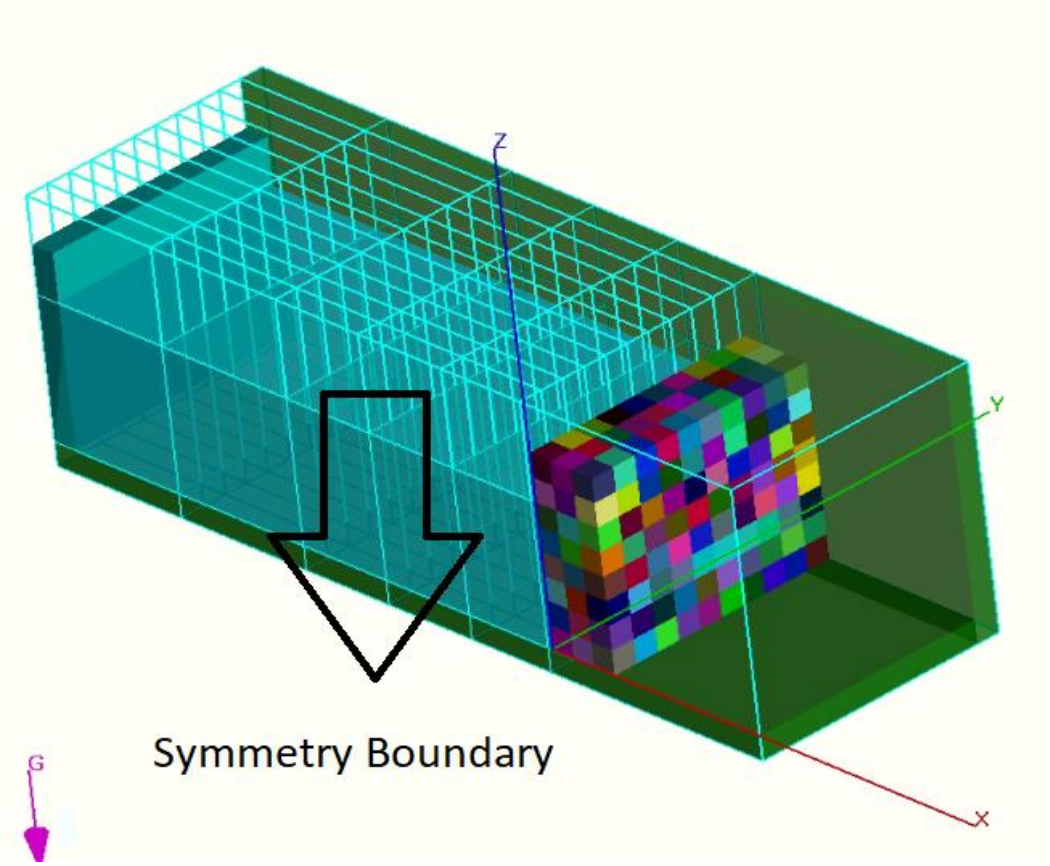

Figure 5.23. 3-dimensional model

Figure 5.23 shows the model used to simulate dam failure in 3D. The dam consists of 240 cubic blocks with a side length of 5 meters, also the height of the water behind

the dam is equal to 30 meters. As in previous models, a reflective wave absorption layer is placed at the end of the reservoir (X_min), its boundary conditions are also considered as stagnation pressure to simulate the infinite volume reservoir. X_max boundary is the outflow and the others are symmetrical. In fact, the length of the dam is 50 meters in the CFD model and it is increased to 100 meters by selecting the symmetrical boundary conditions for the Y_min border. Lastly, friction and restitution coefficients are considered to be equal to 1 and 0.95.

5.3.1 Finite Element Analysis of the Dam's Body

In this part of the research, a model is created to find out the stressful areas on the dam body during a ten-second earthquake with a magnitude of 6.5, using the FSI model, available under the flow 3D software. In this model, the dam's wall, which contains 240 blocks, is considered as the rigid body, then the stresses due to the sum of seismic, hydrostatic and hydrodynamic forces on it are calculated by the software.

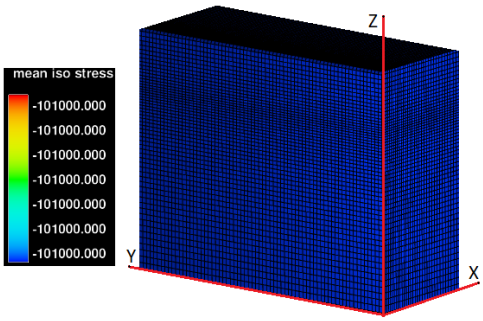

a) t=0s (mean iso stress)

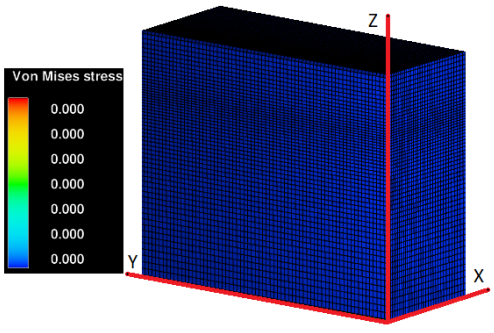

b) t=0s (Von Mises stress)

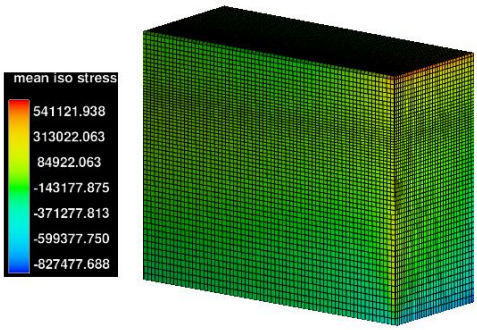

c) t=2s (mean iso stress)

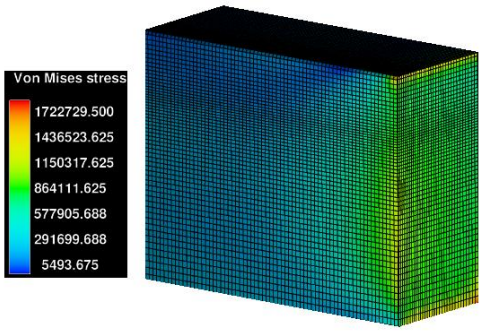

d) t=2s (Von Mises stress)

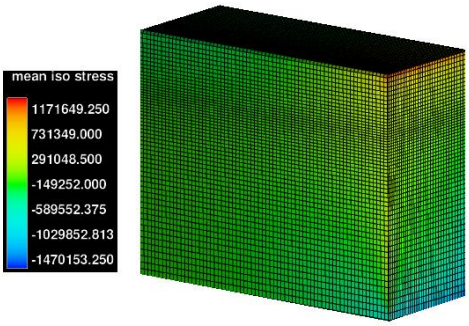

e) t=4s (mean iso stress)

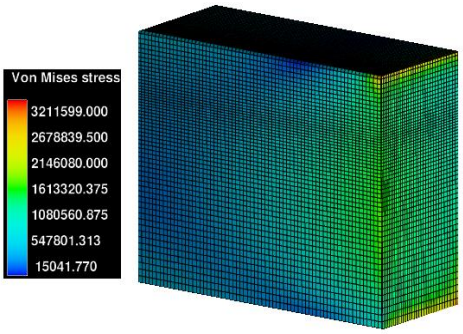

f) t=4s (Von Mises stress)

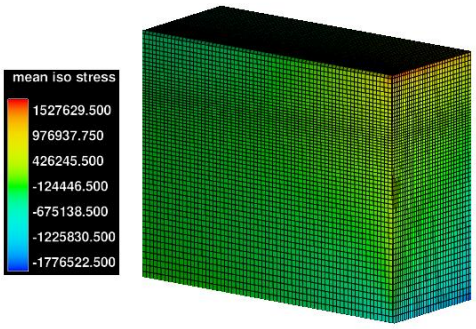

g) t=6s (mean iso stress)

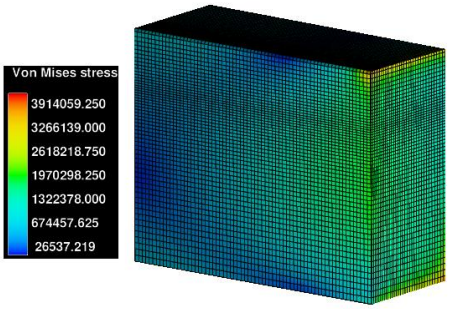

h) t=6s (Von Mises stress)

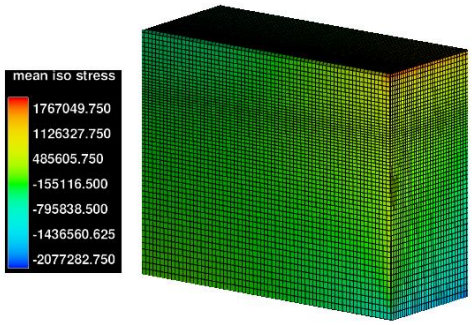

i) t=8s (mean iso stress)

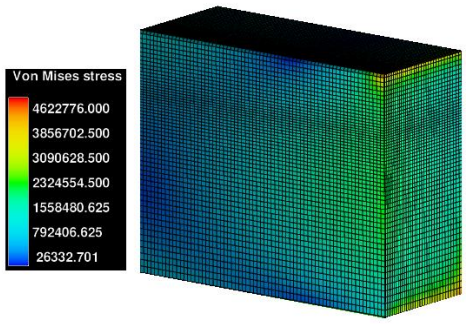

j) t=8s (Von Mises stress)

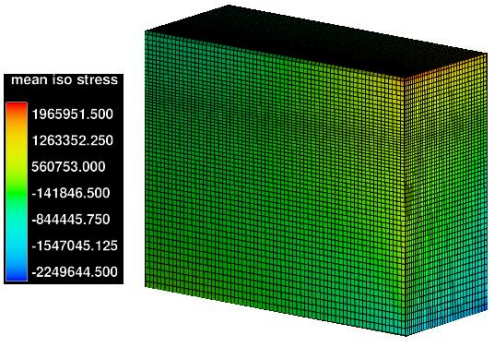

k) t=10s (mean iso stress)

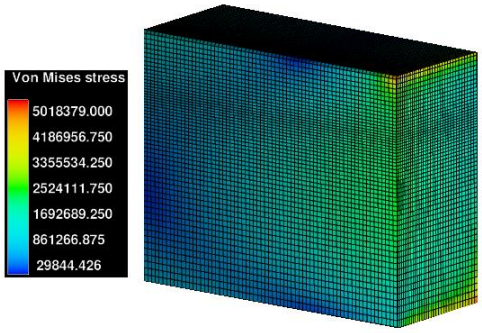

l) t=10s (Von Mises stress)

Figure 5.24. Stress analysis on the dam's body

Figure 5.24 shows the stresses created on the dam body during a ten-second earthquake, from the perspective of the dam reservoir. As can be seen, the middle of the dam, which in the CFD model has a symmetrical boundary condition in the location of Y_min, has the highest stress during the earthquake, so it is expected that the dam will start to break from this part.

5.3.2 Three-Dimensional Inspection of Semi-Gradual Failure

In this section, failure in semi-gradual mode in a three-dimensional model will be investigated. As mentioned, to simulate the most dangerous state of gradual failure,

it is assumed that the failure of the dam begins from the moment the earthquake stops. Therefore, the failure process will start from the tenth second of the simulation.

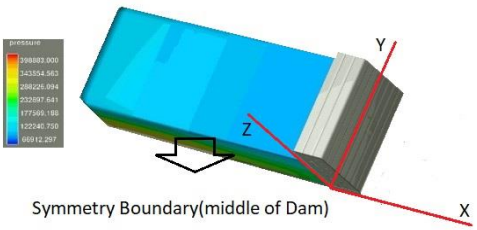

a) t=10s (semi-gradual failure)

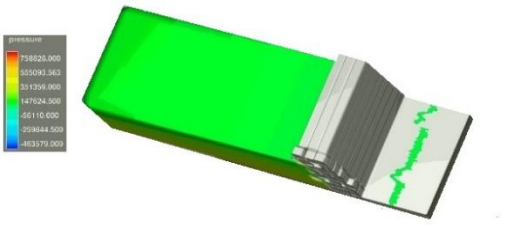

b) t≈10.4s (semi-gradual failure)

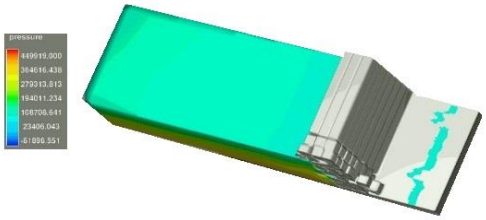

c) t≈10.8s (semi-gradual failure)

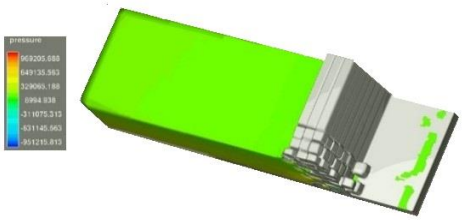

d) t≈11.2s (semi-gradual failure)

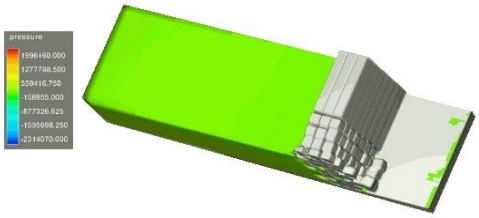

e) t≈11.6s (semi-gradual failure)

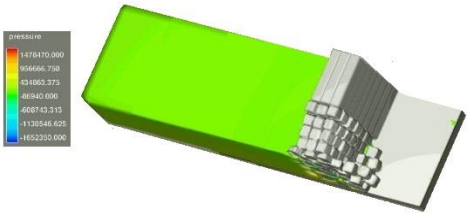

f) t≈12s (semi-gradual failure)

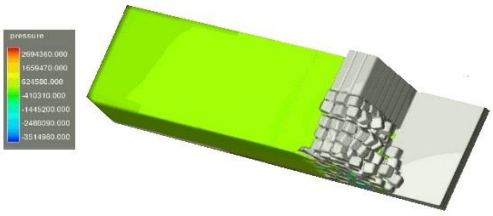

g) t≈12.4s (semi-gradual failure)

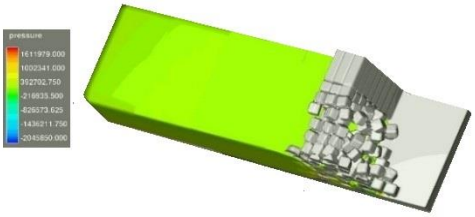

h) t≈12.8s (semi-gradual failure)

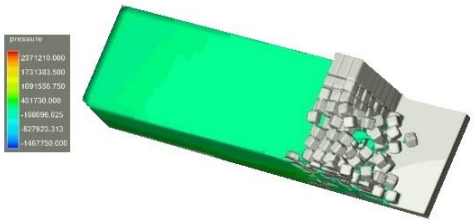

i) t≈13.2s (semi-gradual failure)

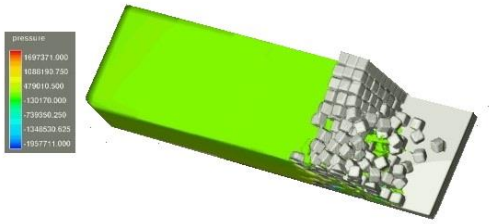

j) t≈13.6s (semi-gradual failure)

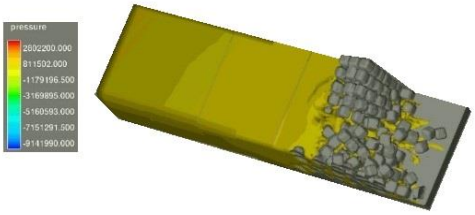

k) t=15s (semi-gradual failure)

l) t=16s (semi-gradual failure)

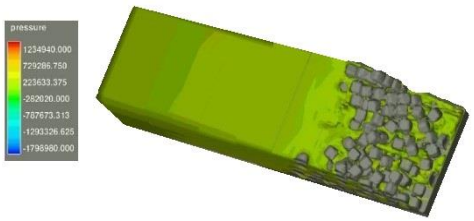

m) t=17s (semi-gradual failure)

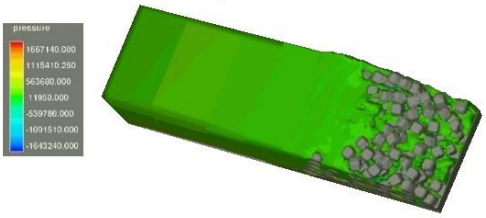

n) t=18s (semi-gradual failure)

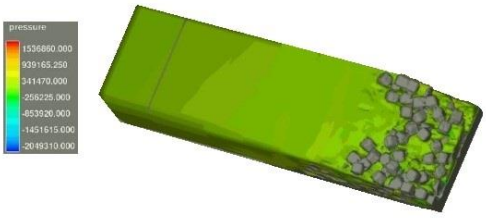

o) t=19s (semi-gradual failure)

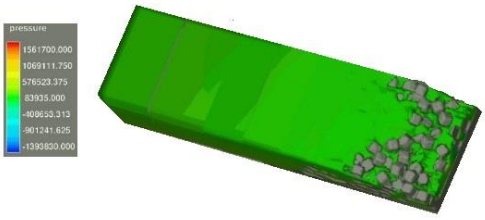

p) t=20s (semi-gradual failure)

Figure 5.25. Semi-gradual failure inspection in three-dimensional dam

As can be seen in Figure 5.25, the dam is completely stable during the earthquake, then the dam begins to fail in the middle at almost t=10.4s. In general, the failure of the dam starts from the middle of it, which is Y_min in CFD model, and with a time step of about 0.4 seconds, the continuous failures continue towards the support of the dam, which is Y_max in CFD model. The important point to note is that although the onset of failure occurs from the middle of the dam, the first flow of water due to the failure of the dam is not observed from this area. In fact, the failure of the dam continues faster from an area about a quarter of the length of the dam from the side wall of the dam. So that the first water flow due to the failure of the dam is observed from a distance of about 25 meters from the support.

5.3.3 Three-Dimensional Inspection of Sudden Failure

In this part of the study, the sudden failure of the 3D dam of the CFD model of the previous part will be examined. In fact, a dam with a wall height of 40 meters, a wall thickness of 15 meters and a length of 100 meters will gradually break due to an earthquake of 6.5 magnitude. But in order to be able to compare the failure in two cases in three dimensions, in this part of the study, the adhesion force of concrete was considered less than its actual value to break the above mentioned dam instantly.

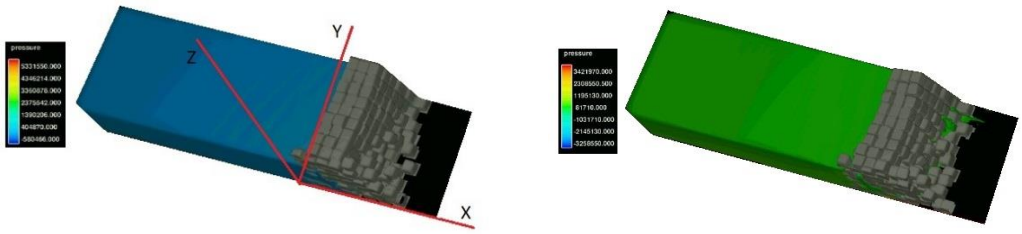

a) t=1s (sudden failure)

b) t=2s (sudden failure)

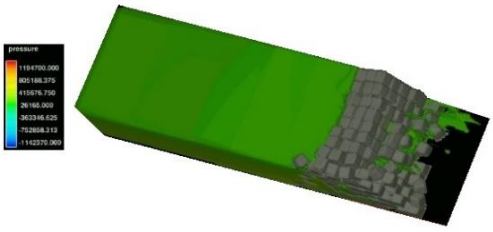

c) t=3s (sudden failure)

d) t=4s (sudden failure)

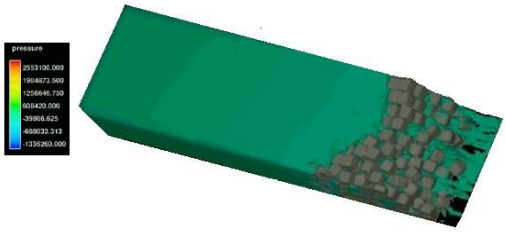

e) t=5s (sudden failure)

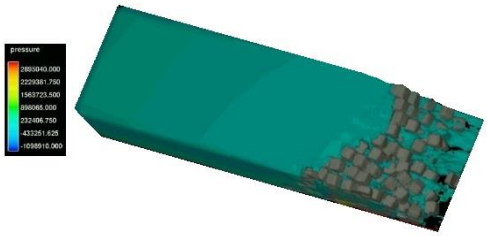

f) t=6s (sudden failure)

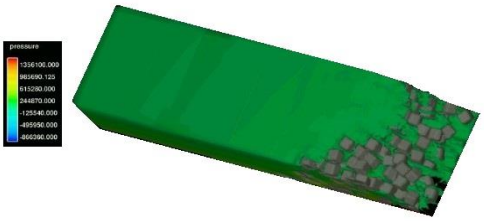

g) t=7s (sudden failure)

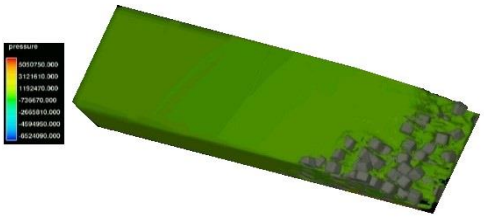

h) t=8s (sudden failure)

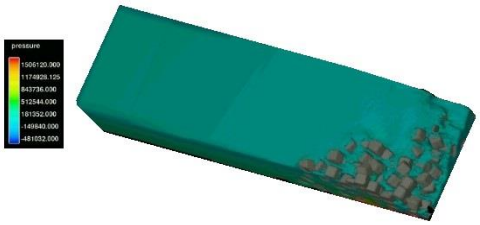

i) t=9s (sudden failure)

j) t=10s (sudden failure)

Figure 5.26. Sudden failure inspection in three-dimensional dam

Given the mechanism of failure of a three-dimensional dam in a sudden state, it can be inferred that, like a semi-gradual failure, the first moving blocks are in the middle region of the dam. However, the movement of blocks located about a quarter of the length of the dam from its side wall is faster than other blocks in other areas. Although the first fractures is observed from the area mentioned in the distance of a quarter of the length of the dam from the side wall, the first flow due to failure was observed in the areas close to the dam support, which is actually the side wall of the dam. The last point is that although the beginning of the movement of the blocks was observed from the middle area of the dam, with the continuation of the process of sudden failure, the lower blocks of this part collapse later than other areas. In other words, two main streams are formed on both sides of the dam and at a distance of about a quarter of its length from the supports, which accelerates the failure of blocks in these areas. (see Fig. 5.28)

5.3.4 Comparison of Semi-Gradual Failure with Sudden Failure in Three-Dimension

As mentioned, the sudden failure of the dam starts from the moment the earthquake starts and by the end of it, which includes ten seconds, most of the dam collapses and only part of the body remains in the middle of the dam. However, in the semi-gradual failure of the dam, the process of which begins after the earthquake, in ten seconds, most of the dam is still standing and only fluid flow are observed at a distance of a quarter of the length of the dam from its side wall. Comparison of discharge hydrographs of the two types of dam fractures, shown in Figure 5.27, gives more accurate results.

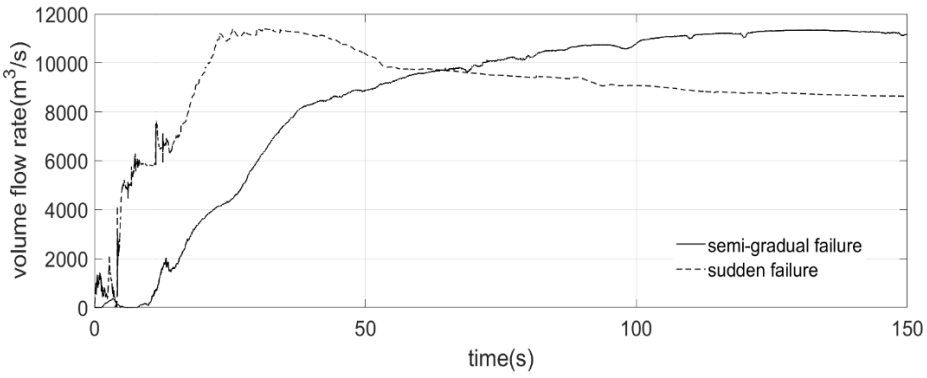

Figure 5.27. Volumetric flow rate comparison of sudden vs. semi-gradual failures

In the sudden failure of a three-dimensional dam, the entire dam breaks in about 70 seconds from the start of the earthquake, so that the flow rate quickly reaches its maximum value. However, in the worst case of semi-gradual failure, up to 350 seconds after the start of the earthquake, there are still standing blocks in the center of the dam, which causes the discharge of semi-gradual failure to be less than the corresponding value in sudden failure.

5.3.5 Comparison of Two-Dimensional and Three-Dimensional Results

Finally, the results obtained from the two-dimensional model and the corresponding three-dimensional model will be compared.

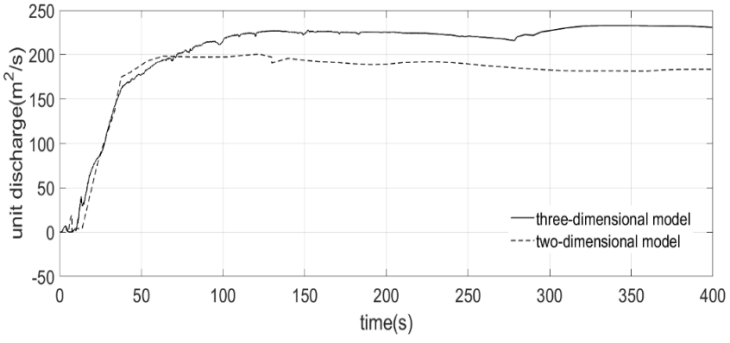

Figure 5.28. Results comparison of 2D and 3D models in semi-gradual failure

A comparison of the discharge hydrographs with the two-dimensional and three-dimensional models shown in the figure reveals interesting results. As can be seen, up to 70 seconds after the onset of the earthquake, the results of the two models are almost identical. Almost 80% of the dam collapsed at the mentioned time, so it can be claimed that the two-dimensional model, like the three-dimensional model, provides accurate information about the failure process, while to obtain the exact discharge caused by the dam failure, using the three-dimensional model is required

The difference in the results of the two models is actually due to the fact that in the two-dimensional model, the two side walls are considered symmetrically, so this model can be considered as a vertical layer with 24 blocks, in the middle of the three-dimensional model containing 240 block. In general, in the two-dimensional model, the three blocks located at the lowest part of the body never collapse, while in the three-dimensional model, all the blocks collapse due to the current generated near the side walls. For this reason, the two-dimensional model yields a lower final discharge value than the corresponding value obtained from the three-dimensional model. In general, if the whole dam collapsed in the two-dimensional model, the results would be better adapted to the three-dimensional model, so the two-dimensional model would be more efficient for the failures, which the whole dam collapses.

5.4 Semi-Gradual Failure Due to Normalized Erthquake in a Single Direction

In the previous section, the failure of the dam in the form of a wall with a length of 100 meters due to the 6.5 magnitude, 1967 Koyna earthquake, which enters the dam in both vertical and horizontal directions, was investigated. To simplify the problem of dam failure in a semi-gradual state in the final part of this analysis, the failure of the dam in the form of a wall with a length of 45 meters under the effect of normalized earthquake in the form of a single direction sine wave is investigated. In order for the failure of the dam to occur at a slower rate so that the failure mechanism

can be more accurately observed, the sine wave frequency is considered to be one Hz, which is far less than the corresponding value in the 1967 Koyna earthquake. The normalized earthquake is shown in the figure below.

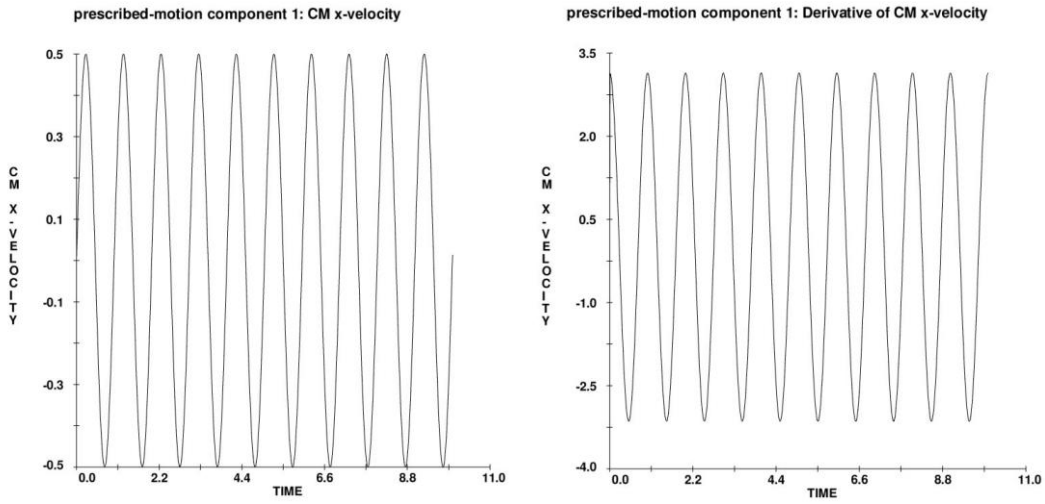

a) Earthquake velocity wave b) Earthquake acceleration wave

Figure 5.29. Normalized earthquake in streamwise direction

5.4.1 CFD Model Generation

The dam simulated in the CFD model consists of a wall 45 meters long, 40 meters high and 24 meters thick, which consists of cubic blocks with 5 meters long sides, which can be seen in Figure 5.30. The size of the dam reservoir is selected so that its size has no effect on the failure mechanism and outlet flow. Thus, its length is selected perpendicular to the dam equal to 200 meters and the boundary condition of the end of the reservoir is set equal to the constant pressure that keeps the water height at this boundary constant. Also, to prevent the effect of return waves from the end of the reservoir in the failure mechanism, a wave absorption layer is created at the end of the reservoir, which is the constant pressure boundary condition. Earthquake force is applied in the form of a velocity wave to three walls, including the side walls and the floor of the canal with a magnitude of 0.5 meters per second

and a frequency of 1 Hz for ten seconds, then the walls are kept motionless. The reason for applying the velocity wave is to prevent the effect of the channel weight on the movement of the blocks separated from the dam body after the collision with the channel.

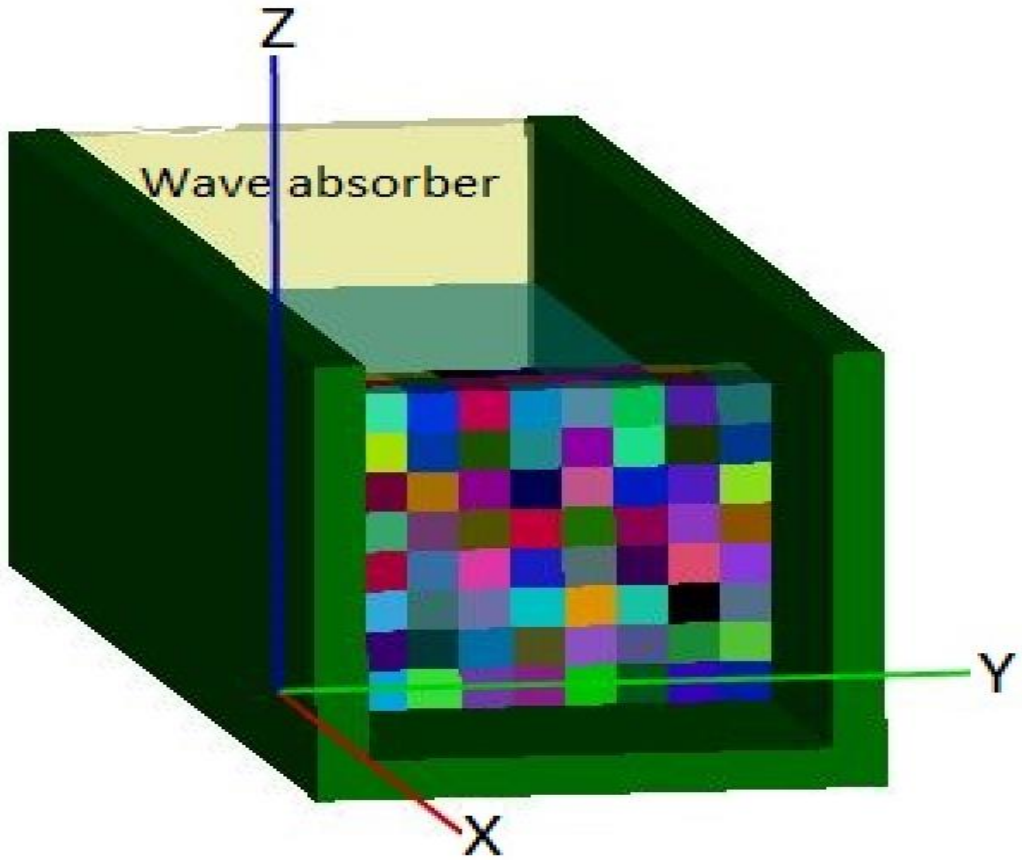

Figure 5.30. CFD model of gradual failure due to normalized earthquake

5.4.2 Semi-Gradual Failure Inspection Due to Normalized Earthquake

As mentioned, the purpose of this part, which is actually the final part of the analysis, is to find out the mechanism of failure in a semi-gradual state, with the difference that the seismic force enters the dam in a single direction and at a low frequency in a normalized way. Due to the fact that the real earthquake enters the body in different directions and frequencies, it is very difficult to predict the dam failure mechanism

without performing the relevant analyzes, so in order to achieve a general answer, the problem is simplified by normalizing the earthquake. Figure 5.31 shows the semi-gradual failure of the dam due to normalized earthquake, starting from the end time of the earthquake (corresponding to the tenth second of the simulation).

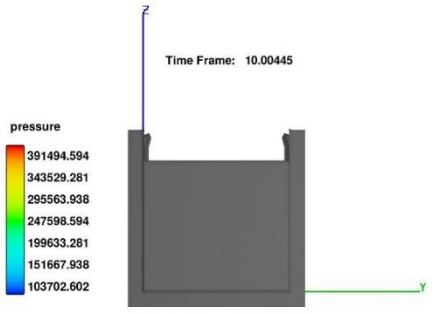

a) t=10s

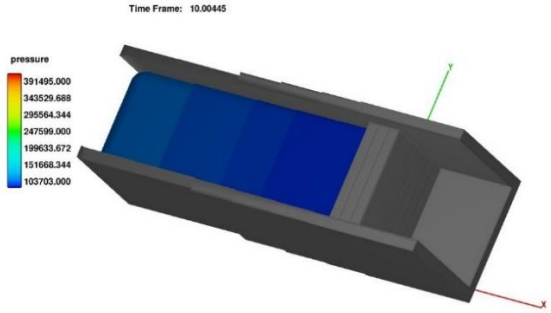

b) t=10s (3D view)

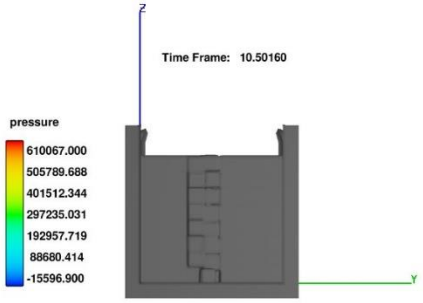

c) t=10.5s

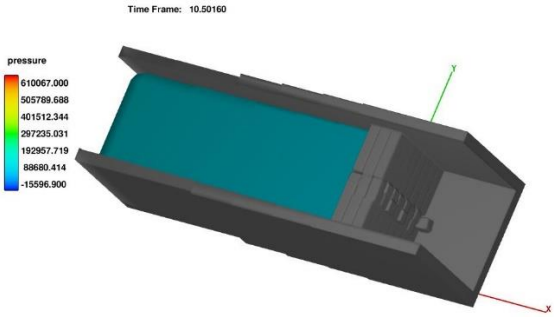

d) t=10.5s (3D view)

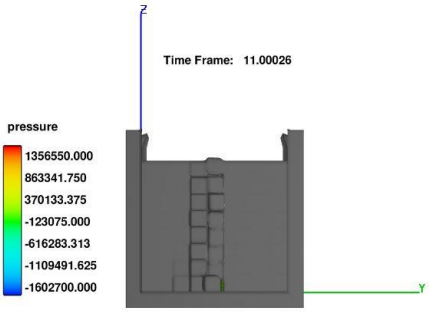

e) t=11s

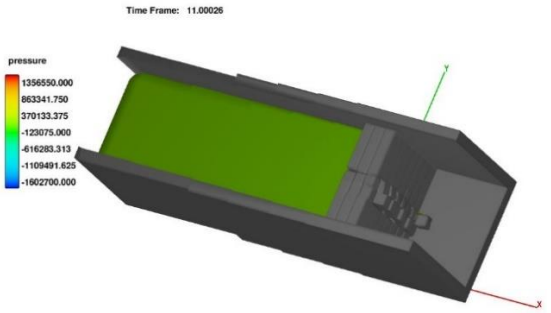

f) t=11s (3D view)

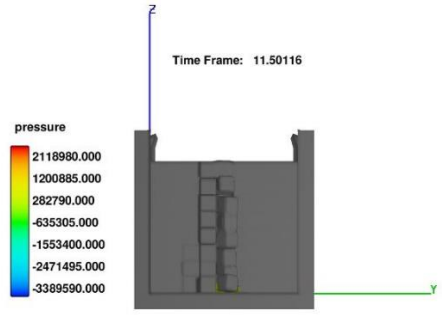

g) t=11.5s

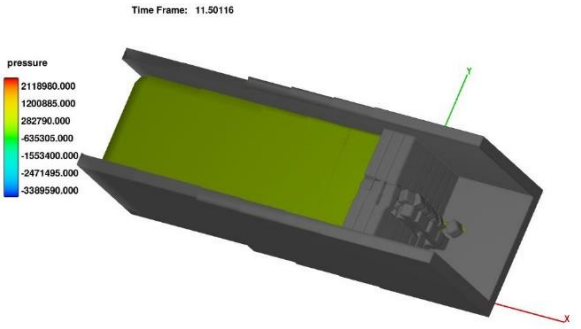

h) t=11.5s (3D view)

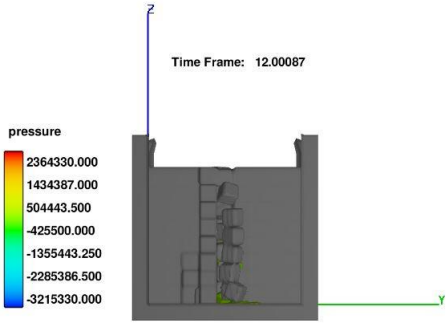

i) t=12s

j) t=12s (3D view)

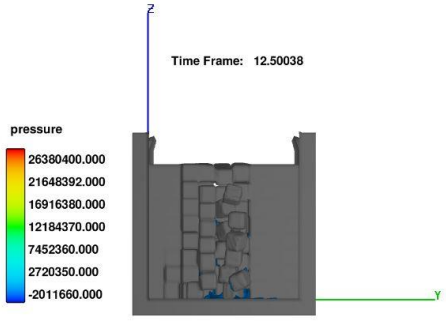

k) t=12.5s

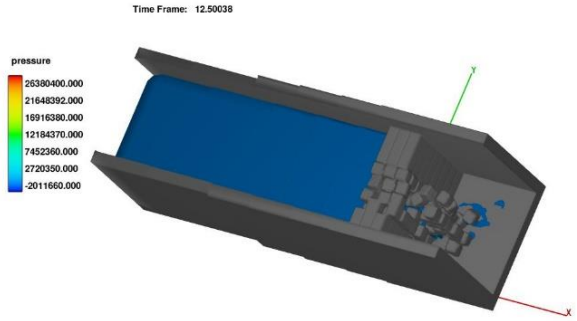

l) t=12.5s (3D view)

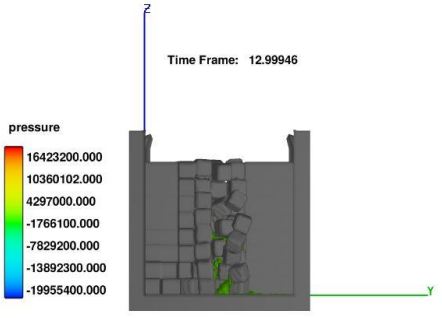

m) t=13s

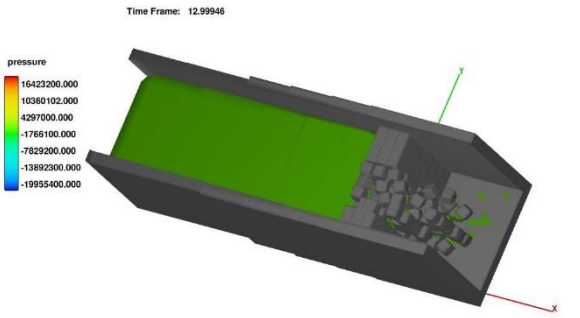

n) t=13s (3D view)

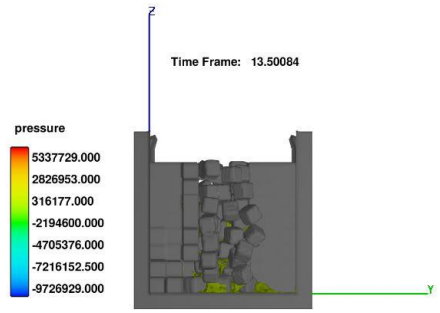

o) t=13.5s

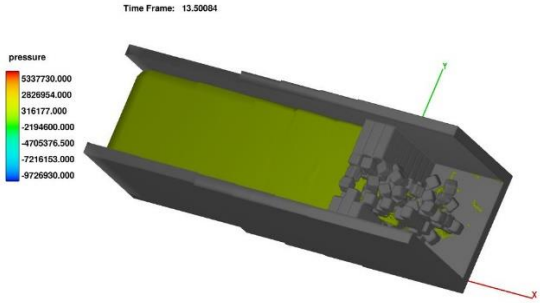

p) t=13.5s (3D view)

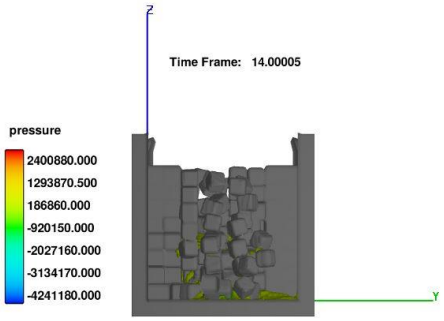

q) t=14s

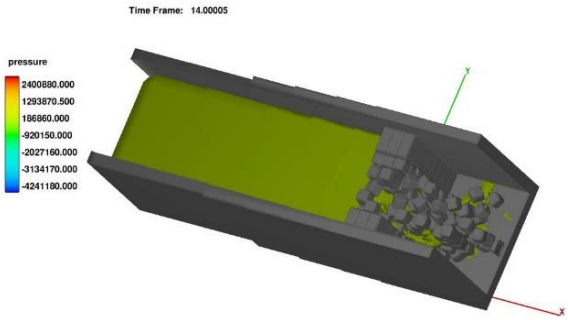

r) t=14s (3D view)

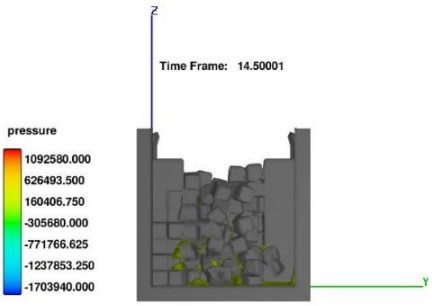

s) t=14.5s

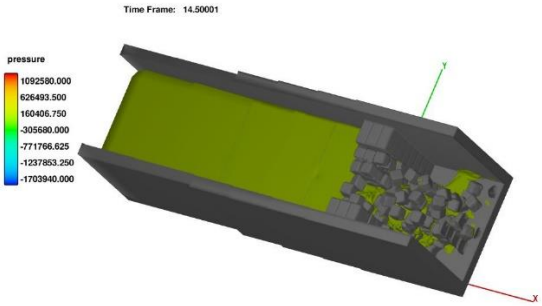

t) t=14.5s (3D view)

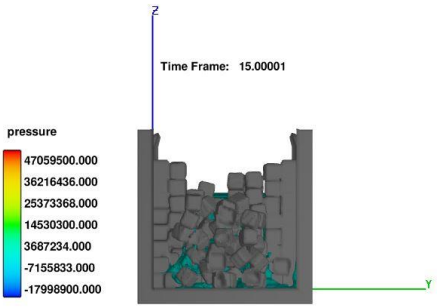

u) t=15s

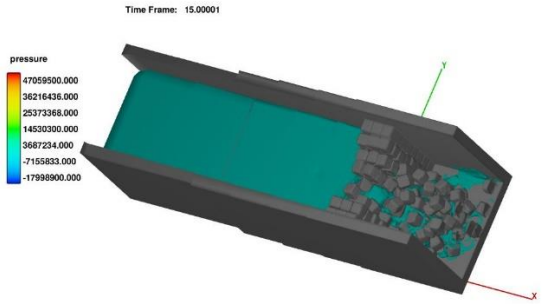

v) t=15s (3D view)

Figure 5.31. Semi-gradual failure of the dam due to normalized earthquake

As can be seen in the Figure 5.31, by applying a normalized earthquake, the 45-meter dam begins to break from the block at the bottom of the body and in the middle of the dam. Unlike the "100-meter-long dam failure due to the 1967 Koyna earthquake" model, which was studied in the previous sections, in the current model, the semi-gradual failure process continues from the middle of the dam, so that the first fluid flow due to the dam failure is observed from the middle of the dam. As the simulation continues, the broken part of the dam grows larger over time and continues toward the side walls, until total failure of the body.

5.4.3 Inspection of the Hydrograph of Symmetric Semi-Gradual Failure

As mentioned, by applying the low frequency normalized sinusoidal earthquake in the single direction, the dam starts to fail from its lower middle blocks, and over time, successive failures continue towards the side walls. Due to the fact that this type of semi-gradual failure is symmetrical with respect to the middle of the dam, it can be called symmetric semi-gradual failure. Another point to note here is that this failure is the most dangerous possible state for the failure of the mentioned dam in gradual mode, as the first failure of the dam was assumed exactly at the earthquake ending time.

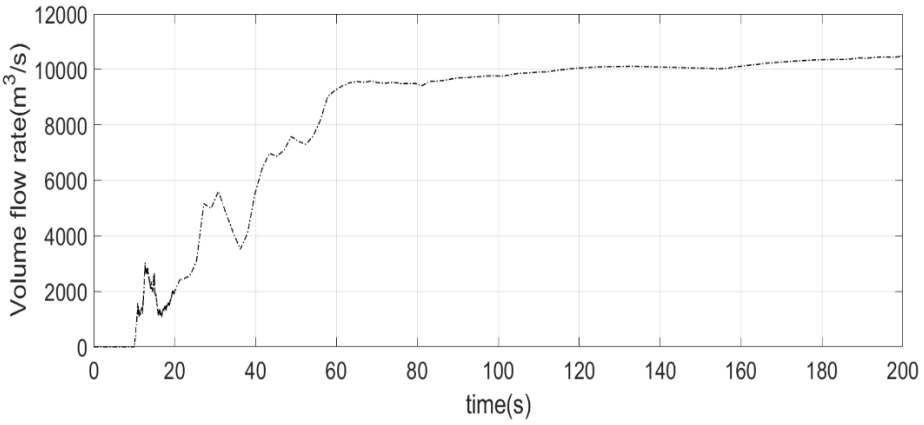

Figure 5.32. Hydrograph of symmetric semi-gradual failure

Based on the discharge hydrograph, as a result of successive failures, the water flow experiences different peaks, which similar to the previous analysis, show a step-by-step incremental behavior. Finally, 200 seconds after starting of earthquake, volumetric flow rate reaches its maximum, which is more than 1E+4 cubic meters per second. It is worth mentioning that this volume of water has been obtained from the failure of a dam with a length of 45 meters and water free surface level of 30 meters.

5.5 Modification of the dam body

At the end of the study, according to the analysis, the dam body is designed to show the greatest resistance to earthquakes. Of course, many factors must be considered for the design of a dam's body, and in this study, according to the findings, only suggestions are presented to structural engineers.

First, according to the analysis of "Koyan Dam failure due to the 1967 earthquake" and "Investigation of the geometric effects of the dam body on gradual failure" presented in the previous sections, parts of the dam body that have a sudden slope change, during the earthquake, are the most stressful zones and are prone to cracking. Therefore, in designing the dam body, sudden change of the body slope should be avoided and these slope changes should be designed using curved lines instead of using angled lines.

The next important point to consider when designing a dam body is that, as shown by three-dimensional analysis, the middle of the dam is the most likely place to start dam failure. In fact, the blocks in the lower middle of the dam were the first blocks to start moving. Therefore, to strengthen the dam body against earthquakes, the middle and lower parts of the dam should be considered to be thicker than the other parts of the body. A simple design of a earthquake resistance dam's body is shown in Figure 5.32.

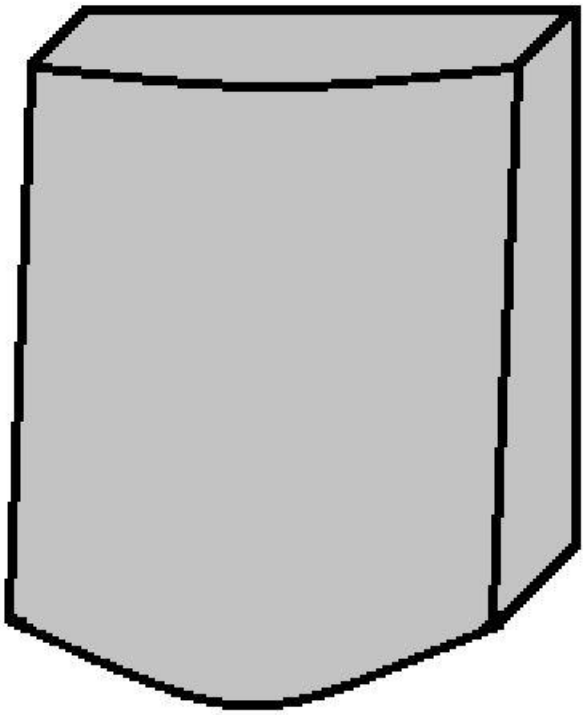

Figure 5.33. Modification of geometry

CHAPTER 6

SUMMARY AND CONCLUSION

In the final part of the study, all the models and analyzes performed under the thesis will be summarized and solutions for future studies will be presented. As mentioned, the main body of the study consisted of three sections of pressure analysis within cracks, rigid body motion analysis, and failure mechanism, and the conclusions of each section are presented separately in this chapter.

6.1 Pressure Inspection

A CFD model is developed to inspect pressure variation with time in the crack area at the time of the earthquake where the earthquake is simulated as a sinusoidal wave with normalized corresponding frequency and magnitude. In order to avoid excessive analysis, just the crack area of the dam by considering constant pressure value in its mouth is utilized.

First of all, the study reveals that the water can penetrate to the crack and partially saturate it during the simulated earthquake. It is observed that, for a constant magnitude earthquake by increasing oscillations' frequency, the pressure value is increased in the crack zone.

Secondly, by going through the crack in the downstream direction, the pressure values are increased and the maximum pressure value is captured at the end of the crack or PT5 with a sufficient value for the propagation of it. Cavitation is observed at the starting of opening and ending of closing cycles, which has larger probability of occurance by moving toward the crack end as well as by increasing the frequency of oscillations.

Thirdly, using the commercial code FLOW-3D, coincident results with experimental data are captured for pressure variation with time, therefore the program is applicable in any similar study, which deals with capturing of fluid properties in narrow cracks among moving objects.

Fourthly, from finite element analysis in the crack zone, the most vulnerable zone inside of the crack is detected at few millimeters before its end, where the water will be in static condition. Due to the finite element analysis and the fact that the maximum pressure was observed at the end of the crack, the cracks tend to expand in the horizontal direction.

Finally, According to the analysis of the effects of crack features on the amount of pressure within it, the amplitude of pressure oscillation increases with increasing crack length at constant crack mouth opening, or with increasing crack mouth opening at constant length. Generally by increasing the crack size with a constant angular velocity the pressure variation increases. This means that, it is not possible to model dam failure experimentally, as the cracks in an actual dam body created by the earthquake will be much larger than it will be in a laboratory model. The pressure changes within a prototype scale are greater, therefore it tend to expand more than a scaled laboratory model.

6.2 Motion Inspection

The behavior of the severed part of a concrete gravity monolith was investigated for three different crack orientations assuming a straight crack geometry. The comparison of the permanent deformation of the top block for the three cases shows that the most dangerous shape is the downstream sloped crack due to the falling possibility of the detached part. Much smaller permanent deformations were obtained for the horizontal and upstream sloped cracks.

Firstly, the motion of the detached part is highly dependent on the value of the restitution coefficient. The recovered kinetic energy after the collision, directly corresponding to higher drift times leading to permanent deformations.

Secondly, the variation of the response due to the coefficient of friction was highest for the downstream sloped case. The variation was the least for the upstream sloped case forming the most stable scenario. It is also not possible to stop a detached part from failing by increasing the friction coefficient as the motion type changes from pure sliding to rock-sliding kind of motion. Overall, Three types of motion were detected for a piece detached from the motion body, including sliding, rocking, and drifting, And a code was developed in MATLAB software to detect these different types.

Thirdly, by comparing the movement of solids isolated with different shapes from the dam body, the most dangerous types of cracks were identified as those that have a slope from upstream to downstream of the dam.

Fourthly, from the analysis in the case with an empty reservoir (neglecting hydraulic forces), the top part's motion is almost the same as the base motion, which means that in the absence of water the top part will mostly fluctuate on its base with negligible detachment from it, however by including hydraulic forces, unlike the empty reservoir case the top part was detached from its base and moved to the downstream direction.

Finally, from discharge analysis by increasing the restitution coefficient the top part of the dam felt sooner, therefore the fluid reached its maximum flow rate earlier. Generally, by increasing the restitution coefficient the top part was easily drifted, and therefore it felt sooner. However, the time of the maximum flow rate was not influenced clearly from the friction coefficient value, because the motion type transforms with the friction coefficient.

6.3 Failure Mechanism Inspection

In this study, two CFD models using FLOW 3D software and concepts of continuum mechanics, for both sudden and gradual failure of Koyna dam due to earthquake base excitation are presented. During the earthquake, due to the excitations of the earth, the blocks are only able to rotate before separating from the main body as there is an adhesion force of concrete in the separated part. After the earthquake, the earth returns to a static state and if cracks are created in the body due to the earthquake, development of these cracks due to the pressure of water penetrating into them will cause the gradual failure of the dam. The water inside the crack is prone to penetration and breaking its stagnant state, so as soon as the crack is completed, the water comes out of the stagnation state and causes the initial movement of the separated block in a sliding type of motion.

Firstly, the failure of the dam in a sudden case that its occurrence was detected during the earthquake is more dangerous than the gradual failure of the dam that occurs after the earthquake as the maximum discharge is reached faster. In the sudden failure of the dam the maximum discharge is reached around 300 seconds after the earthquake. However, for gradual failure, this time is almost three times larger.

Secondly, a closer look at the sudden failure of the dam resulted in the conclusion that although with increasing earthquake acceleration and decreasing oscillation frequencies, the probability of failure in the abrupt state increases. After cracking of the dam body, higher oscillation frequencies will be able to break it in less time. In other words, although large oscillating periods carry a higher risk of cracking of the dam body, smaller periods propagate the resulting cracks more rapidly.

Thirdly, in the gradual failure of the Koyna dam, the failure process began from the sloping area in the body. By the finite element analysis, the same area of the dam has been detected as the most vulnerable zone to cracking, which is consistent with empirical studies of Mridha et al. (2014). Therefore, changes are required to make this part of the dam body stronger.

Finally, According to three-dimensional analysis, the lower middle areas of the dam are the most probable areas on the wall shaped body to start the process of dam failure in a gradual state. Therefore, changes are required to make this part of the dam body stronger.

6.4 Result Inspection

In this study, the failure of the Koyna Dam due to the 1967 earthquake was investigated in two defined failure mechanisms, including 1. sudden that occurs during an earthquake and 2. Gradual that occurs after the earthquake. These methods are applicable for the failure of other dams affected by various earthquakes. The most important suggestion in the context of expanding this issue can be to write a comprehensive computer program that includes all the steps defined in the failure mechanism. Thus, a practical physical model will be provided to dam engineers to identify the sensitive parts of the dam body.

Also, the defined model for gradual dam failure can be used with minor changes for dam failure due to overtopping. Because this model consisted of two general parts, the first part of which showed the cracking of the dam body at the time of the earthquake and the second part of which simulated the gradual failure after the earthquake. The second part of the defined mechanism can be extended and used for failure in the overtopping case.

Finally, considering that in this study we succeeded in obtaining acceptable results by simulating the adhesion force of concrete by increasing the density of blocks by defining some mechanisms. This method can also be extended to different hydraulic and non-hydraulic structures with different materials. The point to be noted here is that in this method, the body of the object is divided into small pieces that have a high weight before the first movement. The initial density value for simulating the adhesion force of a material is determined according to its tensile and compressive strength.

6.5 A Sugession for Future Study

In this section, first some of the limitations we faced in conducting this research will be presented and finally a suggestion for future studies will be presented.

Firstly, as mentioned in the case of the concrete dam failure due to the earthquake, in addition to the need to create very small cells to properly simulate the pressure distribution within the cracks, very small time steps must be used to accurately simulate the seismic effects. This issue greatly increases the simulation time, so that some of the mentioned analyzes took several months to perform, and sometimes three computers were used simultaneously for the simulations.

secondly, FLOW 3D software has limitations that make it more difficult to simulate dam failure. For example, we first intended to simulate failure, using a spring and damper among the blocks , while it is not possible to define a spring with variable stiffness, and the presence of springs in turn greatly increases the simulation time. As another example, a maximum of 500 movable solids can be defined in the software, so we could not study the failure of the Koyna Dam in three dimensions and had to use a simpler geometry for the dam, etc.

lastly, during the research process, many bugs were detected in the software code, which sometimes caused a waste of time. For example, the software can not properly simulate a solid collision with the boundary conditions of the wall, so instead of the wall boundary conditions, we must use another solid object as a wall. Or as another example, the software is not able to simulate the small cycles of pure rocking motion of a solid object, so that after calculating the first few cycles, the object under rocking motion sticks to the fixed body, etc.

In conclusion, due to the mentioned limitations, although we were able to get good answers in the field of study by using Flow 3D software, it is not economical at all in terms of time and equipment required to do it. Therefore, according to the studies and mechanisms defined, it is better to create a code for dam failure case that

regardless of the type and material of dam will be able to provide accurate prediction of its' failure due to earthquake.

REFERENCES

Aleixo, R., Soares-Frazão, S., & Zech, Y. (2010). Velocity-field measurements in a dam-break flow using a PTV Voronoï imaging technique. *Experiments in Fluids*, (6), 1633–1649. https://doi.org/10.1007/s00348-010-1021-y

Aureli, F., Ziveri, C., Maranzoni, A., & Mignosa, P. (2006). Fully-2D and quasi-2D modeling of flooding scenarios due to embankment failure. In *River Flow 2006*. Taylor & Francis. Retrieved from http://dx.doi.org/10.1201/9781439833865.ch157

Biscarini, C., Di Francesco, S., & Manciola, P. (2010). CFD modelling approach for dam break flow studies. *Hydrology and Earth System Sciences*, (4), 705–718. https://doi.org/10.5194/hess-14-705-2010

Bridle, R. (2017). ICOLD Embankment Dams Committee Activities, ICOLD Johannesburg, May 2016. *Dams and Reservoirs*, (2), 87–91. https://doi.org/10.1680/jdare.17.00013

Cao, Z., Pender, G., & Carling, P. (2006). Shallow water hydrodynamic models for hyperconcentrated sediment-laden floods over erodible bed. *Advances in Water Resources*, (4), 546–557. https://doi.org/10.1016/j.advwatres.2005.06.011

Chang, T.-J., Kao, H.-M., Chang, K.-H., & Hsu, M.-H. (2011). Numerical simulation of shallow-water dam break flows in open channels using smoothed particle hydrodynamics. *Journal of Hydrology*, (1–2), 78–90. https://doi.org/10.1016/j.jhydrol.2011.07.023

Chen, S., Liao, B., & Huang, T. (2016). Corrected SPH methods for solving shallow-water equations. *Journal of Hydrodynamics*, (3), 389–399. https://doi.org/10.1016/s1001-6058(16)60642-x

Colagrossi, A., & Landrini, M. (2003). Numerical simulation of interfacial flows by smoothed particle hydrodynamics. *Journal of Computational Physics*, (2), 448–475. https://doi.org/10.1016/s0021-9991(03)00324-3

Collier, N., Radwan, H., Dalcin, L., & Calo, V. M. (2011). Diffusive Wave Approximation to the Shallow Water Equations: Computational Approach. *Procedia Computer Science*, 1828–1833. https://doi.org/10.1016/j.procs.2011.04.198

Dressler, R. F. (1952). Hydraulic resistance effect upon the dam-break functions. *Journal of Research of the National Bureau of Standards*, (3), 217. https://doi.org/10.6028/jres.049.021

Farzin, S., Fatehi, R., & Hassanzadeh, Y. (2019). Position explicit and iterative implicit consistent incompressible SPH methods for free surface flow. *Computers & Fluids*, 52–66. https://doi.org/10.1016/j.compfluid.2018.10.010

Fondelli, T., Andreini, A., & Facchini, B. (2015). Numerical Simulation of Dam-Break Problem Using an Adaptive Meshing Approach. *Energy Procedia*, 309–315. https://doi.org/10.1016/j.egypro.2015.12.038

Gingold, R. A., & Monaghan, J. J. (1977). Smoothed particle hydrodynamics: theory and application to non-spherical stars. *Monthly Notices of the Royal Astronomical Society*, (3), 375–389. https://doi.org/10.1093/mnras/181.3.375

Gopalakrishnan, T. C., & Tung, C. C. (1980). Run-up of non-breaking waves — A finite-element approach. *Coastal Engineering*, 3–22. https://doi.org/10.1016/0378-3839(80)90003-4

Guinot, V., & Soares-Frazão, S. (2005). Flux and source term discretization in two-dimensional shallow water models with porosity on unstructured grids. *International Journal for Numerical Methods in Fluids*, (3), 309–345. https://doi.org/10.1002/fld.1059

Hall, J.F. (1998), “Efficient Non-Linear Seismic Analysis of Arch Dams”, *Earthquake Engineering and Structural Dynamics*, 27, 1425-1444.

Hall, J.F. and Chopra, A.K. (1980), “Dynamic Response of Embankment, Concrete Gravity and Arch Dams including Hydrodynamic Interaction”, Report No: UCB/EERC-80-39, Earthquake Engineering Research Center, University of California, Berkeley, California

Hu, D., Zhu, Y., Zhong, D., & Qin, H. (2017). Two-Dimensional Finite-Volume Eulerian-Lagrangian Method on Unstructured Grid for Solving Advective Transport of Passive Scalars in Free-Surface Flows. *Journal of Hydraulic Engineering*, (12), 04017051. https://doi.org/10.1061/(asce)hy.1943-7900.0001371

Hui Pu, J., Shao, S., Huang, Y., & Hussain, K. (2013). Evaluations of SWEs and SPH Numerical Modelling Techniques for Dam Break Flows. *Engineering Applications of Computational Fluid Mechanics*, (4), 544–563. https://doi.org/10.1080/19942060.2013.11015492

Javanmardi, F., Léger, P., & Tinawi, R. (2005). Seismic Water Pressure in Cracked Concrete Gravity Dams: Experimental Study and Theoretical Modeling. *Journal of Structural Engineering*, (1), 139–150. https://doi.org/10.1061/(asce)0733-9445(2005)131:1(139)

Jansen, R. B. (1980). *Dams and Public Safety*.

Jeon, J., Lee, J., Shin, D., & Park, H. (2009). Development of dam safety management system. *Advances in Engineering Software*, (8), 554–563. https://doi.org/10.1016/j.advengsoft.2008.10.009

Jeong, J. H., & Yang, D. Y. (1998). Finite element analysis of transient fluid flow with free surface using VOF (volume-of-fluid) method and adaptive grid. *International Journal for Numerical Methods in Fluids*, (10), 1127–1154.

https://doi.org/10.1002/(sici)1097-0363(19980615)26:10<1127::aid-fld644>3.0.co;2-q

Kocaman, S., & Ozmen-Cagatay, H. (2015). Investigation of dam-break induced shock waves impact on a vertical wall. *Journal of Hydrology*, 1–12. https://doi.org/10.1016/j.jhydrol.2015.03.040

Kumar, P., Yang, Q., Jones, V., & McCue-Weil, L. (2015). Coupled SPH-FVM Simulation within the OpenFOAM Framework. *Procedia IUTAM*, 76–84. https://doi.org/10.1016/j.piutam.2015.11.008

Löhner, R., Yang, C., & Oñate, E. (2006). On the simulation of flows with violent free surface motion. *Computer Methods in Applied Mechanics and Engineering*, (41–43), 5597–5620. https://doi.org/10.1016/j.cma.2005.11.010

Lohrasbi, A., Dolatshahi Pirooz, M., & Lavaei, A. (2016). Hydraulic Model of Dam Break Using Navier Stokes Equation with Arbitrary Lagrangian-Eulerian Approach. *International Journal of Engineering and Technology*, (4), 249–253. https://doi.org/10.7763/ijet.2016.v6.893

Løkke, A., & Chopra, A. K. (2019). Direct finite element method for nonlinear earthquake analysis of concrete dams: Simplification, modeling, and practical application. *Earthquake Engineering & Structural Dynamics*, (7), 818–842. https://doi.org/10.1002/eqe.3150

Monaghan, J. J. (2012). Smoothed Particle Hydrodynamics and Its Diverse Applications. *Annual Review of Fluid Mechanics*, (1), 323–346. https://doi.org/10.1146/annurev-fluid-120710-101220

Moigne, G. L., & Barghouti, S. M. (1990). *Dam Safety and the Environment*.

Moraga, N. O., Lemus, L. A., Saavedra, M. A., & Lemus-Mondaca, R. A. (2015). VOF/FVM prediction and experimental validation for shear-thinning fluid

column collapse. *Computers & Mathematics with Applications*, (2), 89–100.https://doi.org/10.1016/j.camwa.2014.11.018

Morris, M., Galland, J. C., & Balabanis, P. (1999). Proceedings *of the CADAM Meeting, Wallingford, United Kingdom*. European Commission Directorate-General Research.

Mridha, S., & Maity, D. (2014). Experimental investigation on nonlinear dynamic response of concrete gravity dam-reservoir system. *Engineering Structures*, 289–297. https://doi.org/10.1016/j.engstruct.2014.09.017

Nuss, L.K., Matsumoto, N. and Hansen, K.D. (2012), "Shaken but not Stirred Earthquake Performance of Concrete Dams", *32nd Annual USSD Conference*, New Orleans, Louisiana.

Panicker, P. G., Goel, A., & Iyer, H. R. (2015). Numerical Modeling of Advancing Wave Front in Dam Break Problem by Incompressible Navier-stokes Solver. *Aquatic Procedia*, 861–867. https://doi.org/10.1016/j.aqpro.2015.02.108

Pekau, O. A., & Cui, Y. (2006). Progressive collapse simulation of precast panel shear walls during earthquakes. *Computers & Structures*, (5–6), 400–412. https://doi.org/10.1016/j.compstruc.2005.09.027

Pekau, O. A., Lingmin, F., & Chuhan, Z. (1995). Seismic fracture of koyna dam: Case study. *Earthquake Engineering & Structural Dynamics*, (1), 15–33. https://doi.org/10.1002/eqe.4290240103

Pekau, O. A., & Yuzhu, C. (2004). Failure analysis of fractured dams during earthquakes by DEM. *Engineering Structures*, (10), 1483–1502. https://doi.org/10.1016/j.engstruct.2004.05.019

Pekau, O. A., & Zhu, X. (2008). Effect of Seismic Uplift Pressure on the Behavior of Concrete Gravity Dams with a Penetrated Crack. *Journal of Engineering*

Mechanics, (11), 991–999. https://doi.org/10.1061/(asce)0733-9399(2008)134:11(991)

Sasson, M., Chai, S., Beck, G., Jin, Y., & Rafieshahraki, J. (2016). A comparison between Smoothed-Particle Hydrodynamics and RANS Volume of Fluid method in modelling slamming. *Journal of Ocean Engineering and Science*, (2), 119–128. https://doi.org/10.1016/j.joes.2016.03.004

Saint-Venant, J. de. (1871). Th´eorie du mouvement non-permanent des eaux, avec application aux crues des rivi`eres at `a l'introduction des mar´ees dans leur lit. *Comptes rendus hebdomadaires des s´eances de l'Acad´emie des sciences*, (2), 147– 154.

Savant, G., Trahan, C. J., Berger, C., McAlpin, J. T., & McAlpin, T. O. (2018). Refinement Indicator for Dynamic-Mesh Adaption in Three-Dimensional Shallow-Water Equation Modeling. *Journal of Hydraulic Engineering*, (2), 06017026. https://doi.org/10.1061/(asce)hy.1943-7900.0001394

Shao, S., & Lo, E. Y. M. (2003). Incompressible SPH method for simulating Newtonian and non-Newtonian flows with a free surface. *Advances in Water Resources*, (7), 787–800. https://doi.org/10.1016/s0309-1708(03)00030-7

Shi, Z., Suzuki, M., & Nakano, M. (2003). Numerical Analysis of Multiple Discrete Cracks in Concrete Dams Using Extended Fictitious Crack Model. *Journal of Structural Engineering*, (3), 324–336. https://doi.org/10.1061/(asce)0733-9445(2003)129:3(324)

Shrikhande, M., & Basu, S. (2005). A critique of the ICOLD method for selecting earthquake ground motions to design large dams. *Engineering Geology*, (1–2), 37–42. https://doi.org/10.1016/j.enggeo.2005.02.005

Slowik, V., & Saouma, V. E. (2000). Water Pressure in Propagating Concrete Cracks. *Journal of Structural Engineering*, (2), 235–242. https://doi.org/10.1061/(asce)0733-9445(2000)126:2(235)

Stoker, J. J. (1957). Water waves: The mathematical theory with applications. Wiley-Interscience, New York.

Tate, J. N., Berger, R. C., & Stockstill, R. L. (2006). Refinement Indicator for Mesh Adaption in Shallow-Water Modeling. *Journal of Hydraulic Engineering*, (8), 854–857. https://doi.org/10.1061/(asce)0733-9429(2006)132:8(854)

Uddin, Md. I., & Karim, Md. M. (2017). Application of Volume of Fluid (VOF) Method for Prediction of Wave Generated by Flow around Cambered Hydrofoil. *Procedia Engineering*, 82–89. https://doi.org/10.1016/j.proeng.2017.08.120

Wang, J. S., Ni, H. G., & He, Y. S. (2000). Finite-Difference TVD Scheme for Computation of Dam-Break Problems. *Journal of Hydraulic Engineering*, (4), 253–262. https://doi.org/10.1061/(asce)0733-9429(2000)126:4(253)

Wang, L., & Pan, C. (2014). An analysis of dam-break flow on slope. *Journal of Hydrodynamics*, (6), 902–911. https://doi.org/10.1016/s1001-6058(14)60099-8

Wei, Y., Abadie, T., Henry, A., & Dias, F. (2016). Wave interaction with an Oscillating Wave Surge Converter. Part II: Slamming. *Ocean Engineering*, 319–334. https://doi.org/10.1016/j.oceaneng.2015.12.041

Wu, J., Zhang, H., Yang, R., Dalrymple, R. A., & HéRault, A. (2013). Numerical modeling of dam-break flood through intricate city layouts including underground spaces using GPU-based SPH method. *Journal of*

Hydrodynamics, (6), 818–828. https://doi.org/10.1016/s1001-6058(13)60429-1

Yeh, H. H., Ghazali, A., & Marton, I. (1989). Experimental study of bore run-up. *Journal of Fluid Mechanics*, 563–578. https://doi.org/10.1017/s0022112089002417

Yue, B., & Wang, Z. (2006). Numerical study of three-dimensional free surface dynamics. *Acta Mechanica Sinica*, (2), 120–125. https://doi.org/10.1007/s10409-006-0100-z

Zhang, A., Sun, P., Ming, F., & Colagrossi, A. (2017). Smoothed particle hydrodynamics and its applications in fluid-structure interactions. *Journal of Hydrodynamics*, (2), 187–216. https://doi.org/10.1016/s1001-6058(16)60730-8

Zhang, T., & Feng, P. (2017). Development of a Three-Dimensional Unstructured Mesh Finite-Element Model for Flood Propagation. *Journal of Hydraulic Engineering*, (10), 04017042. https://doi.org/10.1061/(asce)hy.1943-7900.0001358

Zhang, T., Feng, P., Maksimović, Č., & Bates, P. D. (2015). Application of a Three-Dimensional Unstructured-Mesh Finite-Element Flooding Model and Comparison with Two-Dimensional Approaches. *Water Resources Management*, (2), 823–841. https://doi.org/10.1007/s11269-015-1193-6

Zhu, X., & Pekau, O. A. (2007). Seismic behavior of concrete gravity dams with penetrated cracks and equivalent impact damping. *Engineering Structures*, (3), 336–345. https://doi.org/10.1016/j.engstruct.2006.05.002

Farzin, S., Fatehi, R., & Hassanzadeh, Y. (2019). Position explicit and iterative implicit consistent incompressible SPH methods for free surface flow. *Computers & Fluids*, 52–66. https://doi.org/10.1016/j.compfluid.2018.10.010

Shi, Z., Suzuki, M., & Nakano, M. (2003). Numerical Analysis of Multiple Discrete Cracks in Concrete Dams Using Extended Fictitious Crack Model. *Journal of Structural Engineering*, (3), 324–336. https://doi.org/10.1061/(asce)0733-9445(2003)129:3(324)

Løkke, A., & Chopra, A. K. (2019). Direct finite element method for nonlinear earthquake analysis of concrete dams: Simplification, modeling, and practical application. *Earthquake Engineering & Structural Dynamics*, (7), 818–842. https://doi.org/10.1002/eqe.3150

APPENDICES

A. Appendix-Mathlab Code

Developed MATLAB code for extracting motion components consisting of sliding rocking and drifting in cracked Koyna dam model.

```
p1x=x2-10.2-(10.2*(cos(r2+0.0096))-10.2*(cos(0.0096)));
p1y=x2*0;
p1z=z2+0.1+(10.2*(sin(r2+0.0096))-10.2*(sin(0.0096)));
p2x=x2+10.2+(10.2*(cos(r2+0.0096))-10.2*(cos(0.0096)));
p2y=x2*0;
p2z=z2+0.1-(10.2*(sin(r2+0.0096))-10.2*(sin(0.0096)));
p3x=x1-8.8982649-(19.37*(cos(r1+1.093))-19.37*(cos(1.093)));
p3y=x2*0;
p3z=z1-17.228447+(19.37*(sin(r1+1.093))-19.37*(sin(1.093)));
p4x=x1+11.5017351+(20.96*(cos(r1+0.981))-20.96*(cos(0.981)));
p4y=x2*0;
p4z=z1-17.228447-(20.96*(sin(r1+0.981))-20.96*(sin(0.981)));
p1=[p1x,p1y,p1z];
p2=[p2x,p2y,p2z];
p3=[p3x,p3y,p3z];
p4=[p4x,p4y,p4z];
a1 = p1 - p2;
b1 = p3 - p2;
d1 = sqrt(sum(cross(a1,b1,2).^2,2)) ./ sqrt(sum(a1.^2,2));
a2 = p1 - p2;
b2 = p4 - p2;
d2 = sqrt(sum(cross(a2,b2,2).^2,2)) ./ sqrt(sum(a2.^2,2));
a3 = p3 - p4;
b3 = p1 - p4;
d3 = sqrt(sum(cross(a3,b3,2).^2,2)) ./ sqrt(sum(a3.^2,2));
a4 = p3 - p4;
b4 = p2 - p4;
d4 = sqrt(sum(cross(a4,b4,2).^2,2)) ./ sqrt(sum(a4.^2,2));
d=[d1 d2 d3 d4];
dist=min(d,[],2);

dr1=dist>0;
s1=sum(dr1)*0.001;
dr2=dist>0.0001;
s2=sum(dr2)*0.001;
dr3=dist>0.0005;
```

```
s3=sum(dr3)*0.001;
dr4=dist>0.001;
s4=sum(dr4)*0.001;
dr5=dist>0.005;
s5=sum(dr5)*0.001;
dr6=dist>0.01;
s6=sum(dr6)*0.001;
dr7=dist>0.05;
s7=sum(dr7)*0.001;
dr8=dist>0.1;
s8=sum(dr8)*0.001;
dr9=dist>0.5;
s9=sum(dr9)*0.001;
dr10=dist>1;
s10=sum(dr10)*0
```

B. Appendix- Earhquake Simulation methods

In general, four methods can be applied to simulate seismic forces on objects in the CFD model. To do this, a force is applied to a square block (top block) with dimensions of 1 meter resting on a flat plate (bottom block) in the form of a pulse in 0.1 seconds and a magnitude of 1.6 g. Top block movement is compared with the four mentioned methods.

- Method 1: The force applied to the 3DoF top block by considering non-moving base block:

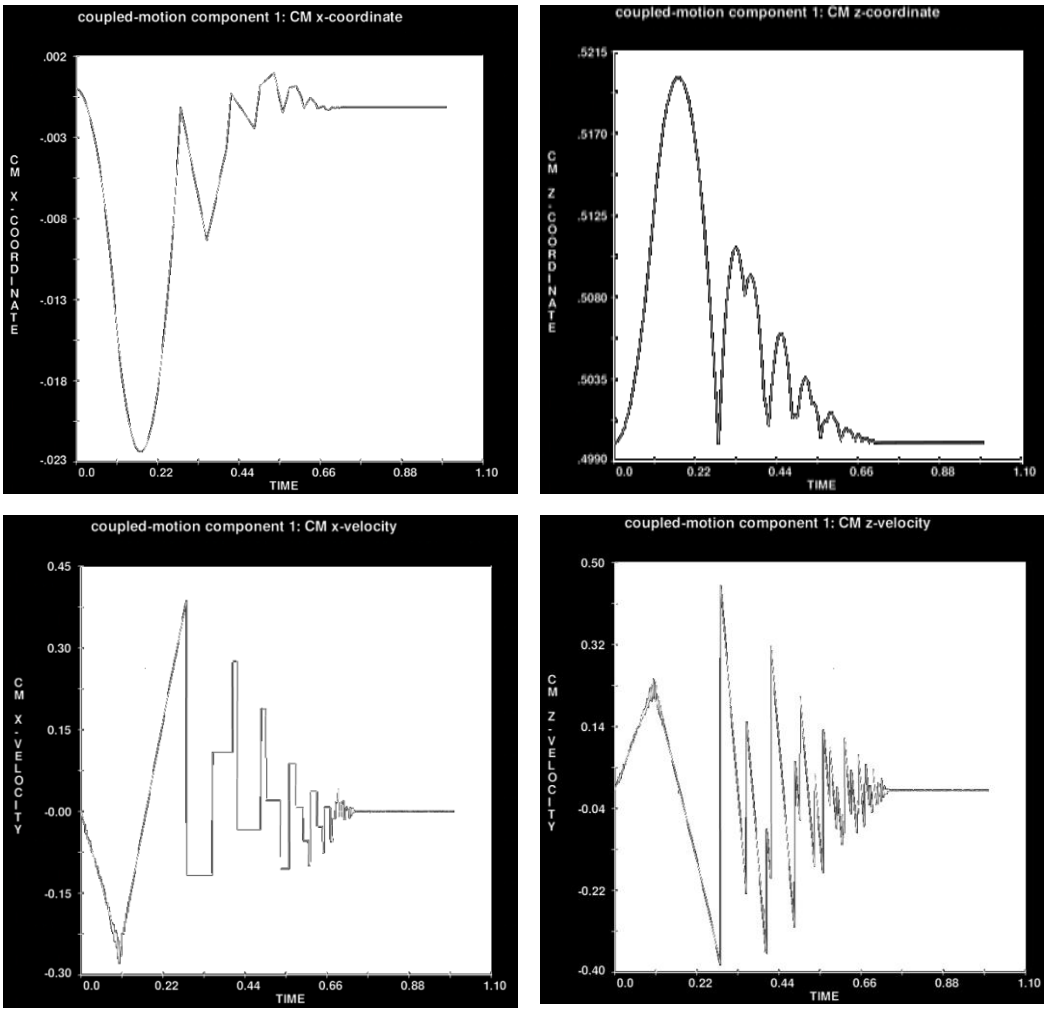

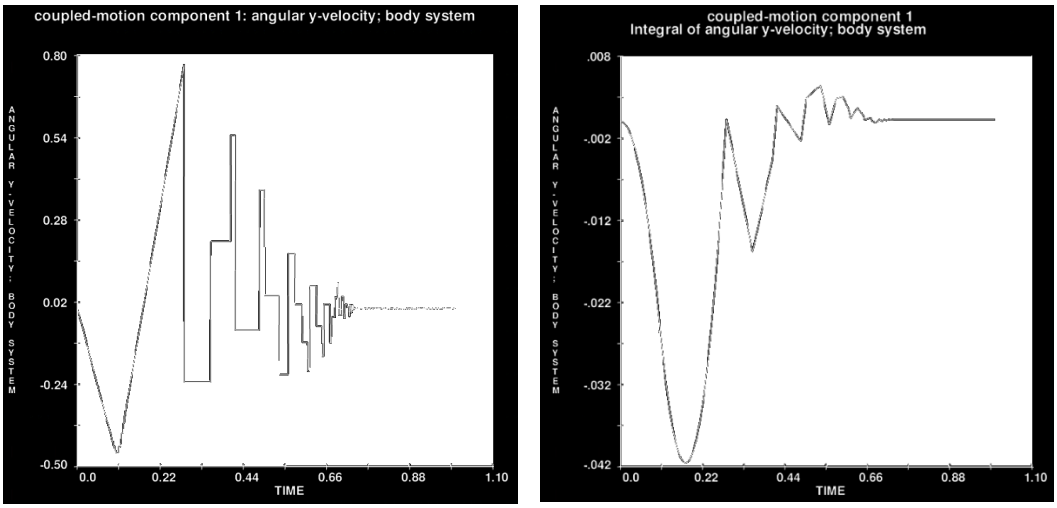

Figure B.1. The motions of the top block due to applied force on it- constant base

- Method 2: The force applied to the top block by considering 6DoF base block with huge density value of 1E+6*ρ:

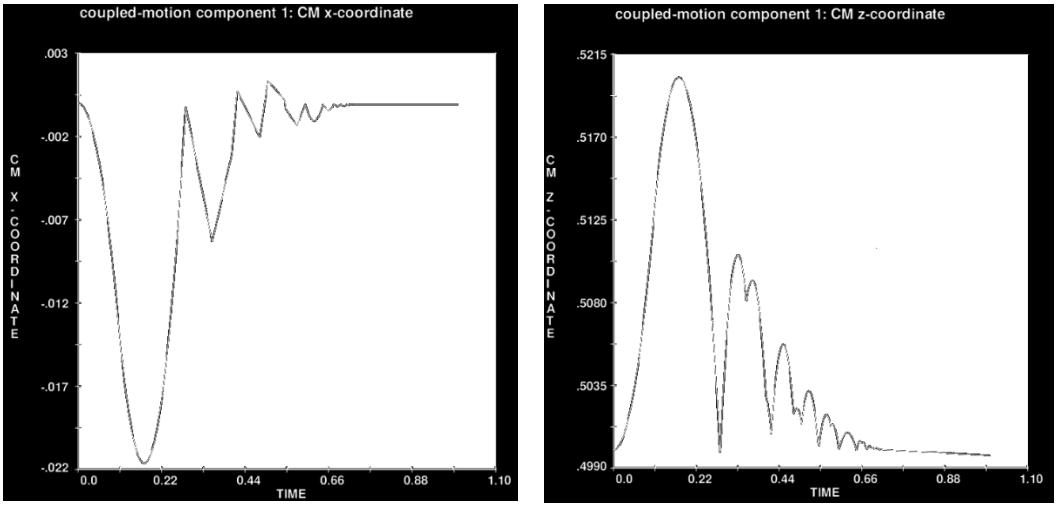

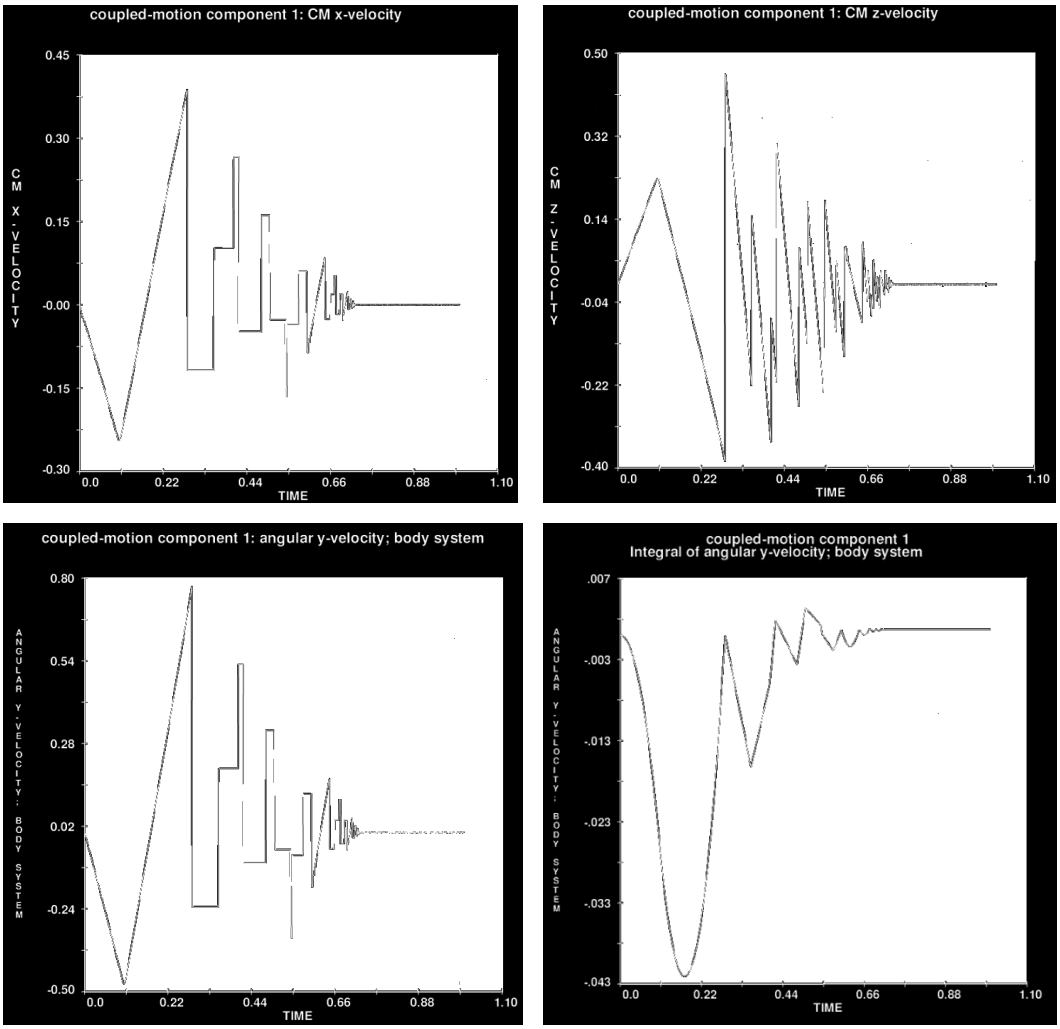

Figure B.2. The motions of the top block due to applied force on it- movable base

- Method 3: The force applied to the dense base block (1E+6*ρ) by considering the top block free to move in three degrees of freedom (X, Z displacement & Y rotation):

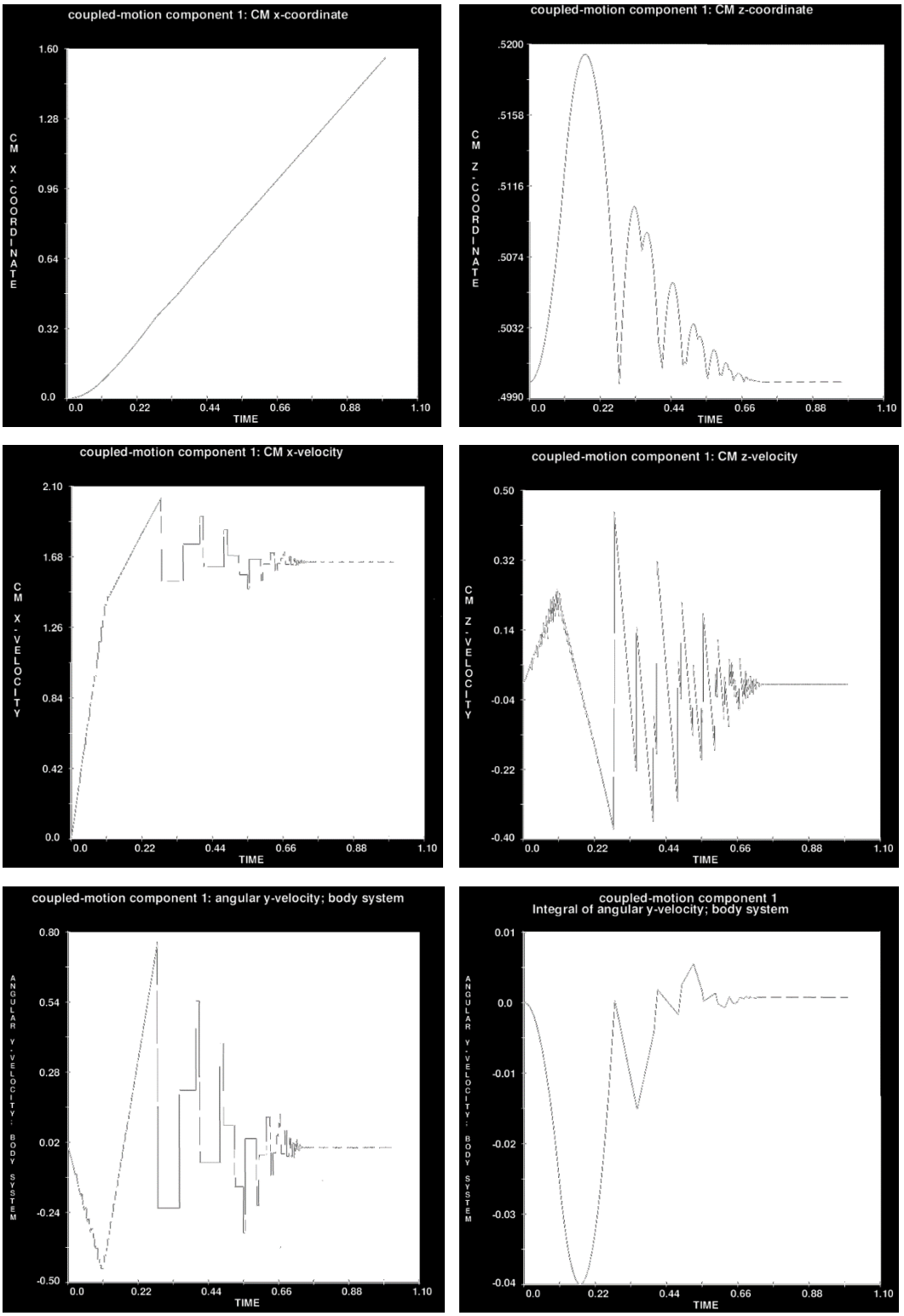

Figure B.3. The motions of the top block due to applied force on the dense base block

- Method 4: The velocity applied to the base block by considering the top block free to move in 3DoF (X, Z displacement & Y rotation):

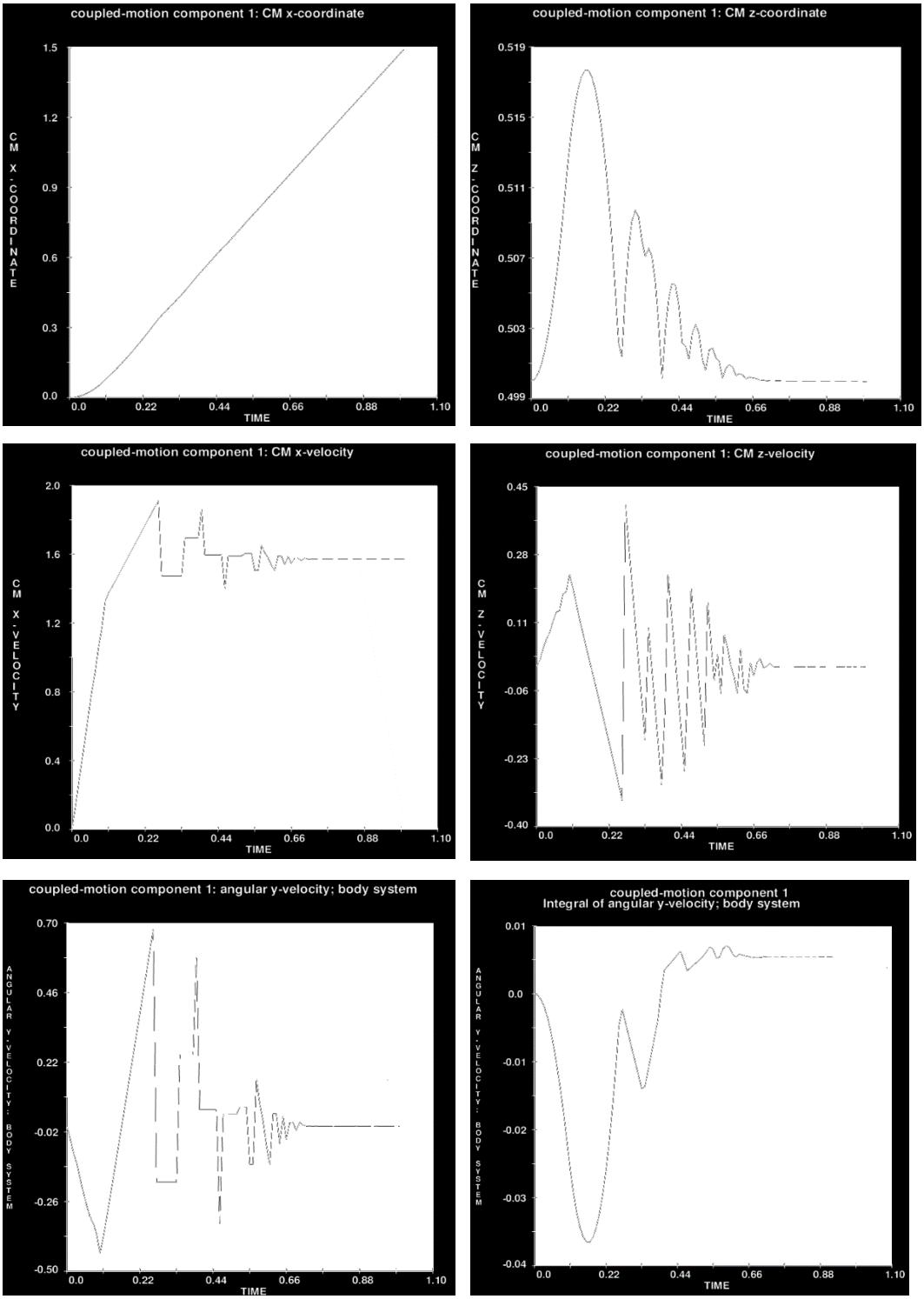

Figure B.4. The motions of the top block due to applied velocity on the base block

For methods 3 and 4, as the base block is moving in the X-direction simultaneously with the top block, to make the motion results of the whole four methods comparable, the top block X displacement and velocity should be considered relative to base one.

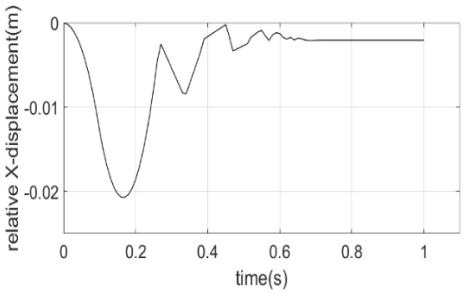

a) Methods 3 &4 relative X-displacement

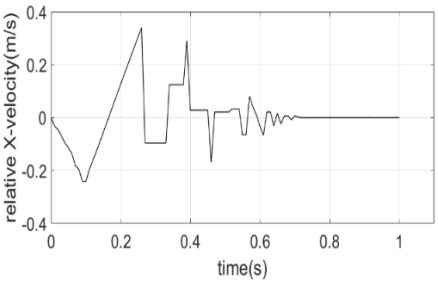

b) Methods 3 &4 relative X-velocity

Figure B.5. The relative motion of the top block concerning the base block

By comparing the results of the four mentioned methods, it was found that all four methods can be used in the CFD model. It should be noted that if the earthquake force directly enters the upper block, which represents the structure, a very high density value should be considered for the lower block, which represents the ground, so that the collisions can be calculated correctly by the software.

C. Appendix-Crack Shape Effects

In this appendix, the effects of hydrostatic and hydrodynamic forces of water on the movement of the separating block from the dam with different crack shapes under the 1967 Koyna earthquake, will be inspected. The second purpose of this appendix is to study the shape of the crack effects on the movement of the detaching block from the main body of the dam.

- One-step case

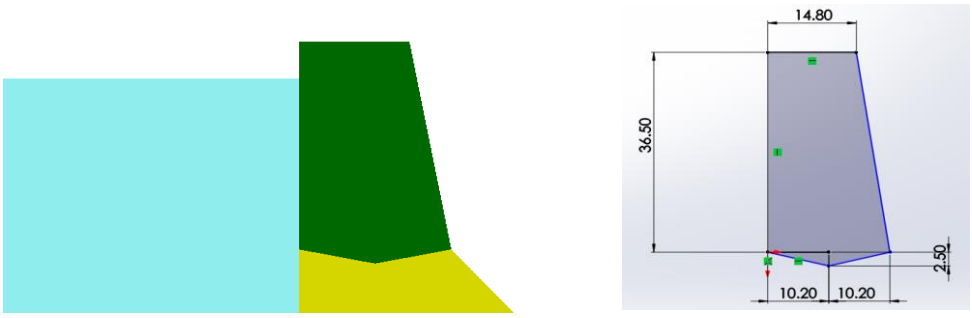

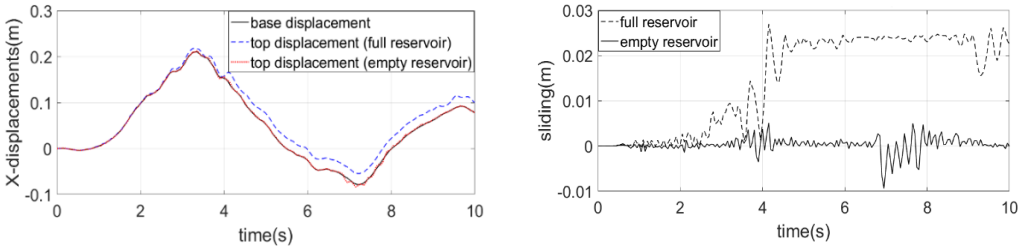

a) Particles absolute displacements b) Particles relative displacements

Figure C.1. One-step case motion in full and empty reservoir conditions

- Two-step case

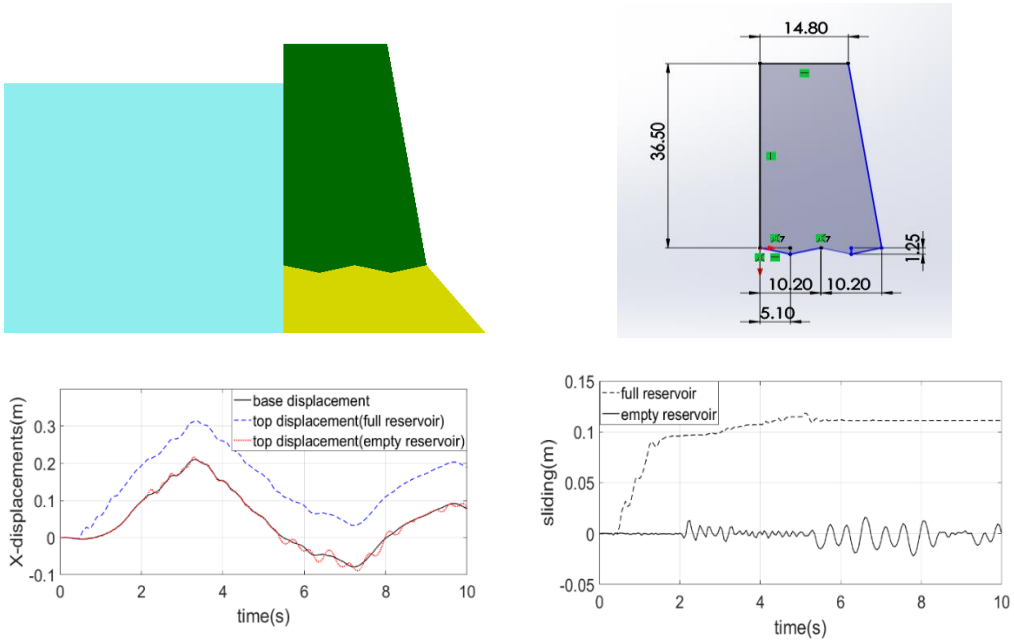

a) Particles absolute displacements b) Particles relative displacements

Figure C.2. Two-step case motion in full and empty reservoir conditions

- Three-step case

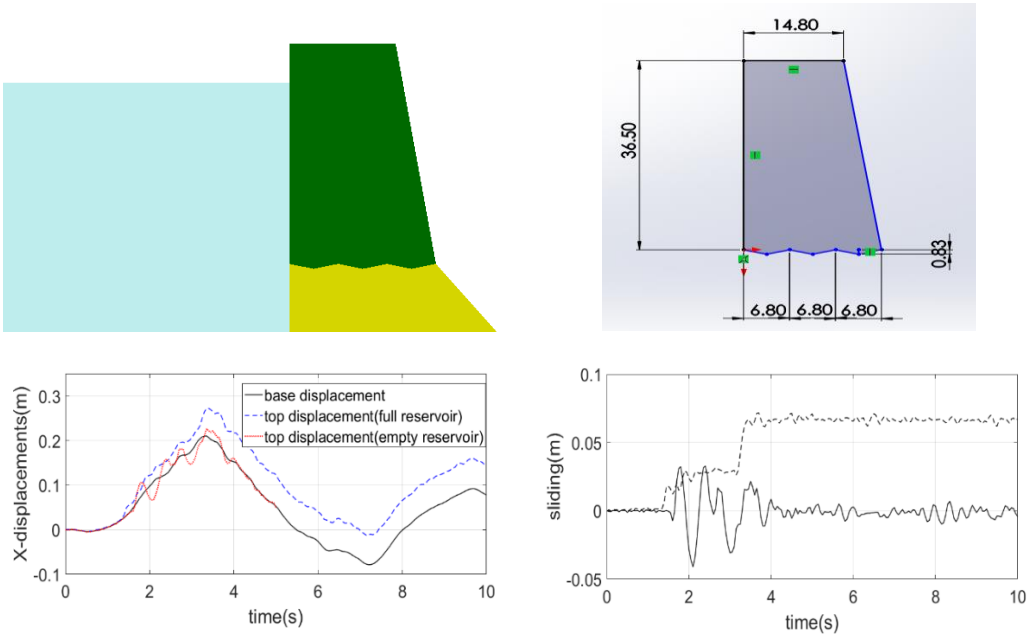

a) Particles absolute displacements b) Particles relative displacements

Figure C.3. Three-step case motion in full and empty reservoir conditions

- Four-step case

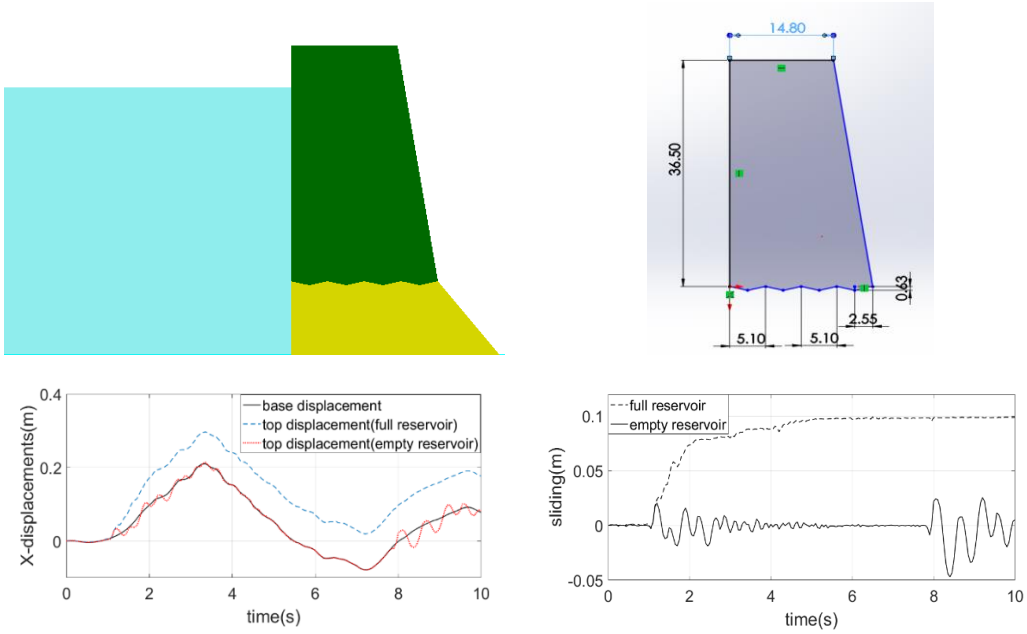

a) Particles absolute displacements b) Particles relative displacements

Figure C.4. Four-step case motion in full and empty reservoir conditions

According to the obtained results, the hydrostatic and hydrodynamic forces of water are the main reason for the separation of the upper block from the lower block. Because, in the empty reservoir, the upper block shows rocking movement in its' place due to seismic force without separating from the lower block.

Another important point to be noted here is that although as the crack shape became more complex, the upper block was expected to show less movement due to the increased frictional force between the two blocks, such a result was not clearly observed. The reason for this phenomenon, as explained in the fourth chapter of the thesis, is that the part separated from the dam body has a combination of three sliding, rocking, and drifting motions, so just increasing the friction force cannot reduce the movement of the detached block.

CURRICULUM VITAE

EDUCATION

Degree	Institution	Year of Graduation
MS	Tabriz University Hydraulic Engineering, Tabriz, Iran	2012-2015
BS	Tabriz University Mechanical Engineering, Tabriz, Iran Tabriz	2007-2011
High School	Shahriar Talented High School, Tabriz	2002-2006

WORK EXPERIENCE

Year	Place	Enrollment
2017-2020	METU Dept. of Civil Eng	Research Assistant
2013-2015	Azar-baharan Co., Tabriz	CEO
2013	Nasim Aras Co., Ahar	Project Manager
1994 August	Zarin Pey Co., Tabriz	Project Engineer

FOREIGN LANGUAGES

Native Persian and Azeri, Advanced English and Turkish, Fluent Arabic, Intermediate German

PUBLICATIONS

1. Khosravi, M ., Mosaddeghi, F., & Khodayari, A. (2015). Aerodynamic drag reduction of heavy vehicles using append devices by CFD analysis. *Journal of Central South University*.

2. Nourdanesh, N., Farrokhi, N., & Mosaddeghi, F. (2015). Geometry optimization of two infinite parallel plates with free convection heat transfer. *Transactions of Famena*.